Blending Optimization of Networks with Uncertain Scenarios (BONUS): An application to hydrogen blending in natural gas networks

Larson Beemster

(2743204)

15 July 2026

Thesis MSc BA - Business Analytics

Thesis committee:

Dr. Alessandro Zocca (supervisor)

Dr. Joost Berkhout (co-reader)

Company Supervisors:

Berend Markhorst (supervisor)

Prof. Dr. Rob van der Mei (supervisor)

Abstract

Within the energy transition, hydrogen gas can become a crucial energy carrier. Currently, the infrastructure for the transportation of hydrogen gas remains underdeveloped. However, hydrogen gas can be transported alongside natural gas, a process called hydrogen blending. To enable hydrogen blending within a natural gas pipeline network, the TSO must account for both technical and market requirements, to which hydrogen blending provides an additional challenge. Furthermore, gas prices and demand are subject to uncertainty, which in turn makes the benefits of hydrogen blending uncertain. Literature has previously provided models for blending on natural gas networks, and has created stochastic linear models to account for uncertainty, but the combination remains underexplored. This thesis proposes a stochastic mixed integer linear program that optimizes the system social welfare of a natural gas pipeline network, subject to both technical and market constraints. In the thesis, the model is applied to a stylized case study of the Norwegian Continental shelf, Europe‘s largest connected offshore pipeline network. Furthermore, to incentivize hydrogen production for blending, the impact of a hydrogen subsidy is examined. In addition, to gauge the effects of changes to the system, sensitivity analyses are executed. Finally, the scalability and stochastic value are examined to provide insight into the practical aspects of the stochastic program.

The following key findings from the results are:

- Hydrogen blending is only economically viable once subsidies lower the production cost to the market price of natural gas, while further subsidies yield diminishing returns.
- Taking into account the cost of carbon emissions, subsidizing hydrogen blending provides a positive social welfare effect.
- The degree of possible hydrogen blending is limited to the strictest connected downstream market, such that cross-market collaboration is needed to reach the full potential of hydrogen blending.
- Hydrogen blending is highly sensitive to the closure of upstream production plants, while pipeline closures can actually increase hydrogen blending under high subsidies.
- Average hydrogen production across scenarios converges to a single value when increasing price volatility, regardless of subsidy.
- The value of the stochastic solution is small but significant to the objective.
- The solve time increases exponentially with the amount of scenarios and nodes, while network structure also impacts performance.

Keywords: Network optimization, Hydrogen Blending, Stochastic Optimization.

Contents

Table 1: List of abbreviations.

Abbreviation	Full term
BONUS	Blending Optimization of Networks with Uncertain Scenarios
CEVPI	Conditional Expected Value of Perfect Information
CO_2	Carbon dioxide
CRN	Common random numbers
CVaR	Conditional value at risk
EASEE	European Association for the Streamlining of Energy Exchange
ENTSOG	European Network of Transmission System Operators for Gas
ETS	Emission Trading System
EVPI	Expected value of perfect information
GCV/HHV	Gross calorific value/ Higher heating value
Gwh	Gigawatt hour
H_2	Hydrogen gas
IEA	International Energy Agency
K	Kelvin
LHV	Lower heating value
Mwh	Megawatt hour
(M)scm	Million standard cubic meter
NG	Natural gas
NOK	Norwegian Krone
ROI	Return on investment
RF	Random Forest regressor
SOS1	Special ordered set of type 1
TSO	Transmission System Operator
VSS	Value of stochastic solution

1 Introduction

To mitigate climate change, the need to transition to carbon neutral fuels increases (Zou et al., 2021). Although solar and wind power generation is increasing, stable power sources are needed for flexibility (R. Egging and Tomasgard, 2018). Hydrogen gas is one of these sources and is expected to play a large role in the transition (Evangelopoulou et al., 2019; Bødal et al., 2020; Jia et al., 2023). However, developing infrastructure for hydrogen gas is time-intensive and costly (Jia et al., 2023; Xie et al., 2024; H. Zhang et al., 2025). Alternatively, hydrogen gas could be sent through existing pipelines used for natural gas (Jia et al., 2023; H. Zhang et al., 2025). This would allow for partial decarbonization of the gas sector, without the need for new infrastructure. Consequently, this thesis develops a model to determine the capabilities and benefits of hydrogen blending within a natural gas network.

A natural gas transmission (pipeline) network is managed by a transmission system operator (TSO) (Dralle, 2018), whose objectives can be optimized by modeling the flow, pressure, and quality of the gas in the network (Egging-Bratseth et al., 2025). Hydrogen blending changes the quality of gas and therefore the amount that can be added is limited (Mahajan et al., 2022). Therefore, modeling must incorporate the ratio between gases, which has been modeled as a mixing transport problem with linear optimization (Tomasgard et al., 2007; Klatzer et al., 2024). Consequently, the developed model incorporates gas quality to accurately model hydrogen blending.

Besides quality restrictions, a TSO also operates under uncertainty, often induced by human behavior. For example, the demand for natural gas could grow, due to an unexpected cold spell, increasing the required flow through the network, as people seek to heat their homes (Pustišek and Karasz, 2017, p. 99). Furthermore, this also affects prices, which maintain an inverse relation with the demand (Midthun et al., 2009; R. Egging, Pichler, et al., 2017). These uncertainties have been modeled using linear stochastic optimization (Fodstad, R. Egging, et al., 2016; Hasturk et al., 2025; Markhorst et al., 2026), or are provided as possible extensions to non-linear models (R. G. Egging, 2010; Grimm et al., 2019). To date, the integration of hydrogen blending in flow models, or more generally gas quality models, with a treatment of uncertainty has not been accomplished. This thesis expands on existing models with an added level of complexity by including both gas quality and uncertainty. In turn, this allows to more accurately represent and optimize the responsibilities of a TSO. To assess the applicability of the developed model, this thesis investigates both the value of stochasticity and the scalability of the model.

Several European countries are starting to allow hydrogen blending in their natural gas networks (IEA, 2025, p. 80). However, Norway, the largest gas supplier in Europe (Aastad, 2025), has only examined the possibilities of hydrogen blending, but currently does not allow blending on its network (IEA, 2025, p. 81). This thesis uses potential hydrogen production plants as well as the existing transmission network in Norway to form a case study on hydrogen blending. In addition, sensitivity analysis is performed to determine the impact of changes in the network on hydrogen blending. Due to the size of the Norwegian transmission network, the case study shows the efficiency and applicability of the model in a real application. Therefore, this thesis aids the investigation into hydrogen blending in Norway by applying the model to their context.

Organization Against this background, this thesis aims to make several contributions. To achieve these contributions, a list of research objectives is shown below. With these objectives in mind, the remaining sections are introduced with a quote by a philosopher, and organized as follows.

First, the literature review focuses on the characteristics of transmission systems and gas physics in networks relevant for modeling, followed by a review of works on gas transmission network optimization. Second, the problem is formalized and constructed as a linear program in the methodology. Third, the case study is outlined and the results on hydrogen blending and model tractability are discussed. Fourth, policy insights on hydrogen blending are derived from the model, and the limitations and possible extensions are discussed. Finally, sensitivity analyses are executed on several aspects of the model to gain insight into the robustness of hydrogen blending, as well as experiments to examine the stochastic value and scalability of the model.

- **Hydrogen blending optimization**: Integrate gas pressure and gas composition constraints into a linear program to model the limitations of hydrogen blending in natural gas networks
- **Incorporation of stochasticity**: Use stochastic linear optimization to enable uncertainty in the network, allowing the model to hedge for different possibilities of prices and contracted demand in the network.
- **Case study**: Show how the resulting BONUS model can be applied to a large system of pipelines.
- **Policy insights on hydrogen blending**: Show the possibilities of hydrogen blending by introducing policy measures on hydrogen blending, enabling the model to quantify the benefits and challenges of hydrogen blending.
- **Sensitivity and scalability**: Conduct sensitivity analyses and scalability experiments to evaluate the adaptability of hydrogen blending across different scenarios and model performance under varying problem sizes.

"All teaching and all intellectual learning come about from already existing knowledge."

— Aristotle

2 Literature Review

The literature review focuses on three topics related to the problem. First, a gas transmission system is examined from the perspective of its actors, focusing mainly on the role and responsibilities of a transmission system operator. Second, the properties required for modeling related to gas flow within a network are discussed and extended to include the additional complexities of hydrogen blending. Finally, optimization models surrounding the problem are compared, to gain insight on how a transmission network can be optimized with the inclusion of hydrogen and uncertainty.

2.1 Gas Transmission Systems

Natural gas is a global commodity that accounts for approximately a fifth of worldwide energy consumption (R. G. Egging, 2010). To supply the energy, gas has to be transported, which is achieved through a natural gas transmission network. A natural gas transmission network involves multiple primary stakeholders, all of whom influence the network. Therefore, in modeling a natural gas network, the importance of each actor must be considered.

Gas suppliers and consumers are the primary stakeholders of a transmission network, who benefit from its transport (Amoiralis and Andriosopoulos, 2017). Natural gas is sold in commodity markets, often virtual (notional) (Pustišek and Karasz, 2017; Egging-Bratseth et al., 2025). Natural gas is sold in both long-term and spot contracts (Egging-Bratseth et al., 2025). Long-term contracts allow for both mitigation of price and demand risk for suppliers (R. G. Egging, 2010). Instead, spot contracts are more volatile in amount and price, but allow for lower consumer prices (R. G. Egging, 2010). Therefore, to accurately optimize for suppliers and consumers, these aspects of uncertainty have to be considered.

In addition, a primary stakeholder is the system operator (Amoiralis and Andriosopoulos, 2017). Transmission system operators are necessary to manage a gas network and transmission market, as well as to maintain and invest in the system. Most countries have their own system operator, and approaches differ (Pollitt, 2012; Dralle, 2018). In small countries such as the Netherlands (GTS) and Denmark (Energinet), a production independent TSO manages transport, balancing, and maintenance of the main pipeline system. In these small countries, the pipeline network is owned by the TSO, thereby ensuring neutrality between suppliers. The main drawback of ownership of pipelines is that economies of scope are lost, leading to operational inefficiency (Growitsch and Stronzik, 2014). However, although uncommon in Europe (Growitsch and Stronzik, 2014), there are also countries where the system operator is not separated from the production operators, which can reduce competition, in turn increasing consumer prices (Dralle, 2018, p. 4). Beyond these responsibilities, a TSO can have other goals. Dralle (2018, p. 138) identified that a TSO has as an objective to increase trading volume. Therefore, a modeling objective can also be to maximize flow in a pipeline network.

Although an independent TSO has no profit motive (Aastad, 2025), maintaining the pipeline system incurs costs. To relieve the financial burden, a TSO posts tariffs on the use of its pipelines (Brandão et al., 2014; Markhorst et al., 2026). The two most common European tariff choices are Postage and entry-exit systems. In a postage system, a supplier pays a fixed rate per unit of gas, regardless of the entry and exit point in the system (Brandão et al., 2014). This system benefits from its simplicity and allows suppliers to switch exit points without engaging in new contracts or trading. However, as the tariff is not location based, it is not entirely cost reflective. Instead, the entry-exit system posts a tariff per unit at each entry and exit point in the system. Suppliers are responsible for balancing the volume they put into and take out of the system. The system allows suppliers in the system to flexibly determine their output, resulting in higher market efficiency. Finally, when all entry-exit tariffs become equal per unit, it reduces the tariff system to a postage system. Consequently, if an entry-exit tariff system is modeled, it also accommodates a postage system.

2.2 Natural Gas and Hydrogen Blending

Natural gas and hydrogen gas are physical commodities that adhere to physical laws. In turn, modeling their behavior can become strenuous. Therefore, this section aims to explicate these properties.

2.2.1 Natural Gas

Natural gas has many applications. It provides warmth to homes and buildings, but is also used to generate electricity (R. G. Egging, 2010; Gassco, 2023). To enable these processes, natural gas must be transported through a transmission network, where the physical properties of the gas must be respected. Egging-Bratseth et al. (2025) indicates that a model of a gas transmission market needs to include three components: Gas flow, pressure, and quality. Flow is always considered in network optimization models (Tomasgard et al., 2007; Ulstein et al., 2007; Gillessen et al., 2020; Klatzer et al., 2024), but the influence of pressure and quality is often ignored for simplicity (Fodstad, R. Egging, et al., 2016; Grimm et al., 2019; Markhorst et al., 2026).

Within a pipeline, flow denotes the amount of gas that passes through it. The amount is often denoted as a standard cubic meter (scm), which is the volume at air pressure at a standardized temperature (temperature differs by region (Pustišek and Karasz, 2017, p. 32)). The flow through a pipeline is constrained. Following other formulations of flow problems, the inflow and outflow of gas between nodes needs to be balanced, such that the outflow cannot exceed the inflow of a pipe. Additionally, each pipe has its own capacity for the amount of gas that can flow through it, but is also dependent on the pressure difference between the in and outlet of a pipe, as well as the gas quality (Egging-Bratseth et al., 2025). An example of the simplified restrictions is given in Figure 1. In this network, each pipe has a capacity of 8 units of gas, and the incoming flow into node C is 13. Suppose node E has overwhelming demand, then the network wants to accommodate for that demand. In this simplified view, the capacity is limited by the pipe, but also ensures that node D cannot receive more from node C than the amount that is left after serving node E.

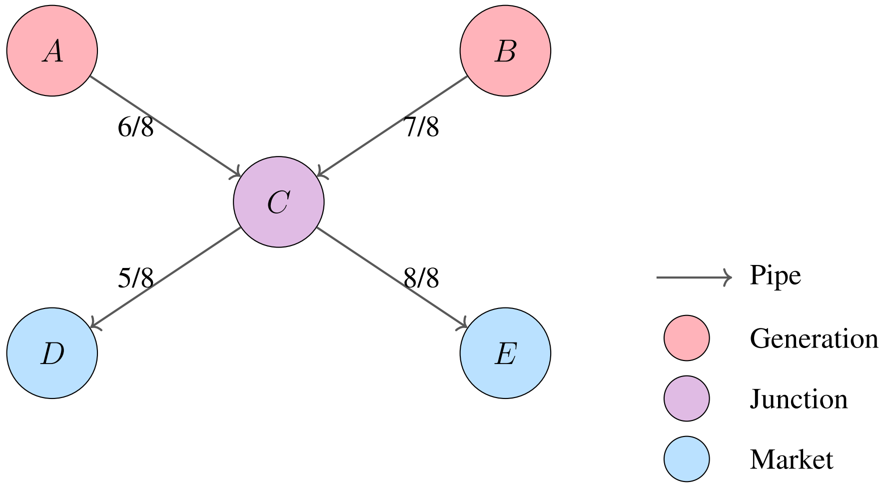

Figure 1: Example of simplified flow constraints within a gas network (similar to examples of Tomasgard et al. (2007) and Rømo et al. (2009)). The flow goes from sources to sinks and is limited by the capacity.

In actual networks, natural gas is put under pressure to create flow. When pipelines are short, the pressure can remain mostly stable and flow through a pipe (Tomasgard et al., 2007). However, when a pipe becomes longer, the flow is given by the difference in pressure between the pipes, known as the Weymouth equation, which is commonly used in optimization models (Wong and Larson, 1968; Midthun et al., 2009; Rømo et al., 2009; Raj et al., 2024; Egging-Bratseth et al., 2025). This relation is given in Equation (1), where f_a denotes the flow through a pipe a and p_{in} and p_{out} represent the pressure in and out of a pipe. Furthermore, K_a denotes the Weymouth constant per pipe, which depends on the length, diameter, ambient temperature of the pipe, as well as the gas composition. A full explanation of the Weymouth constant can be found in Appendix C.4. The relation shows that for a given pipe and gas composition, the flow can be increased by increasing the pressure at the inlet, or dropping it at the outlet. It should be noted that this equation can only be used for single direction pipelines. For bi-directional, pipelines (Babonneau et al., 2009) can be considered, in its squared formulation.

$$f_a = K_a \sqrt{p_{\text{in}}^2 - p_{\text{out}}^2} \tag{1}$$

Besides the pressure difference, to maintain flow, the pressure at the incoming nodes cannot be lower than the pressure at the outgoing nodes (Tomasgard et al., 2007; Klatzer et al., 2024). This is because the pressure difference allows gas to flow to low pressure areas, and it could otherwise not be guaranteed that gas flows in the desired direction. However, to increase pressure within a pipeline, compression units can be used (Nørstebø et al., 2010; Klatzer et al., 2024; Egging-Bratseth et al., 2025). In a compression unit, gas is compressed before being sent further on the line, at the cost of a small percentage (0.2%-5%) of that gas used as fuel (Nørstebø et al., 2010; Egging-Bratseth et al., 2025). In addition to increasing pressure within the network, gas is also stored under pressure, which also incurs similar losses (1%) (Egging-Bratseth et al., 2025). The fuel consumption w_γ is given by Equation (2) per unit of flow f_a, given an inlet pressure p_{in} and the compressed pressure p_{out} (Das et al., 2025; Egging-Bratseth et al., 2025). Here, K_γ denotes a constant which incorporates the compressor efficiency and external conditions, and κ denotes the heat ratio, a quantity dependent on the gas composition. For natural gas, the heat ratio is given as $\kappa = 1.32$ (EngineersToolbox, 2003c). As these losses are significant, they need to be considered when using long pipelines, compressors, or storage.

$$w_\gamma = K_\gamma \frac{\kappa}{\kappa - 1} f_a \left(\left(\frac{p_{\text{out}}}{p_{\text{in}}} \right)^{\kappa - 1/\kappa} - 1 \right) \tag{2}$$

An example of these added restrictions on flow is shown in Figure 2, which updates the previous example. Assume that the losses per unit of compressed gas are 10% and increase the pressure by 10%. Also, assume that all pipes are equal and $K_a = 8$. In the example, we have inserted a storage unit at node C and a compression unit along the route (C, E), which allows us to add more pressure to the pipeline. Furthermore, the pressure at nodes A and B is higher than 1, and the TSO has chosen to let the pressure at C be 1, and at D and E lower than 1. Due to pressure differences, this restricts the flow from node C without compression to $K_a\sqrt{1^2 - 0^2} = 8$. However, a unit of gas ($s = 1$) is stored at node C and the compressor unit is used for the flow in (C, E) resulting in a flow of 9. Since compression costs are incurred, 1 unit of gas is used as fuel and lost in the network. This example shows that adding pressure complicates the problem, especially in larger networks, where system effects can stack up (Midthun et al., 2009).

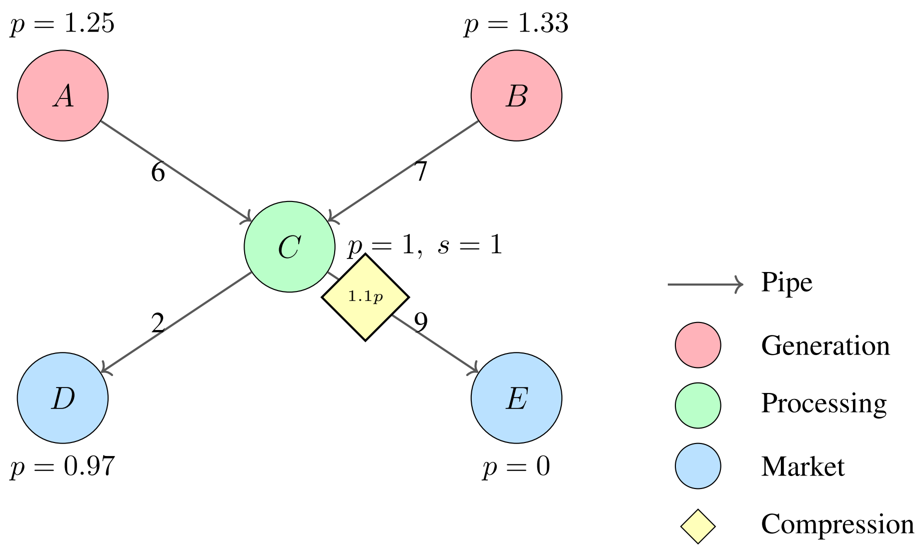

Figure 2: Example of the flow within a network with pressure constraints (similar to examples of Midthun et al. (2009); numbers rounded to two decimals). The pressure at nodes determines the flows through pipes, and the compression node (diamond) increases the pressure by a factor of 1.1.

Finally, the quality of natural gas must be considered. The quality of gas depends on its composition and is restricted by several factors. The European market has requirements on the energy content, density, sulfur content, carbon-dioxide content and dewpoints of the gas (Pustišek and Karasz, 2017, p. 34). However, in modeling, only the energy content, density, and carbon-dioxide content have been considered as bottlenecks (Ulstein et al., 2007; Nørstebø et al., 2010). In line with previous literature, this thesis also considers only these restrictions as quality bottlenecks. Furthermore, the quality constraints on gas apply only to market endpoints, as the quality restrictions are set for consumers (Tomasgard et al., 2007).

The density of the gas is measured as the relative density, also called the specific gravity (Pustišek and Karasz, 2017, p. 32). The formula for this quantity is given in Equation (3), where ρ denotes the relative density, while ρ_{Gas} and ρ_{Air} denote the density of the gas composition, respectively. Furthermore, the density of a gas composition can be calculated as a linear combination of its components (EngineersToolbox, 2003a). The density ensures that the pressure in the pipes can be accurately measured.

$$\rho = \frac{\rho_{\text{Gas}}}{\rho_{\text{Air}}} \tag{3}$$

Second, the energy content can be measured two-fold. First, the Gross Caloric Value (GCV) measures the potential energy of the gas per cubic meter (measured as Kwh/m^3 or MJ/m^3) (Tomasgard et al., 2007; Entsog, 2024). Second, there exists a more complicated unit, named the Wobbe index, used by EASEE (Pustišek and Karasz, 2017; Egging-Bratseth et al., 2025). The Wobbe-index can be used to compare the combustion energy between gases in an appliance such that households can use it for heating or cooking. Equation (4) shows the Wobbe index (W), which depends on the GCV and the relative density. Note that the index changes non-linearly with gas composition, due to the square root in the denominator.

$$W = \frac{\text{GCV}}{\sqrt{\rho}} \tag{4}$$

Finally, the percentage of carbon-dioxide per mol of natural gas is also limited and has been previously modeled (Rømo et al., 2009). Together, these are the necessary restrictions on the European gas market, although there exist regional differences (Pustišek and Karasz, 2017). The range of the three quality restrictions is given in Table 2, as well as the values for natural gas, carbon dioxide and hydrogen gas, which are derived from EngineersToolbox (2003d), EngineersToolbox (2003b), and Quintino et al. (2021).

Table 2: Quality specification according to EASEE.

Parameter	Unit	Min	Max	NG	CO_2	H_2
Wobbe index	kWh/m^3	13.60	15.81	13.71	0.00	13.19
GCV	kWh/m^3	–	–	11.05	0.00	3.35
Relative density	m^3/m^3	0.56	0.70	0.65	1.53	0.07
Carbon-dioxide	mol%	–	2.50	0.00	100.00	0.00

To reach market conditions of natural gas, a TSO has the ability to blend gases (Ulstein et al., 2007; Rømo et al., 2009). Gas can be blended both homogeneously and heterogeneously at a node (Ulstein et al., 2007). Homogeneous blending indicates that every outflowing arc from a node contains the same gas composition, dependent on the compositions and volumes of incoming arcs. In contrast, heterogeneous blending indicates that the TSO can influence the gas composition of each outflowing arc individually, provided that the combined composition of the outflowing arcs matches the total inflow. In both forms, blending can provide an effective tool for managing gas quality, ensuring that market conditions are met.

Quality constraints can make the problem more complex, as gas composition must be tracked to accommodate for the percentage of carbon dioxide and relative density. The example in Figure 1 was again adapted to show the restriction in CO_2, which is shown in Figure 3. In the example, the percentage of CO_2 was limited to 2.5%, and C was assumed to be a homogeneous blending node. When arriving at a node (C), the gas is mixed, providing an average of CO_2, weighted by the flow. In this case, the flow from node B is limited due to its high percentage CO_2. Therefore, the gas composition must also be monitored to ensure that the quality constraints are met.

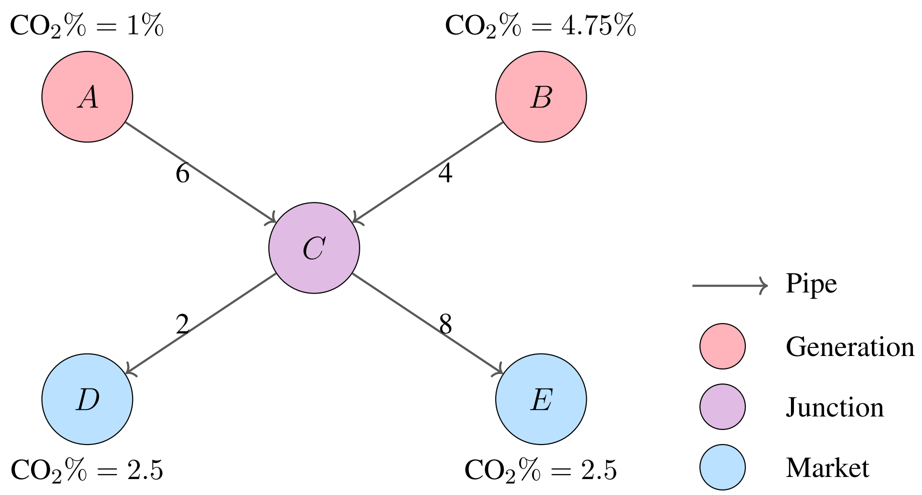

Figure 3: Example of the flow within a network with quality constraints (derived from (Rømo et al., 2009)). The gas is blended at node C, and averages such that more gas can flow to the market nodes.

2.2.2 Hydrogen Blending

Hydrogen can be used in the energy transition as flexible fuel deployment (Zou et al., 2021). To facilitate the development of hydrogen production, hydrogen blending can be used as a transitional solution, without the need for expensive infrastructure (Mahajan et al., 2022; IEA, 2025, pp. 80). Therefore, hydrogen blending is examined in this thesis, to determine the influence on the network.

However, sending natural gas mixed with hydrogen through natural gas pipelines also has limitations. Passing hydrogen gas through steel pipes and storing gas in steel tanks can cause hydrogen embrittlement, which in turn could reduce lifespan (although negative short-term effects could not be determined) (Mahajan et al., 2022; Jia et al., 2023). Therefore, the percentage of hydrogen flowing through a pipe should be limited. Mahajan et al. (2022, p. 25) showed that projects are experimenting with a maximum percentage of 20%-30%, while Quintino et al. (2021, p. 301) note that fractions up to 20% are feasible under the current infrastructure.

In addition to hydrogen embrittlement, the properties of the gas composition also change. In particular, the Weymouth function requires a stable gas composition to determine K_a (Egging-Bratseth et al., 2025). Otherwise, the equation takes on an extra dimension as the specific density plays a role within the formula. As hydrogen has a lower density than natural gas, the flow (m^3) increases artificially, but the energy content does not.

$$f_a = K'_a \sqrt{\frac{p_{\text{in}}^2 - p_{\text{out}}^2}{\rho}} \tag{5}$$

Moreover, the heat ratio κ (used in Equation (2)) increases slightly, to $\kappa = 1.41$ (EngineersToolbox, 2003c). However, if the blend is restricted to 20% hydrogen, then the impact on fuel consumption of compressors is negligible (Das et al., 2025). In turn, the heat ratio can be assumed to be constant when limiting the blend ratio.

The quality of the gas is also impacted. Natural gas is sold as a standard unit and, in turn, has to maintain qualities, of which the Wobbe-index and the relative gas density (specific gravity) can be restrictive for hydrogen (Levinsky et al., 2015; Pustišek and Karasz, 2017). The Wobbe-index decreases by blending natural and hydrogen gas (Zhao et al., 2020; Quintino et al., 2021, pp. 11372, 311). Furthermore, the gas density for hydrogen is lower than that of natural gas and, in turn, decreases linearly in the percentage of hydrogen gas (Quintino et al., 2021, p. 310). However, for both requirements, the impact does not seem to violate the restriction (see Table 2) when limiting the fraction up to 20%.

Finally, there are some external limitations. Currently, international trade limits the inclusion of hydrogen gas at 2% , unless different agreements are initiated (Entsog, 2024). This is due to the fact that the measuring equipment to determine gas quality can deteriorate and is inaccurate when hydrogen and natural gas are mixed (Pustišek and Karasz, 2017; Quintino et al., 2021, pp. 155, 311), due to its lower energy density (Gross caloric value) (Mahajan et al., 2022; Raj et al., 2024). Therefore, with current equipment, an upper limit of 2% may be required at market nodes.

An example that includes some of these constraints is given in Figure 4, adapted from the CO_2 example in Figure 3. The blended hydrogen arrives through node B which can be at most 20%, due to the pipe limit. Again, assume that the split is homogeneous. Furthermore, only one unit can travel through the pipe, as the output at the market nodes is set to 2%. The example shows that if all restrictions are enforced, the amount of blended hydrogen is limited. The difference with the CO_2 example is that entering CO_2 into the system arises from natural gas production, while hydrogen blending is a deliberate action by the hydrogen provider, who aims to enter the highest amount of hydrogen possible into the system.

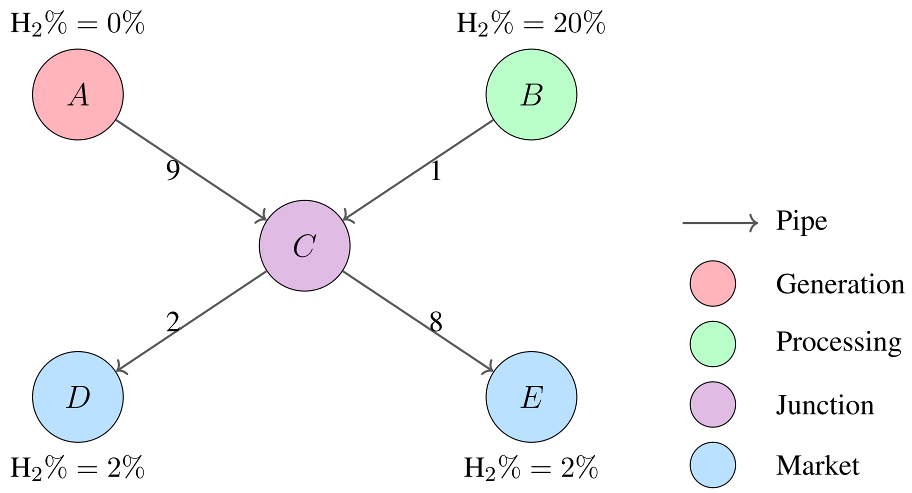

Figure 4: Example of the flow within a network with hydrogen constraints. The flow with hydrogen is highly limited, as the market can only take on 2% hydrogen, and node B provides 20% and thus has to be diluted with natural gas from node A.

Changes in pressure and quality can cause additional strain on the network. Accordingly, it should also be carefully considered which fraction of hydrogen should be allowed through pipes in the network. Therefore, the gas composition must be included to accurately model hydrogen blending.

2.3 TSO Optimization

In line with the goals of the TSO, optimization models have been developed to aid them in decision-making. The models are diverse and represent the different objectives and responsibilities of a TSO. Therefore, to structure the discussion, Table 3 is constructed, which presents the components and methods of the models. The review does not cover all models relating to the TSO, and primarily focuses on European systems. For a more extensive overview, Babonneau et al. (2009), Kotek et al. (2019) and Fodstad, Crespo del Granado, et al. (2022) can be considered.

Table 3 shows that optimization models that optimize for a TSO include flow in their model. This is also reflected by the models' objectives, which mainly include the common TSO goal of flow maximization (Dralle, 2018, p. 138). Some models focus only on the amount of flow to the market (Tomasgard et al., 2007), while others include the price of gas to optimize the value of the flow instead (Callen, 1978; Ulstein et al., 2007; Midthun et al., 2009; Fodstad, R. Egging, et al., 2016; Markhorst et al., 2026). Wong and Larson (1968), Klatzer et al. (2024), Hasturk et al. (2025), and Das et al. (2025) form exceptions to this rule, who instead accept the amount of flow as given and aim to minimize costs given that flow. In addition, Gillessen et al. (2020) does not optimize for market outflows directly, but aims to maximize the pressure at all internal nodes and argues that this allows the most outflow from the system.

The table also shows that pressure and quality are less often included in the models. Models that include pressure employ mainly the Weymouth function (Wong and Larson, 1968) and are often linearized (Midthun et al., 2009; Nørstebø et al., 2010; Fodstad, R. Egging, et al., 2016; Klatzer et al., 2024). However, Grimm et al. (2019) uses a more complicated system of partial differential equations to estimate the flow. In contrast, Das et al. (2025) uses a more complicated formula that assumes a steady flow, but accounts for frictional losses. The inclusion of quality constraints can be found in fewer models, but is united by the linearization of the quality constraints (Ulstein et al., 2007; Nørstebø et al., 2010; Fodstad, R. Egging, et al., 2016). Ulstein et al. (2007) pose the quality constraints as hard constraints, but Tomasgard et al. (2007) argue that to avoid stopping the system entirely, it can be allowed to deliver sub-standard gas, at a penalty, which they also enter as one of their objectives.

Hydrogen blending has more recently become a topic of interest, and literature is still sparse (Klatzer et al., 2024; Hasturk et al., 2025; Das et al., 2025; H. Zhang et al., 2025). Das et al. (2025) returned to the topic of Wong and Larson (1968), to minimize fuel consumption in a pipeline, but allowed for the possibility of hydrogen blending. Instead, both Klatzer et al. (2024) and Hasturk et al. (2025) aimed to minimize the costs of the system that included hydrogen mixing, given the demand, and used linear programming to solve their models. Linear programming refers to a problem in which the objective and constraints are linear functions (Postek et al., 2025, p. 24). However, the scope of their models differs. That is, Klatzer et al. (2024) aimed to make a system that could be used by the TSO to set pressures when including hydrogen, and therefore also models the surrounding gas physics, while Hasturk et al. (2025) wanted to investigate the viability of investments in new pipeline infrastructure and therefore also used stochastic programming to investigate different scenarios. Stochastic programming is a linear program that consists of multiple stages in which decisions can be made (Postek et al., 2025, p. 251). In each stage, multiple scenarios are made into subproblems and the objective takes the expectation over the possible scenarios. This allows the model to optimize for multiple scenarios at once. Finally, while H. Zhang et al. (2025) is not included in the table, they optimized for different investments in energy systems, to find a mixed energy that is cost efficient. In their model, refitting existing infrastructure for hydrogen was included, and they also used stochastic optimization to solve their model.

In addition to hydrogen blending models, other recent TSO models also account for uncertainty (Fodstad, R. Egging, et al., 2016; Gillessen et al., 2020; Markhorst et al., 2026), and use stochastic linear programming to achieve this. However, the work of Fodstad, R. Egging, et al. (2016) marks a deviation from this rule, as they developed multiple models for different scopes and objectives. For their strategic model, they employed stochastic programming to analyze different scenarios. However, for their operational model they included gas physics, but used simulations to determine the optimal solution across scenarios. Furthermore, Gillessen et al. (2020) and Markhorst et al. (2026) also differ from each other, most notably in their objective. Gillessen et al. (2020) use a narrow objective for their analysis, while Markhorst et al. (2026) employs an overarching perspective on the system.

The introduction of different scenarios in stochastic programming can make solving the problem exponentially more difficult. To accelerate the solution process, other methods that take advantage of the structure of the problem can be employed. For example, Hasturk et al. (2025) uses an augmented Lagrangian method, which separates variables in a master problem per subproblem (scenario) and iteratively brings them closer to each other until convergence. H. Zhang et al. (2025) uses benders decomposition instead, which derives cuts from subproblems to solve the main problem (for a detailed explanation of both algorithms, review Wolsey (2020, pp. 201, 235)). Yet, Gillessen et al. (2020) and Markhorst et al. (2026) solve their models without these techniques and still solve in minutes.

Moreover, some models also account for tariff costs in the transmission system, which are levied on the booking market (Grimm et al., 2019; Markhorst et al., 2026). Incorporating these tariffs explicitly captures the influence of suppliers, leading to more accurate decision-making. Both models assume perfect competition, which entails that suppliers cannot influence the market price. While other models do not include the tariff system in their model, several do apply market characteristics (Callen, 1978; Midthun et al., 2009). Instead of assuming perfect market competition and existing demand, they place the TSO as the decision maker of supply, and derive the price as a function of supply, indirectly making the TSO a price setter. In turn, the transmission operator effectively controls the market in these models, which violates the European principle that the TSO must be independent from production. Therefore, for European markets, provided that no other stakeholders act as price setters in the model, perfect competition should be assumed.

Finally, the table shows that the latent aspects in Markhorst et al. (2026) can be addressed by the linear constraints proposed in Tomasgard et al. (2007). This would also make it possible to incorporate hydrogen blending into the model, which is limited by gas quality requirements. The table shows that these aspects have not been combined in linear optimization. Therefore, this thesis extends the model by Markhorst et al. (2026) to address both uncertainty and gas quality in a linear model to optimize the objectives of a TSO.

Table 3: Models used for natural gas TSO optimization ((-) indicates minimization).

Reference	Topic	Objectives	Flow	Pressure	Quality	Hydrogen	Uncertainty	Tariffs	Method	Scope
Wong and Larson (1968)	(-) Pipeline energy	Fuel usage	✓	✓	×	×	×	×	Dynamic Programming	Operational
Callen (1978)	Cost adjusted flow value	Market outflows Flow costs	✓	×	×	×	×	×	Primal-Dual Iteration	Operational
Ulstein et al. (2007)	Flow value	Market outflows Oil production	✓	×	✓	×	×	×	Mixed Integer Linear programming	Tactical
Tomasgard et al. (2007) Rømo et al. (2009) Nørstebø et al. (2010)	Penalty adjusted max flow	Market outflows Flow cost Production difference Quality deviation	✓	✓	✓	×	×	×	Mixed Integer Linear programming	Operational & Strategic
Midthun et al. (2009)	Social welfare	Market outflows Production costs	✓	✓	×	×	×	×	Hand-Solved Examples	Operational
Hellemo et al. (2012) Fodstad, R. Egging, et al. (2016)	Stochastic social welfare	Market outflows Flow costs Production costs Investment costs	✓	✓	✓	×	✓	×	Simulations & Stochastic programming	Operational & Strategic
Grimm et al. (2019)	Multilevel social welfare	Market outflows Flow costs Production costs Tariff income	✓	✓	×	×	×	✓	Multilevel optimization	Operational
Gillessen et al. (2020)	Pressure	Market outflows* Pressure	✓	✓	×	×	✓	×	Stochastic programming	Tactical
Klatzer et al. (2024)	(-) Hydrogen system cost	Production costs CO_2 costs	✓	✓	×	✓	×	×	Mixed Integer Linear programming	Operational
Hasturk et al. (2025)	(-) Hydrogen system cost	Production costs Investment costs Unmet demand costs	✓	×	×	✓	✓	×	Mixed Integer Linear programming	Strategic
Das et al. (2025)	(-) Pipeline energy	Fuel usage	✓	✓	×	✓	×	×	Genetic Algorithm	Operational
Markhorst et al. (2026)	Stochastic social welfare	Market outflows Flow costs Production costs Tariff costs	✓	×	×	×	✓	✓	Stochastic programming	Operational
This work	Stochastic social welfare	Market outflows Flow costs Production costs Tariff costs CO_2 costs	✓	✓	✓	✓	✓	✓	Stochastic programming	Strategic

"The impediment to action advances action. What stands in the way becomes the way."

— Marcus Aurelius

3 Methodology

This section formalizes the aspects of the problem, and introduces the mathematical formulation of the model. First, a description of the problem is given. Second, the relevant sets, parameters and variables are enumerated. Third, an objective function is formulated. Finally, the model is constructed in a stepwise manner, explaining the context of each constraint when introduced. The explanation starts with the flow constraints, followed by the pressure and quality constraints. Subsequently, the entry-exit market constraints are illuminated, as well as an additional constraint surrounding the stochasticity of the model.

3.1 Problem Description

The model is developed to optimize TSO goals, in accordance with the literature examined in Table 3. Recently, TSO goals have shifted towards social welfare (Brandão et al., 2014; Egging-Bratseth et al., 2025), and models have aimed to optimize this welfare (Midthun et al., 2009; Fodstad, R. Egging, et al., 2016; Markhorst et al., 2026). Therefore, the model is also optimized for social welfare, based on the aspects incorporated by Markhorst et al. (2026), with the main component optimizing the value of the amount of gas sold. The pipeline network is modeled as a set of arcs and nodes, with generation and market nodes to model the places of supply and demand, respectively. Gas is modeled as flow through the arcs, and there are restrictions per arc on the flow.

3.1.1 Pressure and Quality

Gas is sold as a single commodity, with restrictions on the qualities of its composition (Tomasgard et al., 2007; Pustišek and Karasz, 2017; Egging-Bratseth et al., 2025, p. 34). Therefore, the price of gas can be assumed singular per market, which is also incorporated by all previous models that optimize for market outflow (Table 3). To model the gas composition, each component obtains its own flow variable. For the model itself, any number of components can be integrated, but the application utilizes three components: Natural gas, carbon-dioxide and hydrogen. The choice of components follows from the restriction of CO_2 in the gas exerted by EASEE (Table 2) and to measure the impact of hydrogen blending. As hydrogen is diffusive in natural gas (Wang, 2026), it is assumed that gas flowing through pipes is homogeneous, except at processing plants where gas can be split heterogeneously into different arcs through processing.

In addition to gas quality, pressure characteristics are also incorporated. Similarly to other models, the Weymouth equation is used and linearized. However, because hydrogen has a lower relative density than that of natural gas, the Weymouth constant changes with the composition. Therefore, a new and slightly more complex linearization approach is applied that enables different relative densities of the gas composition. Pressure can be increased using compressors, which use some of the gas as fuel to function (Wong and Larson, 1968; Das et al., 2025). The fuel consumption from compression has been modeled by linearizing Equation (2) (Tomasgard et al., 2007) and is dependent on the heat ratio of the gas composition. However, for moderate levels of hydrogen gas in the composition, the difference in fuel consumption is negligible (Das et al., 2025), and therefore, the linearization proposed by Hoeven (2004) (Also used in Tomasgard et al. (2007)) can still be applied for each component.

However, not all aspects of pressure are considered for the current model. Unlike Tomasgard et al. (2007), the drop in pressure can be chosen within the model, instead of a hyperparameter fixed per node when solving. For compressors, recycling gas is not considered to model the minimum throughput (Egging-Bratseth et al., 2025), but is instead assumed to be incorporated by fuel consumption. Similar to Tomasgard et al. (2007) it is assumed that the compressor provides a fixed increase in the pressure. This contrasts with Klatzer et al. (2024), who model variable pressure but neglect fuel consumption. In addition, under high pressure, leakage can occur for both natural gas and hydrogen (Xie et al., 2024). However, the amount of gas lost is limited (N. Riddick and L. Mauzerall, 2023), and is therefore neglected for the current model. Finally, in some models, pressure differences are only accounted for when there is flow through a pipe (Tomasgard et al., 2007), however, similar to other recent models (Gillessen et al., 2020; Klatzer et al., 2024) it is assumed that every pipe is in use. Finally, the model is considered static, where time-dependent gas dynamics are not considered.

3.1.2 Markets and Uncertainty

This study aims to model the gas and booking market as a single system. Several assumptions and considerations have to be made with respect to these markets. First, the assumptions for the modeled gas market are discussed, followed by the considerations for the booking market. Finally, from the discussion, the three decision stages for the stochastic model are explicated.

Gas Market A TSO facilitates the network to allow sold gas to be transported to the demand, which is sold on a (notional) market. For this market, several characteristics are assumed. First, akin to Grimm et al. (2019) and Markhorst et al. (2026), perfect competition is assumed, such that the price is exogenous to the decisions of the TSO and the suppliers. Second, suppliers are bound by contractual obligations, where they have to fulfill the taken on demand, but can provide additional gas to market nodes by selling to intra-day spot markets (Pustišek and Karasz, 2017, p. 6). However, from the perspective of the TSO, the contracted demand is uncertain, as this is in the hands of the suppliers. A supplier can own multiple production plants, and can thus meet demand by producing at multiple plants. While gas is sold as a single commodity, the price of gas can differ per market, due to transport costs (Pustišek and Karasz, 2017, p. 163). Therefore, a supplier might prefer delivery to certain market nodes, either because of changes in contracted demand, or market prices.

The gas market is highly connected with other energy markets, such as the Liquefied Natural Gas (LNG) market, and the electricity market, where gas is transferred directly to a different product (Egging-Bratseth et al., 2025). Other models have also considered these markets to better account for the relation between these markets (Fodstad, R. Egging, et al., 2016; H. Zhang et al., 2025; Starreveld, 2026). However, in this thesis, these markets are not considered, and are instead incorporated within the demand for natural gas.

Booking Market In addition to managing the flow of the network, the TSO oversees the booking market of the network. In many European networks, a supplier pays a tariff for entering gas into the network (entry-capacity) and pulling it off (exit-capacity) (Brandão et al., 2014). The capacity is bought via long/medium-term, day-ahead and intra-day booking, where prices that differ between points (GTS, 2023; Gassco, 2024). Based on long-term booking capacity, the TSO makes a provisional planning based on the long-term contracts and adjusts the operational planning after the sale of short-term contracts.

The goals of suppliers and the TSO might not align, as a supplier aims to maximize their own flow value, while the TSO aims to maximize overall social welfare. With fixed entry and exit capacity pricing, conflict is excluded in capacity booking models if suppliers are assumed to book without strategy. Notably, suppliers book the highest capacity they can deliver if the capacity is made available by the TSO. Instead, if the entry or exit capacity is limited by TSO, suppliers would book the amount made available by the TSO. Therefore, assuming the absence of strategic behavior, decisions made on the booking market from the perspective of the TSO maximize social welfare as well as the individual flow of suppliers.

Besides the primary booking market, the TSO allows secondary trading of entry and exit capacities. Competitors can sell and buy booked capacity, enabling higher throughput of the system, without the need to acquire additional capacity. However, a supplier is incentivized to commit to long-term booking contracts, as the capacity of short-term contracts is sometimes limited and secondary trading can result in additional costs. Note that as the secondary market only trades existing entry-exit capacities, the planning does not change from this behavior. Therefore, the secondary market does not have to be included in the model from the perspective of the TSO, as the first market booking contracts determine the maximum flow from an entry node and out of an exit node respectively.

The decision making process is sketched in Figure 5. Suppliers have more knowledge of the demand and prices in later stages, but also pay higher prices for capacity. Therefore, suppliers book capacities beforehand to account for multiple scenarios, but trade and buy additional capacities later to meet contracts and receive higher profits. Suppliers have to account for multiple scenarios, and the long-term decision therefore constitutes a balancing act between overbooking and higher costs in later stages.

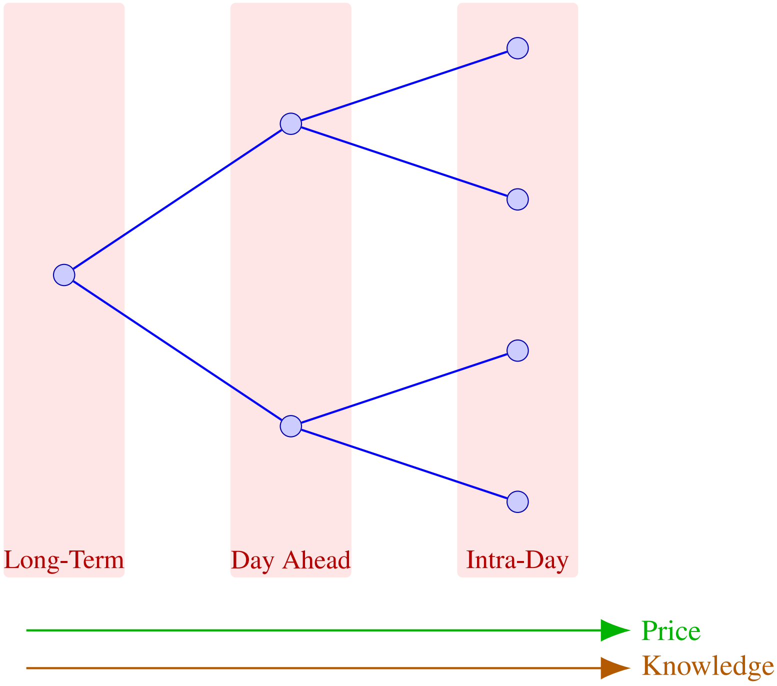

Figure 5: Diagram of scenarios in the model at each stage in the model. The price of booking contracts increase, but so does knowledge of the realized scenario.

Short-term contracts change the operational flows in the system from the provisional long-term planning. Markhorst et al. (2026) argued that the TSO is risk averse and prefers to change the provisional planning as little as possible, ensuring it can meet its obligations to take gas at entry points and deliver it to exit points. Part of the obligations are related to the delivery of a qualitatively sufficient gas at a sufficiently high pressure. In some cases, the TSO can neglect these responsibilities to keep the system operational (Tomasgard et al., 2007), and this flexibility is recommended by the ENTSOG, to accommodate for new gas mixtures, such as hydrogen blending, in the network (Entsog, 2018).

For the current problem, the total difference from the provisional planning is not constrained. Instead, the total violation of the quality commitment across scenarios is constrained. This ensures that the TSO maintains its flexibility, while end users can still expect qualitatively sufficient gas.

3.1.3 Stages

The problem description states that uncertainty presents itself in two forms, spot market price and contracted demand. The contracted demand is uncertain for the TSO when long-term bookings are made, but are fixed, and can be considered known, a day-ahead. However, the spot market price is determined on the day, and is therefore known at a later date. Therefore, suppliers can book long-term capacity in the model, but can additionally change these on a shorter scale. A supplier could prefer to change their entry and exit capacities, due to a change in contracted demand, or a change in the spot market price. However, the short-term contracts are associated with additional risks and cost, that suppliers aim to avoid, which still incentivize them into long-term contracts.

Three stages can be identified to model this process, which are shown in Table 4. The table shows that in the first stage suppliers can book long-term contracts on capacity, while contract demand and spot prices are still unknown. In practice, the TSO exerts control over this process by limiting the entry-exit capacity that can be booked, ensuring a feasible flow. In turn, the booking decisions by the TSO and the suppliers can be modeled simultaneously, as the TSO wants to maximize the total flow, while a supplier wants to maximize their own flow, and both require capacity to be booked. In the second stage, demand becomes known, and long-term entry and exit capacity can be resold on the secondary market, while short-term capacity for the following day can be bought from the TSO, now that demand is known. Finally, the price becomes known on the day, and capacities from the previous two stages can be resold, and intra-day capacity booking becomes available. In addition, in the final stage, the operational flow is calculated.

Table 4: Stages of stochastic program

Stage	**Demand**	**Prices**	**Decision variables**
Stage 1	Unknown	Unknown	Entry–exit capacities
Stage 2	Known	Unknown	Entry–exit capacities
Stage 3	Known	Known	Entry–exit capacities; Operational flow

The operational flow is limited by quality constraints on market nodes. However, the TSO can be flexible in these quality constraints in exceptional cases such that the system does not have to be interrupted. The TSO utilizes this flexibility to release more booking capacity and, in turn, further increase the flow.

3.1.4 Hydrogen Blending

The flexibility also allows for further integration of hydrogen blending in the system. Hydrogen blending impacts the pressure flow relationship and the quality of the gas, and is therefore constrained in its percentage. However, to achieve blending, it is assumed that natural gas flows into a point where it can be directly mixed with the hydrogen and put onto the network via outflowing arcs. Due to the diffusive nature of hydrogen, it is assumed that the mixing is immediate, and does not require more extensive planning than putting natural gas onto the network. In turn, the model does not require additional variables in the second stage to determine production planning. The implementation of the gas characteristics with multi-stage stochastic linear optimization has not yet been achieved, and the following model therefore expands on studies on network blending models, and can be applied to study the feasibility of hydrogen blending in natural gas networks.

3.2 Sets, Parameters and Variables

The model formulation extends previous formulations. Consequently, it contains numerous sets that require an introduction, all of which are shown in Table 5. In the model, N denotes the set of nodes in the network, and A denotes the arcs in the network, in other words, the pipelines. Some nodes have specific purposes in the network, and are therefore given an extra index. That is, $N_{h,g}$ denotes the set of gas production nodes for each supplier, each with their own composition; N_d denotes market nodes, each with their respective quality requirements; N_γ denotes nodes where a compressor is placed, which can increase the pressure at a fuel cost; and N_s denotes arcs where the gas is homogeneously split into fractions, also referred to as junctions. Likewise, for arcs, A_n^+ denotes the set of incoming arcs into node n, while A_n^- denotes the set of outgoing arcs from node n. In addition to the network, multiple commodities are included and C denotes the set of commodities (In the current context the relevant commodities are $C \in \{\text{Natural gas}, \text{CO}_2, \text{H}_2\}$).

Special ordered sets of type 1 are used to model single choice decisions (Wolsey, 2020, p. 125). Z_θ denotes the set of choices for an upper bound on the relative density and is used to obtain the Weymouth constant for different gas compositions. Z_v instead denotes the choices for splitting gas homogeneously between pipes. To model the nonlinear relationship between flow and pressure, the set of cutting planes L is introduced. Finally, K, M_k and $M_k(m)$ denote the set of stages, scenarios per stage, and predecessors of scenario m, respectively.

Table 5: Sets.

Symbol	Description	Index
N	Nodes in the network (production platforms, processing facilities, markets)	n
$N_{h,g}$	Production nodes	n
N_d	Market nodes	n
N_γ	Nodes where a compressor is placed	n
N_s	Nodes where gas is split homogeneously	n
A	Arc which transport gas	a
A_n^+	Incoming arcs to node n	a
A_n^-	Outgoing arcs from node n	a
C	Components of the gas mix {Natural gas, CO_2, H_2}	c
Z_θ	Special order set of type 1 corresponding to density upperbound	z
Z_v	Special order set of type 1 corresponding to homogeneous splitting	z
L	Set of cutting planes	l
H	Set of suppliers	h
K	Set of stages	k
M_k	Set of scenarios in stage k	m
$M_k(m)$	Predecessors of scenario m in stage k	k', m'

Decision variables are introduced to represent and optimize the decisions made by the TSO. Table 6 shows descriptions of all the variables used in the model and their respective range. The flow through arcs is modeled by $f^c_{a,m}$, where each gas component is represented by an individual flow. To obtain flow, the pressure differences between pipelines are modeled by variables at each inlet and outlet of a pipe, denoted by $p_{a,\text{in},m}$ and $p_{a,\text{out},m}$, respectively. Third, to model the constraints on pressure and quality, auxiliary variables are introduced. That is, $\theta_{a,z,m}$ denotes an auxiliary variable to relate the flow to pressure, while $v_{n,z,m}$ provides an auxiliary variable for homogeneous splitting. In addition, $e^c_{n,z,m}$ allows the total inflow to be connected to the fractional outflow per arc. In the model, $w^c_{n,m}$ denotes the fuel consumption of a compressor for each individual component. Finally, $x^+_{n,k,m}$ and $x^-_{n,k,m}$ represent booked entry and exit capacity, respectively. Note that it represents the total bought capacity across suppliers, instead of the capacity per supplier, which simplifies the model and can speed up computation time. Finally, to allow for quality deviations without halting the flow, it could be allowed to relax market constraints in a scenario. This is made possible with the introduction of δ_m.

Table 6: Variables.

Symbol	Description	Range
$f^c_{a,m}$	Flow through arc a of component c under scenario m	$\mathbb{R}^+$
$p_{a,\text{in},m}$	Inflow pressure at arc a under scenario m	$\mathbb{R}^+$
$p_{a,\text{out},m}$	Outflow pressure at arc a under scenario m	$\mathbb{R}^+$
$\theta_{a,z,m}$	Choice z of lower bound of relative density at arc a under scenario m	{0,1}
$v_{n,z,m}$	Choice z of fractional flow in node n under scenario m	{0,1}
$e^c_{n,z,m}$	Flow through node n of component c used for splitting under scenario m	$\mathbb{R}^+$
$w^c_{n,m}$	Fuel consumption at compression node n of component c under scenario m	$\mathbb{R}^+$
$x^+_{n,k,m}$	Booked entry capacity at node n in stage k under scenario m	$\mathbb{R}^+$
$x^-_{n,k,m}$	Booked exit capacity at node n in stage k under scenario m	$\mathbb{R}^+$
δ_m	Indicator of allowed market quality deviation in scenario m	$\{0, 1\}$

Third, the model is subject to parameters that provide the context in which the model operates. Table 7 shows a complete list of the used parameters. The objective (O) contains the prices and costs for each part of the objective ($o^d_{n,m}$, $o^g_{n,m}$, o^p_a, $o^x_{n,k,m}$), which is subject to a weighted sum given by the scenario probability $\pi_{k,m}$ and, in part, the gross caloric value of each component r^c. The parameters $G_{n,m}$ and $D_{n,m}$ reflect the maximum production and minimum demand per node, where α^c_n represents the fraction of each component at generation. $\bar{F}_a$ and $\bar{F}_n$ indicate the upper limit on the flow through, respectively, an arc and a node, and function as big-M parameters. The parameters ρ_z and ρ^c help provide an upper limit on the relative density of the gas composition. $K_{a,z}$ and $E_{a,z}$ represent parameters that are used when the corresponding binary variables are active. The constants $K^c_{p_{a'},\text{in}}$, $K^c_{p_a,\text{out}}$ and $K_{f^c_a}$ are used to linearize the fuel consumption of a compressor. Furthermore, several parameters are introduced to ensure pressure constraints ($P_{\text{in},l}$, $P_{\text{out},l}$, $\bar{P}_{a,\text{in}}$, $\underline{P}_{n,\text{out}}$, $\hat{P}_n$). In addition, parameters are introduced that ensure that quality constraints are met at market nodes (q^{c+}_n, q^{c-}_n), while q^{c+}_a and q^{c-}_a allow percentage constraints on the arcs to ensure the longevity of the pipeline. Finally, Δ denotes the percentage of scenarios that are allowed to deviate from market quality restrictions.

Table 7: Parameters.

Symbol	Description
O	Objective to be maximized
$\pi_{k,m}$	Unconditional probability of scenario m in stage k
$o^d_{n,m}$	Market price of gas at node n under scenario m
$o^g_{n,m}$	Generation cost of gas at node n under scenario m
o^p_a	Pressure cost of gas at arc a
$o^x_{n,k,m}$	Booking cost of entry-exit capacity at node n in stage k under scenario m
r_c	Gross caloric value of component c
$G_{n,m}$	Maximum produced gas composition at production node n under scenario m
α^c_n	component c byproduct fraction (percentage) of total generation at node n
$D_{n,h,m}$	Minimum demand at market node n for supplier h under scenario m
$\bar{F}_a$	Upper limit on the flow through arc a
$\bar{F}_n$	Upper limit on flow through node n
ρ_z	Upperbound on the relative density in choice z
ρ_c	Relative density of component c
$K_{a,z}$	Weymouth constants for arc a at choice of pressure z
$E_{a,z}$	Fraction of flow corresponding to choice z at arc a
$K^c_{p_a,\text{in}}$	Fuel consumption constant for the discharge pressure into arc a'
$K^c_{p_a,\text{out}}$	Fuel consumption constant for the intake pressure out of arc a
$K_{f^c_a}$	Fuel consumption constant for the flow out of arc a
$P_{\text{in},l}$	Taylor expansion constant l of inlet pressure
$P_{\text{out},l}$	Taylor expansion constant l of outlet pressure
$\bar{P}_{a,\text{in}}$	Maximum allowable inlet pressure on arc a
$\underline{P}_{n,\text{out}}$	Minimum allowable outlet pressure on node n
$\hat{P}_n$	Compression factor at node n
q^{c+}_n, q^{c+}_a	Maximum percentage of component c at node n / through arc a
q^{c-}_n, q^{c-}_a	Minimum percentage of component c at node n / through arc a
Δ	Maximum percentage of scenarios with allowed deviation

The following sections use the explained symbols throughout, while some are re-explained for emphasis. However, for other symbols Tables 5, 6 and 7 can be re-examined.

3.3 Objective Function

The objective function of the model is given in Equation (6) and is aimed at representing the goals and responsibilities of the TSO. The objective is derived mainly from Markhorst et al. (2026), with some changes to represent the costs related to pressure and gas quality. The objective remains to maximize the flow value and includes the operational cost of gas generation. The value of the flow in markets is measured in €/Mwh, while the flow variable is measured in Mscm. To compute the value of the gas, a transformation is required. Here, r_c is the gross caloric value (Mwh/Mscm) of component c, which allows the computation of the flow value in the objective.

Flow costs have been replaced with a pressure penalty, which are the underlying producer of flow costs, which is also taken into account by the objectives of Tomasgard et al. (2007) and Fodstad, R. Egging, et al. (2016). This functions as a substitute for actual costs generated by pressure, as it avoids unnecessary high pressures. Finally, the cost of entry and exit capacity is included in the final term. Suppliers do not benefit from overbooking, and the model should account for this. Furthermore, R. G. Egging (2010, p. 72) argues that under the assumption that maintenance costs are minimized by the TSO themselves per pipeline, entry-exit capacity costs represent these costs, as an independent TSO does not have a profit motive. This is further substantiated by the construction of the entry-exit unit cost of a TSO, which consists of maintenance and investments cost, divided by the amount of usage (NOD, 2024; GTS, 2026a). The tariff costs are therefore a welfare transfer of these actual costs. Therefore, the system models the social welfare created by the model, as a function of the total transported gas, reduced with the costs of transporting the gas.

$$
\begin{aligned}
\max \quad O = \quad & \sum_{m \in M_3} \pi_{3,m} \Bigg(\underbrace{\sum_{n \in N_d} \sum_{a \in A_n^+} \sum_{c \in C} o^d_{n,m} r_c f^c_{a,m}}_{\text{Value of gas delivered to market nodes}} \\
& - \underbrace{\sum_{n \in N_{h,g}, h \in H} o^g_{n,m} \sum_{c \in C} \Big(\sum_{a \in A_n^-} f^c_{a,m} - \sum_{a \in A_n^+} f^c_{a,m} \Big)}_{\text{Operational cost of gas generation}} \\
& - \underbrace{\sum_{n \in N} \sum_{a \in A_n^-} o^p_a p_{a,\text{in},m}}_{\text{Pressure operational cost}} \Bigg) \\
& - \underbrace{\sum_{k \in K} \sum_{m \in M_k} \pi_{k,m} \sum_{n \in N} o^x_{n,k,m} (x^+_{n,k,m} + x^-_{n,k,m})}_{\text{Entry-Exit Capacity cost}}
\end{aligned} \tag{6}
$$

3.4 Gas Constraints

As previously discussed, expressing gas dynamics with parametric variables yields inherently non-linear governing equations, a behavior that becomes more pronounced with hydrogen blending (see Section 2.2). In the model, only static gas flows are considered on a daily basis, instead of the time-dependent flow dynamics. To integrate the equations into a linear stochastic program, these equations must be linearized. This section explicates the linear constraints corresponding to the bilinear and conic gas behavior equations on pressure and quality, accounting for the added difficulties of hydrogen blending.

3.4.1 Flow Constraints

The model aims to optimize the network based on the flow from production to demand at market nodes. To ensure that the flow is correctly modeled, several constraints are formulated. First, production per production plant is limited and demand must be satisfied, both by the amount of supply entered by the supplier and the actual amount delivered to the market node. This results in the constraints shown in Equations (7), (8) and (9). In Equations (7) and (8) the gas generation in a node is given by the difference between the inflow and outflow. Taking the difference between inflow and outflow allows for network structures where inflow occurs at generation points. For the current application this is especially useful, as the generated hydrogen can be immediately blended from its production node, without the need to include intensive new infrastructure for hydrogen production.

$$\sum_{c \in C} \left(\sum_{a \in A_n^-} f_{a,m}^c - \sum_{a \in A_n^+} f_{a,m}^c \right) \leq G_{n,m} \forall\, n \in N_{h,g},\ h \in H,\ m \in M_3 \tag{7}$$

$$\sum_{c \in C} r_c \sum_{n \in N_{h,g}} \left(\sum_{a \in A_n^-} f_{a,m}^c - \sum_{a \in A_n^+} f_{a,m}^c \right) \geq \sum_{n \in N_d} D_{h,n,m} \quad \forall h \in H,\ m \in M_3 \tag{8}$$

$$\sum_{a \in A_n^+} \sum_{c \in C} r_c f_{a,m}^c \geq \sum_{h \in H} D_{h,n,m} \quad \forall\, n \in N_d,\ m \in M_3 \tag{9}$$

Note that there exists an additional constraint on the structure of the network of generation nodes. A hydrogen production plant must have access to an inflow of natural gas to blend their hydrogen with the natural gas. However, this can be assumed if the hydrogen production plants included in the model are chosen accordingly.

A further constraint is that a gas plant produces a fixed gas composition, with each component as a fraction of total output. This is modeled by Equation (10), where the fraction of each component is defined by a constant and the sum of all components, keeping the generation stable regardless of the amount produced. In the equation, both the left and right sides employ the difference between inflow and outflow as the generation. The difference in flow is required to enable blending. At blending nodes, the composition ratio of generated gas is $\alpha_n^{\mathrm{H}_2} = 1$, while the other components are zero, yielding flow balance for the other components, while allowing hydrogen gas to be added into the composition.

$$\sum_{a \in A_n^-} f_{a,m}^c - \sum_{a \in A_n^+} f_{a,m}^c = \alpha_n^c \sum_{c \in C} \left(\sum_{a \in A_n^-} f_{a,m}^c - \sum_{a \in A_n^+} f_{a,m}^c \right) \quad \forall c \in C\ n \in N_{h,g},\ h \in H,\ m \in M_3 \tag{10}$$

In addition, the total inflow into a node has to match the outflow from a node. This needs to hold for each component individually, to ensure no flow is lost. The flow balance constraint is given in Equation (11). Note that this constraint already incorporates heterogeneous splitting, as the model gets to decide how much flow is pushed to each outgoing node. The constraint does not hold for generation ($N_{h,g}$) and market nodes (N_d) as these function as sources and sinks in the network. Furthermore, it is not true for compression nodes (N_γ), where fuel costs reduce flow.

$$\sum_{a \in A_n^+} f_{a,m}^c = \sum_{a \in A_n^-} f_{a,m}^c \quad \forall\, n \in N \setminus \{N_{h,g}, N_d, N_\gamma\},\ c \in C,\ m \in M_3 \tag{11}$$

Finally, the total flow per arc is limited to a maximum, to avoid deterioration of pipes. This constraint is shown in Equation (12).

$$\sum_{c \in C} f_{a,m}^c \leq \bar{F}_a \quad \forall \quad a \in A, m \in M_3 \tag{12}$$

3.4.2 Weymouth Flow Constraints

On long pipes, the difference in pressure determines the amount of flow. Previously, the Weymouth equation was used with the relative density of the gas composition considered fixed, even when considering different gas compositions (Tomasgard et al., 2007; Klatzer et al., 2024). However, the relative density changes with the gas composition and should be taken into consideration, especially when blending hydrogen. Therefore, Equation (5) needs to be linearized. As the equation is bilinear in relative density and conic in in- and outlet pressures, the constraint is enforced in two steps. First, a special ordered set of type 1 (SOS1) is introduced. A special ordered set of type 1 is a set of integer variables where exactly 1 variable can become nonzero (Wolsey, 2020, p. 125). Equation (13) ensures this constraint.

$$\sum_{z \in Z_\theta} \theta_{a,z,m} = 1 \quad \forall\, a \in A,\ m \in M_3 \tag{13}$$

Second, the relative density of a gas composition can be calculated as a linear combination of the relative density of the individual components (EngineersToolbox, 2003a). The objective aims to maximize the value of the flow, while limiting the cost of pressure. Furthermore, a lower relative density increases the flow in the Weymouth equation, and therefore the model prefers a lower density to allow for more flow. This fact yields an upper bound on relative density, shown in Equation (14) allowing separation of the Weymouth equation for different gas compositions. Given the upper bound on the relative density, the corresponding Weymouth constant can be calculated. Namely, parameters $K_{a,z}$ are introduced, which are constants given by equation (15).

$$\rho_z \sum_{c \in C} f^c_{a,m} + \bar{F}_a\big(1 - \theta_{a,z,m}\big) \geq \sum_{c \in C} \rho^c f^c_{a,m} \quad \forall\, a \in A,\ z \in Z_\theta,\ m \in M_3 \tag{14}$$

$$K_{a,z} = \frac{K_a}{\sqrt{\rho_z}} \tag{15}$$

With the extra parameters, the Weymouth equation can be linearized using Taylor expansion, which is commonly applied (Midthun et al., 2009; Nørstebø et al., 2010; Fodstad, R. Egging, et al., 2016; Klatzer et al., 2024). The Taylor expansion functions as an upperbound on the original function. Namely, let $g(p_{in}, p_{out}) = \sqrt{p_{in}^2 - p_{out}^2}$ be the conic part of Equation (1). This is concave over its physically relevant domain ($p_{in} - p_{out} \geq 0$), as the square root function is concave and on the relevant domain the inner part is concave. This provides the ability to construct the following cutting planes shown in Equation (16), around the fixed points P_{in} and P_{out}. Since the function is concave on the relevant domain, the Taylor approximation gives an upperbound on the Weymouth flow, which, due to Euler's theorem of homogeneous functions (Weisstein, 2026b) is equal to the flow when $P_{in} = p_{in}$ and $P_{out} = p_{out}$, as $g(tp_{in}, tp_{out}) = tg(p_{in}, p_{out})\ \forall\ t \geq 0$. Carefully constructing multiple tangent planes in this form therefore provide a strong linear upperbound constraint on the Weymouth flow.

$$
\begin{aligned}
g(p_{in}, p_{out}) &= \sqrt{p_{in}^2 - p_{out}^2} \\
&\leq g(P_{in}, P_{out}) + \left(\frac{\mathrm{d}g(P_{in}, P_{out})}{\mathrm{d}P_{in}} (p_{in} - P_{in}) + \frac{\mathrm{d}g(P_{in}, P_{out})}{\mathrm{d}P_{out}} (p_{out} - P_{out}) \right) \\
&= \sqrt{P_{in}^2 - P_{out}^2} + \frac{P_{in}}{\sqrt{P_{in}^2 - P_{out}^2}} (p_{in} - P_{in}) - \frac{P_{out}}{\sqrt{P_{in}^2 - P_{out}^2}} (p_{out} - P_{out}) \\
&= \frac{P_{in}}{\sqrt{P_{in}^2 - P_{out}^2}} p_{in} - \frac{P_{out}}{\sqrt{P_{in}^2 - P_{out}^2}} p_{out} \\
&\quad + \sqrt{P_{in}^2 - P_{out}^2} - \frac{P_{in}^2 - P_{out}^2}{\sqrt{P_{in}^2 - P_{out}^2}} \\
&= \frac{P_{in}}{\sqrt{P_{in}^2 - P_{out}^2}} p_{in} - \frac{P_{out}}{\sqrt{P_{in}^2 - P_{out}^2}} p_{out}
\end{aligned} \tag{16}
$$

Equation (17) shows the constructed constraint. In the equation, the flow cannot exceed the value given by any tangent cutting plane $l \in L$. In the constraint, the set of cutting planes together approximate the original function when the constraint is tight. Note that the big-M value ensures that only the constraint relating to the chosen constant $K_{a,z}$ is active, while the other constraints are relaxed. The bound of $\bar{F}_a$ is always valid, as flow is already limited to this value, such that it does not unnecessarily restrict the value further. It should be noted that this constraint only accounts for single directional pipelines. Instead, to account for bidirectional pipelines, Appendix A.1 can be consulted. It should be noted that it is not necessary to enforce the relevant domain ($p_{in} - p_{out} \geq 0$), as the range of the flow is non-negative, and exiting the relevant domain would force the flow to be negative. Therefore this constraint can be omitted.

$$
\sum_{c \in C} f_{a,m}^c \leq \; K_{a,z} \left(\frac{P_{in,l}}{\sqrt{P_{in,l}^2 - P_{out,l}^2}} p_{a,\text{in},m} - \frac{P_{out,l}}{\sqrt{P_{in,l}^2 - P_{out,l}^2}} p_{a,\text{out},m} \right) + \bar{F}_a \big(1 - \theta_{a,z,m} \big) \qquad \forall \; a \in A, \; z \in Z_\theta, \; l \in L, \; m \in M_3 \tag{17}
$$

An example of this constraint is given in Figure 6. The Figure shows the Weymouth side of Equation (17), with a fixed outlet pressure of $p_{a,\text{out}} = 30$, and 3 cutting planes on the active constraint. The activated Weymouth equation is depicted in the blue line, indicating that the respective Weymouth constant is applied. The function is then linearized by applying the cutting planes shown in green, which limit the flow. Finally, the orange constraints depict the constraints that are relaxed by increasing them by $\bar{F}_a$. Therefore, the flow is effectively restricted only by one set of cutting planes, and only one of the cutting plane constraints is tight for each arc. Finally, note that when the inlet pressure $p_{a,\text{in}}$ is close to the fixed outlet pressure, the function becomes more curved, yielding a looser upper bound. Therefore, the cutting plane points must be more dense when the inlet and outlet pressure are close. An illustration of this procedure, along with the associated formula, is provided in Equation (63) and Figure 42 in Appendix C.1. Furthermore, an examination of the efficiency and impact on model solutions is given in Appendix C.2, which also defines the choice made on the number of upper bounds for the case study.

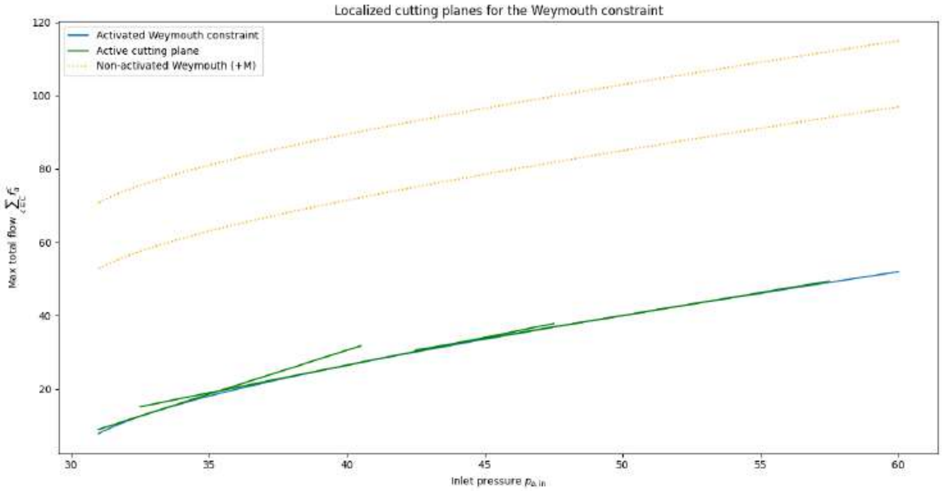

Figure 6: Example of the Weymouth constraint for different inlet pressures (Bar) and corresponding max-flow (Mscm). The dashed line show the constraint that are relaxed, while the green line shows the activated approximated cutting planes.

3.4.3 Other Pressure Constraints

In addition to modeling the Weymouth Equation, pressure within a pipeline is also limited. The flow in a pipeline is one directional, so, at non-compressor nodes, the pressure delivered into outgoing arcs cannot exceed the pressure received from incoming arcs. This is ensured by Equation (18). This does not hold for compression nodes, which can instead increase the pressure. The inequality stems from the option to drop the pressure at nodes, to get the pressure difference into an arc that achieves the related flow. The pressure within a pipe is also restricted to a maximum value and a minimum pressure at the market nodes (Tomasgard et al., 2007; Klatzer et al., 2024). These constraints are modeled by Equations (19) and (20).

$$p_{a,\text{in},m} \leq p_{a',\text{out},m} \quad \forall \quad a \in A_n^-,\ a' \in A_n^+,\ n \in N \setminus N_\gamma,\ m \in M_3 \tag{18}$$

$$p_{a,\text{in},m} \leq \bar{P}_{a,\text{in}} \quad \forall a \in A,\ m \in M_3, \tag{19}$$

$$p_{a,\text{out},m} \geq \underline{P}_{n,\text{out}} \quad \forall \quad a \in A_n^+,\ n \in N_d,\ m \in M_3, \tag{20}$$

Lastly, fuel consumption of compressors must be taken into account. A linearization of Equation 2 can be used to model the fuel consumption of a compressor (Hoeven, 2004; Nørstebø et al., 2010; Egging-Bratseth et al., 2025), which is shown in Equation (21). To model fuel consumption, it is assumed that the compression node has one outflowing arc, i.e $\mid A_n^- \mid = 1 \ \forall \ n \in N_\gamma$. This assumption allows for the linearization proposed by Hoeven (2004), using constants, $K_{p_{a'},\text{in}}$, $K_{p_{a'},\text{out}}$ and $K_{f_a^c}$,which depend on the standard operations of the compressor. After the power consumption is calculated, the flow is balanced by reducing the flow by the power consumption. This is achieved in Equation (22). Finally, since the pressure increase is assumed to be fixed, Equation (23) ensures that the pressure increase is applied. Note that a compressor also has a maximum pressure input, but this is already achieved by the constraint shown in Equation (19).

$$w_{n,m}^c = K_{p_{a'},\text{in}}^c \, p_{a',\text{in},m} - K_{p_a,\text{out}}^c \, p_{a,\text{out},m} + K_{f_a^c} \, f_{a',m}^c$$
$$\forall\, a \in A_n^+,\; a' \in A_n^-,\; n \in N_\gamma,\; c \in C,\; m \in M_3 \tag{21}$$

$$\sum_{a \in A_n^+} f_{a,m}^c - w_{n,m}^c = \sum_{a \in A_n^-} f_{a,m}^c \quad \forall\, n \in N_\gamma,\; c \in C,\; m \in M_3, \tag{22}$$

$$p_{a,\text{in},m} = \hat{P}_n p_{a',\text{out},m} \;\forall\, a \in A_n^+,\; a' \in A_n^-,\; n \in N_\gamma,\; m \in M_3 \tag{23}$$

3.4.4 Quality Constraints

The gas quality is determined by the gas composition. In addition, the composition is restricted in the amount of hydrogen, to avoid hydrogen embrittlement (Mahajan et al., 2022), as well as market viability (Quintino et al., 2021). Therefore, to model gas quality, the gas composition within a pipeline has to be modeled, by modeling each component as its own flow. The decomposition into individual flows enables the formulation of quality constraints on the composition. That is, the restriction of maximum and minimum percentages at market nodes can be formulated per component, which are shown in Equations (24) and (25), respectively. The constraint can be relaxed by δ_m, which allows the TSO to maintain flow of the system in the scenario, even when market quality is not met.

$$\sum_{a \in A_n^+} f_{a,m}^c - \delta_m \bar{F}_n \leq \; q_n^{c+} \sum_{a \in A_n^+} \sum_{c \in C} f_{a,m}^c \quad \forall\, n \in N_d,\; c \in C,\; m \in M_3 \tag{24}$$

$$\sum_{a \in A_n^+} f_{a,m}^c + \delta_m \bar{F}_n \geq \; q_n^{c-} \sum_{a \in A_n^+} \sum_{c \in C} f_{a,m}^c \quad \forall\, n \in N_d,\; c \in C,\; m \in M_3 \tag{25}$$

Similarly, to ensure pipeline longevity, percentage restrictions can be put per arc. These constraints are shown in Equations (26) and (27). For hydrogen blending, the percentage of hydrogen per pipe is limited, to avoid, among other issues, hydrogen embrittlement. Therefore, this constraint ensures that hydrogen gas requires natural gas to flow alongside it.

$$f_{a,m}^c \leq \; q_a^{c+} \sum_{c' \in C} f_{a,m}^{c'} \quad \forall\, a \in A,\; c \in C,\; m \in M_3 \tag{26}$$

$$f_{a,m}^c \geq \; q_a^{c-} \sum_{c' \in C} f_{a,m}^{c'} \quad \forall\, a \in A,\; c \in C,\; m \in M_3 \tag{27}$$

Finally, heterogeneous splitting was already modeled by the balance constraint in Equation (11). However, for homogeneous splitting, this constraint is not sufficient. Instead, the model must keep the ratio between every component to each outgoing arc equal. Since the ratios divide decision variables, the constraint is bilinear.

To linearize this, Tomasgard et al. (2007) used integer variables to denote the fraction of the total flow to go to each outgoing arc. The reformulation was only integrated for a homogeneous split into two arcs. However, the current model extends the formulation for any number of arcs to split on. They reformulated Equation (28) by introducing an SOS1 choice. For the current problem, variables $v_{n,z}$ denote these variables, and Equation (28) ensures that only one choice can be made.

$$\sum_{z \in Z_v} v_{n,z,m} = 1 \quad \forall\, n \in N_s,\; m \in M_3 \tag{28}$$

Second, using the upper limit on a node $\bar{F}_n$ and variables $e^c_{n,z}$ denoting the flow of component c through node n in the case where scenario z is chosen, they ensure that only one of these flows is non-zero by enforcing the constraint shown in Equation (29). In turn, when the binary choice is made, this equation ensures that the flow through is multiplied with the chosen fractions into each arc.

$$\sum_{c \in C} e^c_{n,z,m} \leq \bar{F}_n \, v_{n,z,m} \quad \forall \, z \in Z_v, \; n \in N_s, \; m \in M_3 \tag{29}$$

Third, fractions $E_{a,z}$ are introduced, which denote the fraction of the total flow that is sent to node a in choice z. Since the split is between outflowing edges, the parameters are given as $\sum_{a \in A_n^-} E_{a,z} = 1$. These fractions can then be used to denote per component how much flow should go to either arc. Equation (30) denotes this relation and determines, based on the choice $v_{n,z}$, how much flow should go to each arc. The binary choice, together with Equation 29, ensures that for each junction node, only one flow $e^c_{n,z,m}$ matches the actual flow through the node. Then, given this chosen option z, it is multiplied by the corresponding fractions $E_{a,z}$ which denote the fraction for each component. Since the fraction is equal for all components, the ratio between the components is kept equal in both arcs. In turn, it models homogeneous splitting, as the total flow can still be divided between outflowing arcs, while the fraction is maintained equivalent between arcs. It should be noted that the flow for each component $e^c_{n,z,m}$ matches the actual flow through the node, instead of following the upperbound shown in Equation 29, as the sum of the flows over the outgoing arcs is limited by the balance Equation (11), while Equation (30) uses a strict equality. Together, the fractions $E_{a,z}$ effectively give choices of fractions to divide the flow over arcs. Therefore, Equations (28) to (30) effectively model a homogeneous split, with added limitations on the fraction of split flow.

$$f^c_{a,m} = \sum_{z \in Z_v} E_{a,z} \, e^c_{n,z,m} \quad \forall \, a \in A_n^-, \; n \in N_s, \; c \in C, \; m \in M_3 \tag{30}$$

To illustrate this constraint, the example on quality constraints can be re-examined to describe the linear reformulation, which is shown in its decomposed structure in Figure 7. Here, a system with only natural gas (NG) and CO_2 is examined. The demand nodes D and E receive only 2% CO_2 in their gas mixture, exactly at the limit, which is enforced by Equation (24). The flow coming in is balanced due to Equation (11), which indicates that $e^{\mathrm{NG}}_{n,z} = 9.75$, while $e^{\mathrm{CO_2}}_{n,z} = 0.25$. In addition, the chosen split between nodes D and E is given by $E_{(C,D),z} = 0.2$ and $E_{(C,E),z} = 0.8$. This results in the outgoing flows due to Equation (30), for example $f^{\mathrm{NG}}_{(C,D)} = E_{(C,D),z} e^{\mathrm{NG}}_{n,z} = 1.95$, which is equivalent to the flow of natural gas to node D.

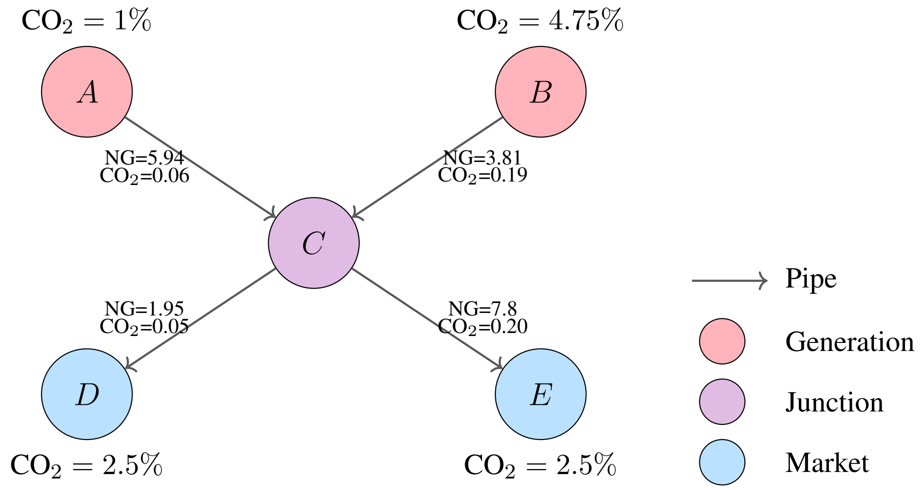

Figure 7: Homogeneous splitting under quality constraints, with different commodities.

While these equations provide a linearization of the bilinear constraint of homogeneous splitting, it generates two limitations, that form a tradeoff against each other. First, increasing the amount of possible fractions that can be chosen increases the number of binary variables in the model, which in turn can drastically increase solve times. However, limiting the amount of possible fractions can instead lower the objective. The model deals with both demands and prices, where demand must be satisfied while high-priced markets drive the objective. Therefore, to achieve optimality, the flow has to be carefully split across the network, to both fulfill demand and maximize the gas flows to high-priced markets. When many, finely grained, splits are available, gas can be distributed through the network such that it the objective obtains minimal loss. However, limiting the amount of possible splits can lower the objective, as additional gas is routed to markets where demand is satisfied, but prices are relatively low. Therefore, this tradeoff needs to be carefully considered upon implementation. Appendix C.3 goes into further depth on this topic, and quantifies the trade-off.

3.5 Entry-Exit Market

To model the gas market, the booking market cannot be omitted. The TSO provides booking capacity at entry and exit capacities in the market, via booking rounds in the first stage. In a later stage, suppliers can book additional capacity, or trade capacity with each other to accommodate for demand, or deliver gas to high-priced markets. As the model is viewed from the perspective of the TSO, the secondary market can be disregarded, as the variables represent the bought capacity in aggregation. This gives rise to two constraints. Equation (31) ensures that if more gas flows out of the node then comes in (generation nodes), entry-capacity must be booked for that node. Similarly, if more gas flows to a node than comes out of it, exit-capacity needs to be booked at that node (market nodes), which is shown in Equation (32). In consequence, capacity is only booked when flow is imbalanced, with the exception of compression nodes.

$$x^+_{n,3,m} + \sum_{k,m' \in M_3(m)} x^+_{n,k,m'} \geq \sum_{c \in C} \left(\sum_{a \in A^-_n} f^c_{a,m} - \sum_{a \in A^+_n} f^c_{a,m} \right) \quad \forall \quad n \in N \backslash N_\gamma, m \in M_3 \quad (31)$$

$$x^-_{n,3,m} + \sum_{k,m' \in M_3(m)} x^-_{n,k,m'} \geq \sum_{c \in C} \left(\sum_{a \in A^+_n} f^c_{a,m} - \sum_{a \in A^-_n} f^c_{a,m} \right) \quad \forall \quad n \in N \backslash N_\gamma, m \in M_3 \quad (32)$$

Finally, suppliers are required to book at least as much entry capacity as exit capacity. This is ensured by the constraint shown in Equation (33). Here, following the aggregation over the supplier, the constraint is also simplified. This ensures that, system-wide, more entry than exit capacity is bought, but ignores whether individual suppliers can meet this constraint. If each supplier does meet it, then the system does too. Thus, assuming all suppliers respect the constraint, it also holds in aggregate and is sufficient to restrict capacities.

$$\sum_{n \in N} x^{+}_{n,3,m} + \sum_{k,m' \in M_3(m)} x^{+}_{n,k,m} \geq \sum_{n \in N} x^{-}_{n,3,m} + \sum_{k,m' \in M_3(m)} x^{-}_{n,k,m} \quad \forall \quad m \in M_k \tag{33}$$

3.6 Stochasticity

The uncertainty in the demand and prices are modeled by different scenarios. In some scenarios, the quality might not be maintained at market nodes, while a technically feasible flow can still be achieved. To limit the deviation from quality standards across scenarios, the number of scenarios where deviation from quality is allowed is limited. This is ensured by the constraint in Equation (34). In the equation, the parameter Δ can be set to zero to ensure a qualitatively feasible flow is achieved for all scenarios. With this constraint, the model is complete and ready to be used for applications.

$$\sum_{m \in M_3} \pi_{3,m} \delta_m \leq \Delta \tag{34}$$

"To collect into one by reasoning things that are scattered, so that by defining each thing one may make clear what one wishes to teach."

— Plato

4 Case Study

With the generic formulation fully specified, it can be applied to a real world setting. This requires several assumptions regarding the data, as well as reviewing assumptions of the general model. Therefore, to determine the tractability and effectiveness of the model, this section formulates a case study based on the Norwegian Continental Shelf. The Norwegian Continental Shelf is the largest integrated gas transmission network in the world (Gassco, 2023), and therefore provides a substantially complex case study. This section explains the derivation of the parameters involved and provides necessary context for the choices made in the model application.

4.1 Uncertainty

The case study is applied to a different number of scenarios in stage two and three, to gauge the efficiency of the model. However, the main experiments are executed on branching 8 times to stage 2 and 8 times to stage 3, yielding 64 total scenarios. For all applications the probability of scenarios is equal, i.e. $\pi_{k,m} = \frac{1}{|M_k|}$. The choice of hyperparameters can be found in Appendices C.1 (weymouth cutting planes), C.2 (density bounds) and C.3 (homogeneous splits).

4.2 The Norwegian Continental Shelf

Norway is the largest gas supplier to Europe (Adomaitis and Buli, 2025; Aastad, 2025). The network is connected with other European markets, generating additional complexity with regard to demand requirements. In addition, Norway has a potential competitive advantage in generating (blue) hydrogen and has taken a leadership role in developing hydrogen technology (Cheng et al., 2024).

Because of the complexity of the network and the large trading volumes, it provides a highly interesting case study, to determine the efficiency of the model, as well as an indication of the scale on which hydrogen blending can be applied. Therefore, this section illuminates the characteristics of the Norwegian transmission system, focusing on the TSO, as well as the hydrogen infrastructure that Norway is developing.

4.2.1 Norwegian Transmission Network

The Norwegian Continental Shelf consists of several Transmission Systems, with the largest operated by Gassco (Dale, 2025). For the case study, the system operated by Gassco was considered, as they operate the largest system, and the end-points to their pipelines provide gas to international markets. Pipeline data was collected from Dale (2025), which contains pipelines from multiple operators, and the active gas pipelines operated by Gassco were selected for the case study. The dataset was checked against a graphical representation in Aastad (2025), and it was found that the direction of some edges should be reversed to obtain a reasonable flow. Namely, from the original dataset, Europipe II, Norpipe and a pipeline from Gjøa were reversed back to the actual direction. In addition, two pipelines were removed from consideration, as they rely on pipelines from other operators to connect to a market node. Finally, the individual pipelines were converted to a comprehensive graph by making the endpoints of the pipelines into nodes, and merging nodes if they were 20 km or less away from each other. With these adaptations, the network for the case study is shown in Figure 8. Appendix B.1 provides the network in a hierarchical form to aid in understanding routing decisions.

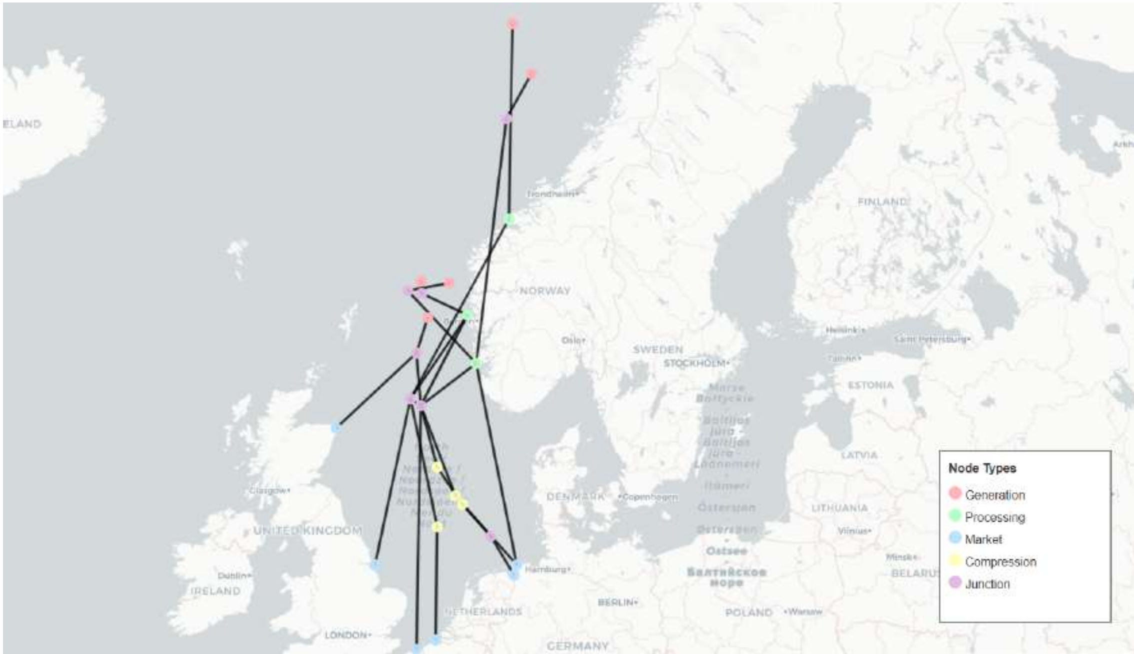

Figure 8: Geographical view of the network. The different colors represent the different node types.

In the network, the nodes were manually separated into categories, based on their presumed function. This is indicated by the colors in the figure. Each of the, generation, processing and market nodes were given their respective roles based on known characteristics. For, nodes in the sea with multiple incoming or outgoing arcs are considered junctions, where homogeneous splitting must be applied. Finally, if there is only one node coming in and going out to the node, even when considering other operators, then this is assumed to be a compression node.

In addition to the main case study, the amount of stylization of the network can also be changed such that two additional networks are created to determine the scalability of the linear model. The derivation and structure of these networks is given in Appendix B.4.

4.2.2 Generation Nodes

For each of the generation nodes, the supplier and the generation limit were derived from data from Norwegian Petroleum (2025), the second using Equation (35). Here, $g_{T-4,n}$ to $g_{T,n}$ represent the gas production over the past 5 years, while $g_{i,n}$ represents the remaining gas in the reservoir. The five year time frame was chosen to obtain a reasonably accurate value for the production limit, while reflecting the current situation of production. The production was provided in yearly format, so the found number was divided by the number of days in a year to obtain a feasible daily flow.

$$G_n = \frac{\min\{\max_{t=0}^{4}\{g_{T-t,n}\}, g_{i,n}\}}{365} \tag{35}$$

In addition, the gas production cost is calculated by the investment costs ($\hat{o}^g_{t,n}$) over the past 5 years divided by the production the following year, as shown in Equation (36). Note that this is a substitute of the average costs, rather than the marginal costs, which are more common. Finally, records on the gas composition at generation fields are not made public, and were therefore chosen based on realistic values from other fields (Hoeven, 2004; IEA, 2005; Nørstebø et al., 2010; Poe and Mokhatab, 2012). They are varied to show the capabilities of the model to mix appropriately for sales at market nodes. The resulting parameters are given in Table 8.

$$o^g_{n,m} = \frac{\sum_{t=1}^{5} \hat{o}^g_{T-t,n}}{\sum_{t=0}^{4} g_{T-t,n}} \quad \forall m \in M_3 \tag{36}$$

Table 8: Parameters of selected gas fields.

Location	Operator	Capacity (Mscm/day)	Cost (€/Mscm $\times$ 1000)	CO_2 percentage (%)
Aasta Hansteen	Equinor	24.44	10.90	2
Gjøa	Vår Energi ASA	9.32	19.62	2
Norne	Equinor	0.27	34.05	1
Oseberg	Equinor	22.93	42.28	1
Visund	Equinor	15.78	26.20	3

4.2.3 Compression Nodes

Following the construction of the network, compression nodes are designed to have exactly one outflowing arc, following the model assumption used in Equation (2). The compression nodes were designed solely for this case study and, in turn, data stemming from these nodes does not exist. Instead, example data is created, based on real data used in previous studies. The compressibility factor is derived from Nørstebø et al. (2010), who suggest compressibility factors of 1.9 which are adopted here. This is further substantiated by Das et al. (2025, p. 504), who optimized for fuel usage under hydrogen blending, and observed compressibility factors of $\hat{P} \in [1.8, 2.06]$ for NG and H_2 mixtures up to 20%. Second, the fuel consumption constants were derived, with data from Nørstebø et al. (2010). The full derivation is shown in Appendix C.5, based on a hydrogen free solution. Table 9 shows the resulting values for each compressor. Note that based on these parameters, the fuel consumption is moderate, but still reduces the flow of the arcs they are placed between.

Table 9: Compression parameters shared by compression nodes. The compressibility factor and $K_{f^c_a}$ do not depend on the component.

Parameter	NG	H_2	CO_2
Compressibility factor	1.9	1.9	1.9
$K^c_{p_a,\text{in}}$	5.667×10^{-5}	0	1.157×10^{-6}
$K^c_{p_a,\text{out}}$	1.077×10^{-4}	0	2.197×10^{-6}
$K_{f^c_a}$	2.706×10^{-4}	2.706×10^{-4}	2.706×10^{-4}

4.2.4 Market Nodes

Finally, the gas is sold at exit points of the network, namely, the market nodes. For each market node, the spot market price and the contracted demand are be sampled per scenario. Sampling allows to compare scenario trees, which in turn allows to execute multiple runs to obtain statistically significant results. To compare, the results for a manually constructed tree can be found in Appendix D.1. For the spot market price, the markets are regulated at trading hubs. For example, gas in Germany is traded on the Trading Hub Europe (THE, 2026a), while the UK uses the NBP (Clever Markets, 2025). These markets also operate under different price mechanisms, for example, working with daily futures (ICE, 2026b), or with prices to deviate from contracted demand (THE, 2026b). For simplicity, this study only considers a single spot price per market. The average prices per market node were taken as the scenario average proposed in Markhorst et al. (2026, p. 24).

However, instead of sampling regardless of the stage 2 branch, prices are sampled based on the average price given in the parent node, with added variance based on the duration of the stage. Namely, for each node there exists an average price, to which a long-term variance is applied to get the average day-ahead price (when demand is revealed) and a short-term variance is applied to get the actual prices per scenario. The variance is applied by multiplying the price by a normal distribution of the form $\mathcal{N}(1, \sigma_{k,n})$, where $\sigma_{k,n}$ represents the standard deviation applied in stage k at market node n. This enables the prices to be dependent on the previous stage and in turn reflect a more realistic behavior of changing prices. For convenience, the prices are truncated at zero. The long-term standard deviation was estimated by examining the 6 months change of the intraday-futures price market of both the TTF market (ICE, 2026a) and the NBP market (ICE, 2026b) for mainland Europe and the United Kingdom, respectively. Furthermore, the day-ahead standard deviation was estimated by examining the changes between consecutive days.

In addition to price, the average contracted demand was also taken directly from the case study by Markhorst et al. (2026, p. 24). As this study does not incorporate all operators on the Norwegian Continental Shelf, only the demand of time block one is considered. The variance was estimated by examining the change in open interest (required deliverables) of the long-term gas futures market (ICE, 2025). This provides an indication for the change in contract size, as the futures market is in itself a contract market for delivering gas. The demand is sampled using the lognormal distribution, following empirical results (Ajinkya and Jain, 1989). It should be noted that the total demand is given here, and that suppliers obtain a share of these contracts. The shares of contracts per node are given when hydrogen suppliers are introduced. Finally, there exist quality requirements on the gas in terms of minimum pressure at the market nodes, as well as a maximum percentage of CO_2. For this, the publicly available terms and conditions from Gassco were used (Gassco, 2026a). The resulting values for the parameters are given in Table 10.

Table 10: Market prices and demand per node

	Dunkerque	Easington	St. Fergus	Emden	Dornum	Zeebrugge
Market	France	UK	UK	Germany	Germany	Belgium
Average Price (€/Mwh)	30	26	26	28	28	29
Long-term std. (%)	15	10	10	15	15	10
Short-term std. (%)	1	1	1	1	1	1
Average total Demand (Gwh)	50	12.5	12.5	25	25	25
Standard deviation (%)	30	30	30	30	30	30
Minimum pressure (bar)	60	70	41	45	84	80
Maximum CO_2 (%)	2.5	2.5	4	2.6	2.5	2.5

4.2.5 Nodes and Arcs

In addition to node-type-specific parameters, there are parameters that are required for all nodes and arcs. For all nodes, the maximum capacity was set at $\bar{F}_n = \sum_{n' \in N_{g,h}} G_{n'}$, as the capacity is higher than the flow that is possible at any node, and therefore provides an upper bound required for the big-M parameter. Instead, for every arc, the capacity limit was chosen manually by examining the interactive Gassco map (Gassco, 2026c), and applying the given limit if available, while setting it to $\bar{F}_a = 40$ for the remaining arcs. Otherwise, the maximum inlet pressure, also known as the maximum allowable operating pressure (MAOP) needs to be computed for each arc. Das et al. (2025, p. 499) provide a formula to compute this based on the diameter of the pipe. However, assuming this formula is correct, and using the diameters of pipes given on the Gassco map, all pipes have a maximum operating pressure of $\bar{P}_a \in [149.76, 150.46]$ bar. Therefore, for each pipe in the case study the operating pressure was set to an equal $\bar{P}_a = 150$. Furthermore, the cost of pressure for each arc was also set equal, and was set at a magnitude smaller value compared to the flow value, $o_a^p = 100$€/Bar (the objective is in the millions while the pressure costs take on costs near half a million), following the claim of Tomasgard et al. (2007) that it is a secondary objective that should be minimized given that the flow is already optimized. Finally, the Weymouth constant was calculated for each pipe. The constant depends on the diameter and length of the pipe, taken directly from the pipline dataset (Dale, 2025). Other required constants are taken from previous research that use the Weymouth equation, of which the full derivation is shown in Appendix C.4. A full list of the arcs is given in Appendix B.2, alongside the allowed capacity.

4.2.6 Gassco & the Entry-Exit System

The Norwegian state-owned TSO, Gassco (Gassco, 2023), operates neutrally with regard to suppliers, but does not own its pipelines (Petroleum, 2025). Gassco indicates two responsibilities in the form of special and normal operatorships (Gassco, 2023; Aastad, 2025). Special operatorship covers system operation, capacity, and quality control, as well as conducting studies on effective pipeline development. Normal operatorship instead covers the maintenance of its assets and projects, such as the pipeline network. The case study can be applied for responsibilities within its special operatorship, as the integration of hydrogen gas within the system covers system operation and capacity and quality control, while only indirectly affecting the maintenance of the system through its outcomes. These considerations are in line with recent literature that optimizes social welfare in the system (see Table 3).

Gassco manages different areas, namely areas A-P. Per area, there exist different regulations relating to its place in the network. For example, area D covers most exit points to other national markets (NOD, 2024), and suppliers are obliged to supply more to the network than they plan to extract using these points (Gassco, 2024, p. 13). While the areas provide extra restrictions, they present incidental constraints and are for the most part not relevant to the modeling decisions made by the TSO. Therefore, they are not considered in the case study. However, the areas do give rise to the different tariffs that are levied.

Gassco employs an entry-exit system to collect tariffs (Dahl, 2001, p. 49). The tariff per standard unit (NOK/scm) for each entry and exit point is determined by Equation (37), where $C = 1/\text{sm}^3$ denotes the capital cost element, I_p denotes the base investment per expected unit of gas through area p and E_n denotes the expansion factor of these investments in year n (Dahl, 2001, p. 160, NOD, 2024). Furthermore, O denotes the operation cost of the entire network, and Q_n the total expected quantity transported in year n. This formula is employed for each entry, exit, and process points in all areas. When investments for each area are equal, all entry-exit tariffs become equal per unit, in turn reducing the tariff system to a postage system. The booking costs per area were computed using the latest component cost per area of Gassco (Gassco, 2026b), and applied to each node within that area (NOD, 2024). The full table of the base booking tariffs can be found in Appendix B.3.

$$t_{p,n} = (CI_p E_n) + \frac{O}{Q_n} \tag{37}$$

In the actual Gassco system, the booking price is stable, regardless of the booking duration (yearly, day-ahead or intra-day) (Gassco, 2024). However, they maintain a first-come first-served system for short-term capacity while contracts are available, such that suppliers are incentivized to engage in long-term booking contracts. To model this behavior, the booking costs are instead considered to increase with each stage, such that the model is incentivized to mimic the behavior of suppliers. The price increase is directly taken from Markhorst et al. (2026, p. 22), with an increase of 4% at stage two and 8% at stage three compared to the base cost.

4.3 Hydrogen Production

To mix hydrogen gas into the network, it has to be produced in a power plant and connected to the pipeline network. Lakeit et al. (2023, p. 8) identified two large scale hydrogen production in the last stage before production. However, both have since been put on hold (S&P Global, 2024; Lea, 2024; IEA, 2025). There are other smaller scale projects that run along the coast of Norway, mainly to be transported by boat (GreenH, 2026; HYDS, 2026). If these projects were located near the main pipeline network, they could have been considered for hydrogen blending. Figure 9 provides an overview of these projects. However, for the case study, only the larger projects that are put on hold are considered. This choice is made because these are the only production plants near an existing network point, enabling direct network entry without additional costly hydrogen pipelines.

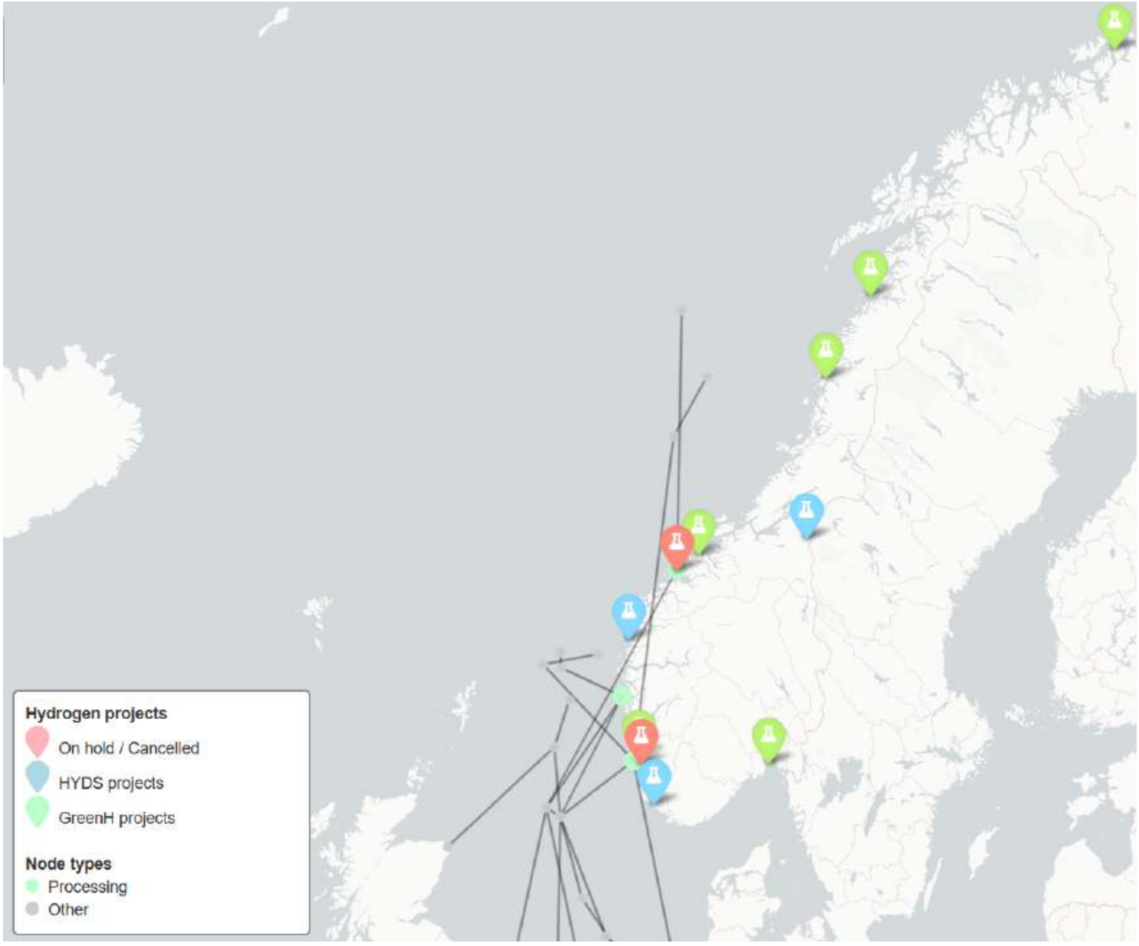

Figure 9: Hydrogen Production plants in Norway, with the case study network given in gray. While these examples are numerous, they do not represent a comprehensive list.

This gives rise to two new generation nodes at the processing nodes, where production parameters need to be determined. While the projects have been put on hold, Lakeit et al. (2023) did provide yearly production capacity after 2030, which after a conversion of units, are used for the case study, and shown in Table 11. However, the same report estimates the cost of hydrogen at 70-110 Euro/Mwh, which equates to approximately 195-307 Euro/ Mscm $\times 1000$, converted using the lower heating value (LHV) of hydrogen gas (≈ 2.79 Gwh/Mscm), which is used in the report (Lakeit et al., 2023, p. 6), and therefore needs to be adapted here for the costs. Note that as the transmission system uses the GCV as the selling price (see Table 2), the production cost per Mwh does not equate one to one with the selling price. Nonetheless, the average cost is about twice the selling price of hydrogen gas (see Table 10), such that the production of hydrogen is economically infeasible. Therefore, in the case study, the effectiveness of subsidy on the total flow is examined. In the case study, the subsidy is applied per Mwh using the LHV, and the production is also shown in the metric, to match the units of hydrogen reports, such as Lakeit et al. (2023) and IEA (2025).

Table 11: Hydrogen Generation nodes.

Location	Operator	Capacity (Mscm/day)	Cost (€/Mscm $\times$ 1000)
Nyhamna	Shell	14.74	195
Kårstø	Equinor	14.74	195

There exist limits on the percentage of hydrogen that can flow from an arc. As discussed, it is safe to flow up to 20% of hydrogen gas through an arc, therefore $q_a^{c+} = 0.2$. However, the limit per market is distinct, and the allowed blending rate is taken from IEA (2025, p. 80) for each node. Additionally, all suppliers are mentioned, such that the contract ratios can be given. The supplier contracts are divided to reflect the production, as well as maintain similarity to the contract division from Markhorst et al. (2026), who created a fair division among suppliers. The resulting division and maximum percentage of hydrogen gas per market node is given in Table 12. It was chosen not to give Shell a mandatory demand size, as hydrogen production and shipping is both limited and hypothetical, and the natural gas plants from Shell are not included in the model, unlike the model by Markhorst et al. (2026).

Table 12: Contract divisions and maximum hydrogen percentage

Location	Equinor (%)	Shell (%)	Vår Energi ASA (%)	maximum H_2 percentage (%)
Dunkerque	100	0	0	6
Easington	100	0	0	0.1
St. Fergus	100	0	0	0.1
Emden	100	0	0	10
Dornum	80	0	20	10
Zeebrugge	100	0	0	0

4.4 Computational Setup

The experiments have been developed in Python 3.13 (Python, 2024), using Pyomo (Bynum et al., 2021) to allow the models to be solved with different solvers. For the experiments, the Gurobi solver (Gurobi, 2026) was employed, where presolve, cutting planes are enabled and the precision set to 0.2% gap, with the other parameters left at the default parameters. The experiments were run on a high performance computing cluster (HPC) on 48 cores, each with two gigabytes of memory.

"One of the main functions of an analogy or model is to suggest extensions of the theory by considering extensions of the analogy"

— *Mary Hesse*

5 Results

The case study provides the ability to discuss the benefits and challenges from several angles. To provide an understanding of the current situation, the characteristics of the model in the form above are shown first, under the guise of an example usage of the model. Second, the impact of policy measures for hydrogen gas is examined. Third, the sensitivity of the model to technical restrictions, such as changes in the allowed percentage of hydrogen through pipelines and the closure of pipelines and natural gas generation points critical for hydrogen blending. Fourth, the sensitivity of the model to higher price fluctuations is examined, to gauge the influence on hydrogen blending and booking decisions. Finally, the stochastic value and the scalability of the model are analyzed. For each finding, unless stated otherwise, all claims of statistical significance are based on t-tests (Chicco et al., 2025) conducted at a significance level of $\alpha = 0.05$, with Bonferroni-adjusted p-values used to account for multiple comparisons (Weisstein, 2026a). Furthermore, the code which is used to generate the results is provided on a Github repository (Beemster, 2026).

5.1 Example Usage

The case study is executed in its explained form to define the model behavior and determine the impact of allowing hydrogen blending under current circumstances. An initial note for the base model is that under current hydrogen prices, hydrogen production designed for blending is not economically feasible, as the production price (70€/Mwh) is over twice the price and is therefore not relevant in the base setting.

First, the distribution of flows from the generation points and to the market points is given as a violin plot, which are shown in Figure 10. The figure on the left shows that the production of natural gas at each generation node remains rather unvaried, which shows that a nearly equal amount of natural gas is produced in each scenario. Together with the production capacity shown in Table 8, the maximum amount of gas is always produced, indicating that no matter the scenario, operators should always produce natural gas to maximize social welfare. On the other hand, the direction the gas is directed to differs per scenario very frequently. At lower-price markets, such as the English markets, usually only long-term contracts are fulfilled, creating the large lower tail, and the route sends extra gas there only when prices are favorable, which is rare, given the low base price. On the other hand, the high base price in Dunkerque often yields higher gas routing, but is limited by the demands (contract sizes) of other market points, such that the upper tail of the delivery is higher, and still varies. Finally, this figure shows that gas can effectively be routed to market points across scenarios.

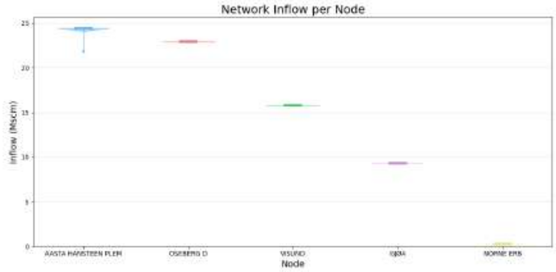

(a) Net inflow (Mscm) into the network from generation nodes. The inflow is stable across scenarios, indicating different prices and demand rarely change production.

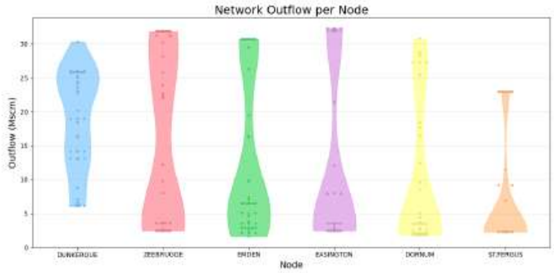

(b) Net outflow (Mscm) out of the network to market nodes. The outflow is unstable, corresponding to the changes in demand and prices at these nodes.

Figure 10: Net inflow and outflow distributions

Second, the bought entry and exit capacities per node averaged across scenarios is shown in Figure 11. The left figure shows that entry capacity is only bought in stage 1, which corresponds to the unvaried production, as capacity needed to fulfill the production in the earliest can already be bought, as it is always beneficial to produce. Second, corresponding to the changing flow, the model reduces overdraft of capacity by booking capacity at stage two and three depending on the demand and prices at market nodes. The capacity bought at the third stage is smaller, which originates from the structure of price generation, where the day-ahead price determines the intraday price, thereby partially revealing the price in the second stage.

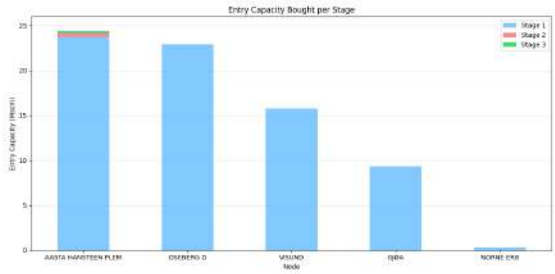

(a) Entry capacity per node (Mscm). The entry capacity is bought in the first stage mostly, which is related to the stable inflow.

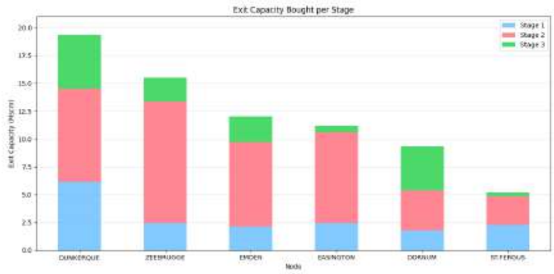

(b) Exit capacity per node (Mscm). The exit capacity is bought in different stages, to account for the changing gas flow.

Figure 11: Comparison of entry and exit capacity per node

Third, the pressure differences on arcs should also be examined. For three different arcs, the inlet and outlet pressures are plotted as violin plots across the scenarios as violin plots, which is shown in Figure 12. For this figure, an edge from a generation node (Visund) was chosen, an edge to a compression node (B-11), as well as to a market node (Zeebrugge), to see the difference in pressure dynamics in the model.

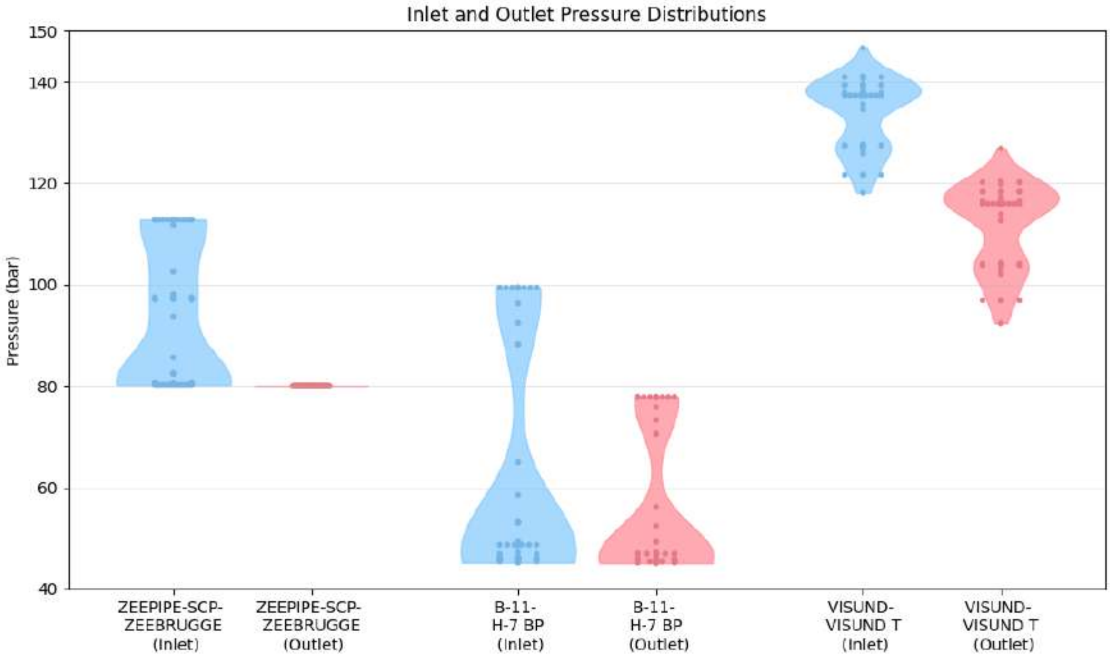

Figure 12: Distribution of inlet and outlet pressures (Bar) for 3 example arcs. The pressures depend on the position of the pipe in the network. Where market nodes only have changing inlet pressure from upstream gas (Outlet Zeebrugge), generation nodes have both changing inlet and outlet (Inlet Visund), depending on downstream market dynamics.

The figure shows that for the generation arc, the inlet and outlet pressures do change, but move simultaneously up and down, indicating the flow remains the same, while the required pressure later in the network changes. The opposite is true for the arc towards Zeebrugge, where the outlet pressure stays at the minimum required value (see Table 10), but the inlet pressure differs, based on the amount of gas delivered to Zeebrugge. At B-11, the outlet pressure is extremely low, as the compressor increases the pressure again afterwards, reducing the cost component of pressure. Therefore, this figure shows that pressure requirements are appropriately handled for different types of nodes.

Finally, the components of the objective are examined. Figure 13 shows that the generated revenue is a magnitude larger than the cost, and the main goal of the model is therefore to maximize the revenue, and only as a secondary objective minimize the costs. Otherwise, the revenue differs per scenario, which underscores the need to optimize for different scenarios, to get a more comprehensive picture of both the tactical and operational decisions of the TSO.

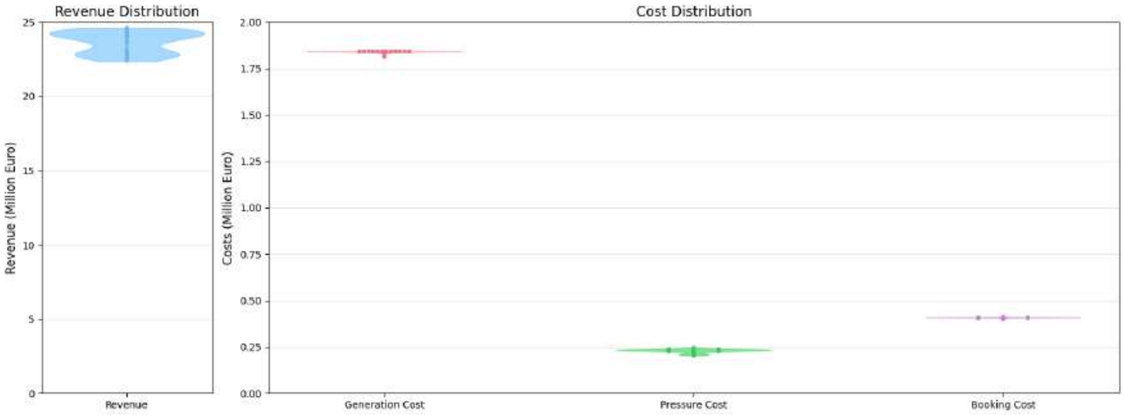

Figure 13: Distributions over the scenario of revenue and costs (Million €). The revenue is a an order of magnitude higher than the cost, but is also more varied across scenarios.

In summary, the model can be used on an operational level by the TSO, to monitor gas routing decisions, gas quality and pressure dynamics throughout the system. In addition, the stochastic formulation allows the TSO to examine the entry-exit capacity market in aggregated form, and see the impact of the system of different scenarios in pricing and demand. Therefore, the model can function as a strategical tool for the TSO.

5.2 Subsidies and Allowed Deviation

Hydrogen production is not viable for blending, due to the high production costs. To combat these costs and stimulate hydrogen blending, a subsidy per generated Mwh of hydrogen can be introduced. As hydrogen production costs are taken as 70 €, subsidies are chosen within the range of $o_{s_i} \in [0, 70]$, where $i \in I$ denotes the index of the experiment. The subsidies are directly applied to the production cost of the gas, such that effective production cost becomes $o^{gi}_{n,m} = o^{g}_{n,m} - o_{s_i}$ for hydrogen plants. The subsidy and subsequent hydrogen production are shown using the LHV, to match the units of reports of European hydrogen production (Lakeit et al., 2023; IEA, 2025).

In addition to different subsidies, the TSO is also allowed to sometimes deviate from market quality restrictions, to maintain flow in the system. This characteristic, hereafter named deviation, can be used to possibly generate extra hydrogen flow when prices or demand are high, such that the need for blended hydrogen can be justified. The allowed number of scenarios where market deviation is allowed consists of $\Delta \in \{0\%, 5\%, 10\%, 20\%, 100\%\}$ to generate a comprehensive picture on the impact on the strictness of the market.

The model is run four times using Common Random Numbers (CRN) between each deviation and subsidy, to eliminate noise generated from the tolerance and scenario generation respectively.

5.2.1 Subsidy Impact

The resulting hydrogen production is shown in Figure 14, alongside the shaded standard error. The figure shows that for any number of scenarios where deviation is allowed, a subsidy is required to be higher than 30 €/MWh to significantly impact hydrogen blending, as hydrogen blending then becomes economically viable in some scenarios where market prices of gas are high. Furthermore, the impact of the subsidy decreases, as the hydrogen gas production stagnates as the subsidy increases. However, if the market restrictions are ignored, the possibilities of hydrogen production increases further with the subsidy, but also declines as the effective cost of hydrogen production decreases to zero. Note that if the actual production costs of hydrogen turn out to be higher, the projected impact would move to the right, but retain its shape, as hydrogen blending would become still become economically viable at the corresponding effective cost.

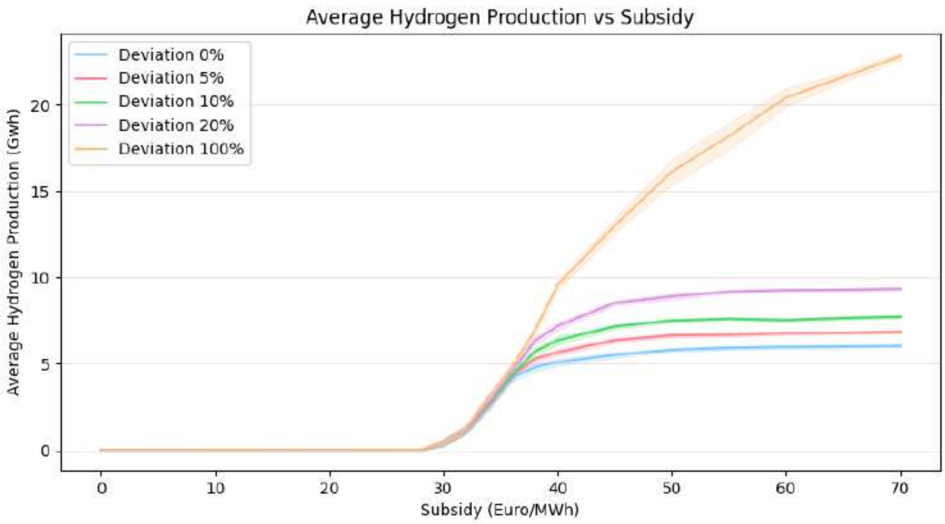

Figure 14: Hydrogen production (Gwh) for different subsidy levels (€/Mwh) and allowed market deviations (%). The hydrogen production grows with the subsidy.

The subsidy generates additional social welfare within the system, which corresponds to the objective, but also reduces social welfare by incurring the cost of the subsidy. The effects can be computed according to Equation (38). Here, O_i denotes the objective corresponding to experiment i, while O_0 denotes the objective corresponding to the case without subsidy.

$$\begin{aligned} \bar{O}_i &= O_i - O_0 \\ C_i &= o_{s_i} \left(\sum_{n \in N_{h,g}} \sum_{a \in A_n^-} f_{a,m}^{H_2} - \sum_{a \in A_n^+} f_{a,m}^{H_2} \right) \end{aligned} \tag{38}$$

These effects are shown in Figure 15, where the changes from zero subsidy are given. The left figure shows that with the subsidy increase, the objective increases quadratically when the hydrogen production increases, but otherwise seems to become linear, indicating that the additional subsidy is then directly taken into account, but does not increase it more than the cost of the subsidy. The right figure shows a similar picture, where the costs increase drastically at the beginning, but become linear when hydrogen production has stabilized. For both plots, the effects are larger for a higher deviation, where the corresponding hydrogen production is bigger. The figures also show that the costs of hydrogen production are greater than the increase in objective value, indicating that direct social welfare is lost due to the subsidy. Therefore, subsidy should be carefully weighed against the benefits of hydrogen production.

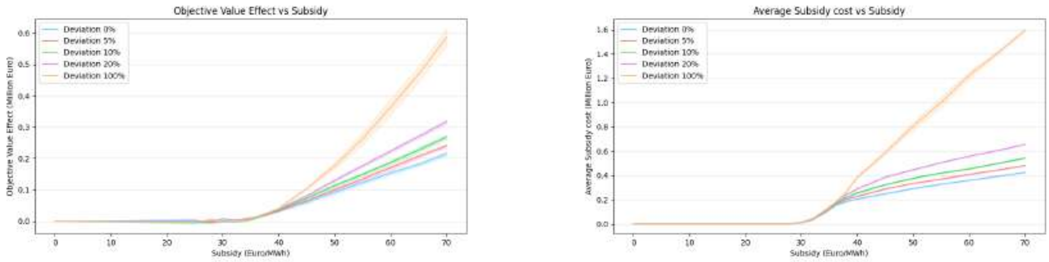

(a) Objective change (Million €) for different subsidy levels (€/Mwh) and allowed market deviations (%). The objective increases super-linearly with hydrogen subsidy.

(b) Subsidy cost (Million €) for different subsidy levels (€/Mwh) and allowed market deviations (%). The cost of the subsidy increases with hydrogen subsidy.

Figure 15: Relationship between subsidy, objective value, and subsidy costs.

One of the benefits is that hydrogen gas can replace in part the carbon intensive fuel of natural gas, thereby removing carbon emissions. To calculate this effect, the difference in carbon emissions per Mscm of produced hydrogen gas, scaled for energy contents, is calculated between natural gas and green hydrogen gas (Millieu Centraal, 2025). To measure the monetary effect, the social welfare cost per tonne of CO_2 emissions is taken as 185\$, following the findings of Rennert et al. (2022). This quantity was translated to Euro using 2020 as the base year (27.6% inflation), and the\$/€exchange rate of 01-05-2026 (0.85\$/€), such that the cost becomes 200.65€. The full social cost of carbon is used instead of the prevailing Emission Trading System (ETS) price (Emissieautoriteit, 2025), as the subsidy is conceived from a regulatory perspective that prioritizes overall social welfare rather than cost minimization within the existing emissions trading framework. This results in the savings in the social welfare cost shown in Equation (39) of $o_c = 118483.32$€/Mscm of produced hydrogen.

$$o_c = \underbrace{200.65\text{€/tCO}_2}_{\text{Cost of emission}} \cdot \left(\underbrace{2134\text{tCO}_2\text{/Mscm}}_{\text{Emissions NG}} \cdot \underbrace{\frac{12.7}{39.8}}_{\text{HHV Ratio}} - \underbrace{90.45\text{tCO}_2\text{/Mscm}}_{\text{Emissions green H}_2} \right) \tag{39}$$

The net welfare effect of a given subsidy and deviation ($i \in I$) can then be calculated according to Equation (40), where the savings of carbon emissions and increase in the system social welfare are weighed against the cost of the hydrogen subsidy.

$$W_i = \bar{O}_i + \sum_{m \in M_3} \pi_{3,m} (\sum_{n \in N_{h,g}} \sum_{a \in A_n^-} f_{a,m}^{H_2} - \sum_{a \in A_n^+} f_{a,m}^{H_2})(o_c - o_{s_i}) \tag{40}$$

Figure 16 displays the net effect for the different subsidies and deviations. The plot shows that the net effect increases to 45 €, but then decreases again slowly. However, when the deviation is 100%, meaning market restrictions may always be ignored, the effect drastically decreases further. The reason for this is because when the subsidy removes the production cost of gas, and every market is available, the TSO can decide to reroute gas towards to lower priced markets, to facilitate extra hydrogen blending. This reduces social welfare, as the revenue from the natural gas itself becomes lower. However, when the system is restrained, the possibilities for this behavior are less prevalent, and therefore affect the net welfare effect less.

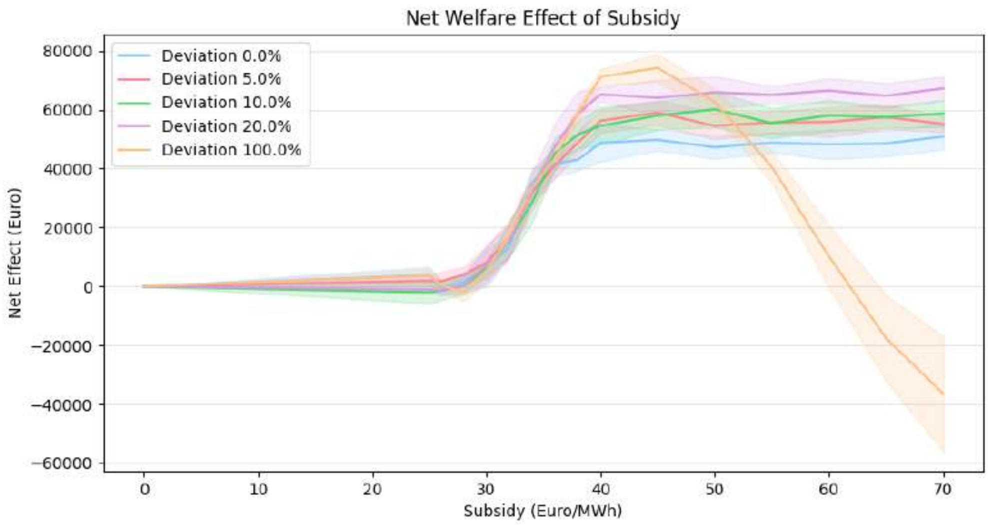

Figure 16: Net social welfare effect (€) for different subsidy levels (€/Mwh) and allowed market deviations (%). The net effect peaks at 45€/Mwh, but shows different patterns for different market deviations.

However, while the net effect of the subsidy is largest at 45, it might not weigh against the high subsidy cost. The return on investment (ROI) should also be examined, such that $\mathrm{ROI}_i = \frac{W_i}{C_i}$. For the subsidy levels with significant hydrogen production, the ROI is shown in Figure 17, and shows that besides the large standard error at the start, the ROI is quite high, but decreases with the amount of needed investment. Therefore, it is in the best interest of institutions to balance between the absolute impact and the return on investment of hydrogen blending. Furthermore, the return on investment is lower, given the same subsidy when not alleviating market restrictions, due to the fact that the hydrogen production is higher, yielding to a higher cost and therefore a lower ROI.

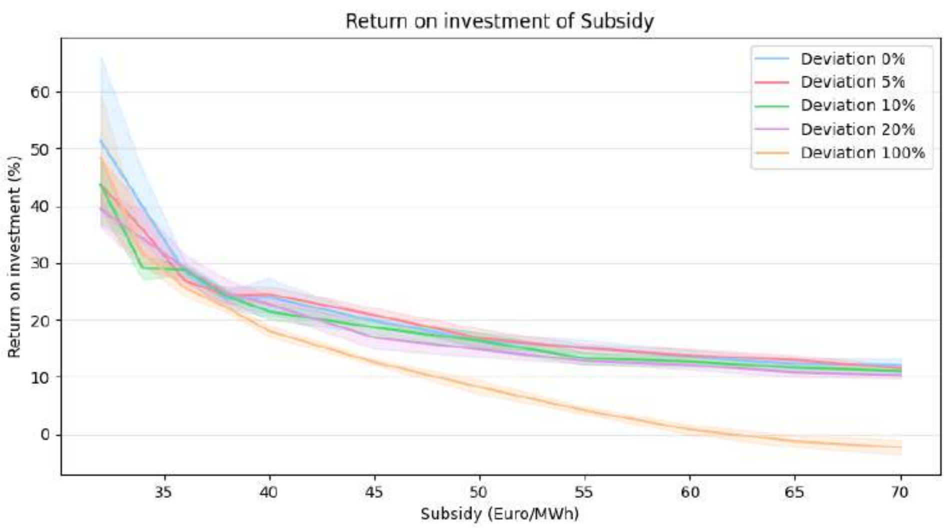

Figure 17: Return on Investment (%) for different subsidy levels. The ROI decreases as the total investment increases.

Together, these findings show that subsidies can enable hydrogen blending, alongside its challenges. Subsidy allows hydrogen to become economically viable, and generate a positive net welfare effect when considering subsidies.

5.2.2 Hydrogen Flow Structure

To assess the impact of hydrogen blending, the average hydrogen flow can be analyzed by examining the full network. To this aim, the average flow over the scenarios was taken, as well as the percentage of hydrogen that flow consists of and plotted for each arc. For subsidies of 45€/Mwh (highest welfare) and 70€/Mwh (zero effective cost) as well as full and no market restrictions, the flows are given in Figure 18. The figure shows that when market restrictions are enacted only the hydrogen production facility in Kårstø is able to provide blended gas, for both the welfare optimum and zero cost subsidy, while the facility in Nyhamna remains inactive. This is due to the fact that Nyhamna delivers to homogeneous splitting nodes. At these nodes, where the composition of the gas is split in even fractions over the pipes, each connected market node receives an equal fraction of hydrogen gas within their composition. If one of these markets does not allow hydrogen blending, in this case Zeebrugge, then any other market also connected to the splitting node cannot receive hydrogen from that point, due to the equal splitting. However, when the market restrictions are alleviated, such that only the technical pipe limitations apply, then the possible hydrogen production facility in Nyhamna also becomes relevant for hydrogen blending. Note that while this finding applies to the case study, it also applies to any system where downstream markets are reached by homogeneous splitting. In that case, the amount of possible hydrogen blending is limited to the strictest market. Therefore, to fully benefit from hydrogen blending, cross-market collaboration is required.

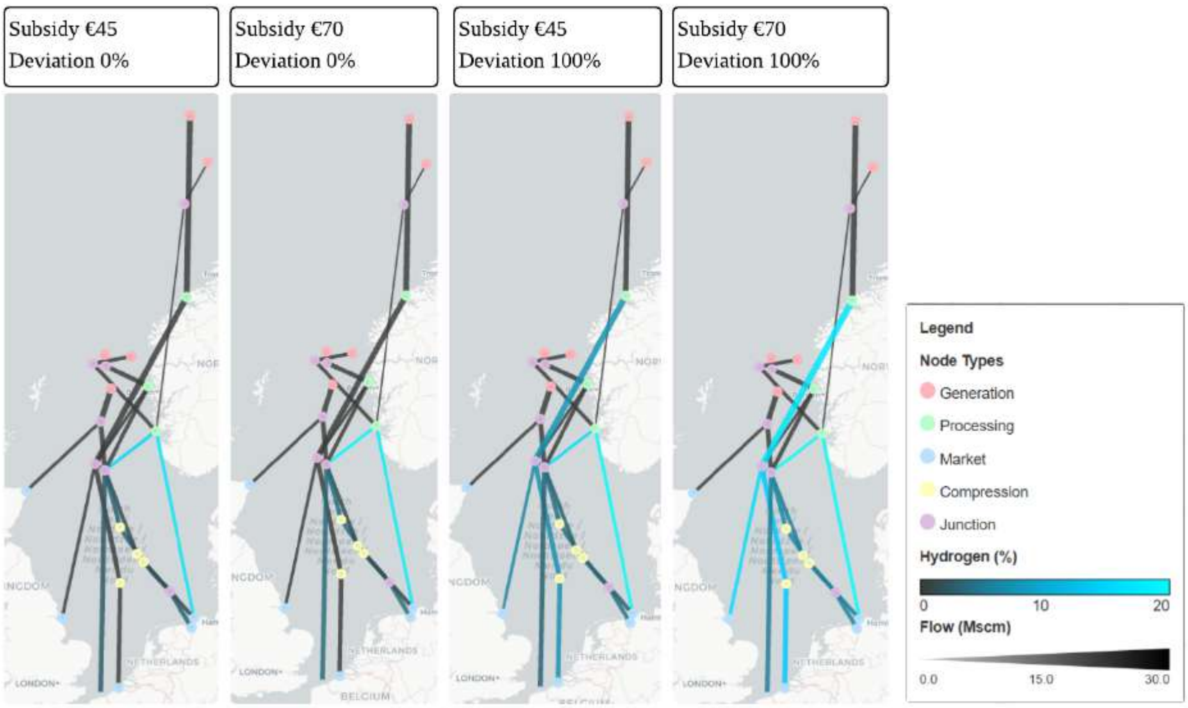

Figure 18: Network structure for different subsidy and deviation levels. The hydrogen flow is limited to the plant in Kårstø, but when market restrictions are relaxed, the plant in Nyhamna also becomes useful.

Under the welfare optimum subsidy, the effect is marginal, but when hydrogen is given an effective production cost of zero, the full effect is realized. Moreover, the transition to a lower net welfare effect can also be shown with the aid of Figure 19. When the net welfare effect is at its highest, natural gas is routed to the Easington market point and hydrogen gas is moved alongside it when possible. However, when the subsidy gets higher the model reroutes gas to these market points in some scenarios, even though it is not the optimal natural gas disposition. This is to enable extra hydrogen flow, which obtains a lower cost than natural gas. However, the rerouting of natural gas cuts into the growth in objective, while the cost of the subsidy keep rising, yielding a negative net effect. Therefore, making the subsidy too high can cause negative effects for the net social welfare when considering hydrogen blending.

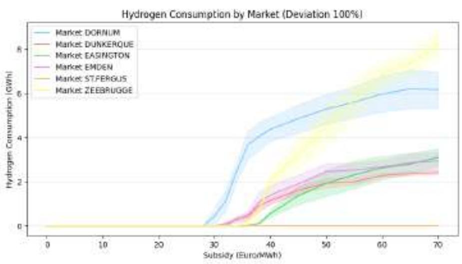

(a) Hydrogen consumption (Mwh) per market point. Hydrogen production increases at each market point with increased subsidies.

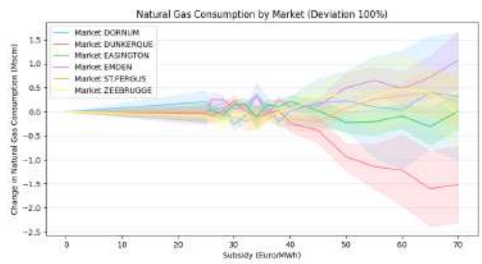

(b) Change in natural gas consumption (Mscm) per market point. The gas routed to the highest value market (Dunkerque) decreases while the one to Easington increases, indicating that subsidies change the direction of natural gas flow.

Figure 19: Comparison of hydrogen and natural gas consumption per market point, at deviation of 100%

When market restrictions are neglected more often, more hydrogen blending is possible. However, when market restrictions are maintained, the only feasible hydrogen blending location is found to be Kårstø, as offshore junctions restrict hydrogen blending to the strictest market. Again, this shows that to reach the full benefit of hydrogen blending, cross market collaboration is needed. When market restrictions are fully released, concern should be raised to avoid the rerouting of gas to enable additional hydrogen blending, which can reduce the net welfare effect, and should therefore be avoided.

5.2.3 Entry-Exit System Impact

Finally, a subsidy and the corresponding hydrogen production could disrupt the entry-exit system that governs the capacity market. With disruption of the entry-exit system, the TSO could in turn lose some of its control over the direction of the gas, while booking partners on the network can overpay for capacity. To measure this risk, the amount of overprovision, the difference between the bought and used capacity, was calculated for each scenario,and then summarized according to Equation 41 for both the entry (χ^+) and exit (χ^-) capacity respectively. When the total bought capacity is zero ($\sum_{n\in N} x^+_{n,k,m}$ and $\sum_{n\in N} x^-_{n,k,m}$), the quantity is set to zero, although this does not occur for any of the current experiments.

$$\chi_i^+ = \sum_{m \in M_3} \pi_{3,m} \frac{\sum_{n \in N} x^+_{n,3,m} + \sum_{k,m' \in M_3(m)} x^+_{n,k,m'} - \sum_{c \in C}(\sum_{a \in A_n^-} f^c_{a,m} - \sum_{a \in A_n^+} f^c_{a,m})}{\sum_{n \in N} x^+_{n,k,m}}$$
$$\chi_i^- = \sum_{m \in M_3} \pi_{3,m} \frac{\sum_{n \in N} x^-_{n,k,m} + \sum_{k,m' \in M_3(m)} x^-_{n,k,m'} - \sum_{c \in C}(\sum_{a \in A_n^+} f^c_{a,m} - \sum_{a \in A_n^-} f^c_{a,m})}{\sum_{n \in N} x^-_{n,k,m}} \tag{41}$$

The entry and exit capacity overdraft was determined for several of the subsidies, when market restrictions are respected. The resulting overprovisions are shown in Figure 20. The figure shows that the percentage of leftover entry capacity increase when hydrogen blending is introduced, indicating that hydrogen blending increases the uncertainty in the system for operators. However, there are additional trends visible. Namely, the amount of leftover entry capacity is larger than the exit capacity. This originates from the fact that part of the exit capacity is booked in later stages, while the model seems to prefer booking entry capacity in earlier stages, as it expects to produce. When the subsidy hovers near market prices, the amount of unused entry capacity increases the most. This is instead due to the difference in price levels between scenarios, where in some scenarios, the model uses up the capacity, while in others it does not see a benefit in hydrogen blending, but has bought the capacity in case the other scenario actualized, resulting in unused capacity. Furthermore, as hydrogen gas has to flow with natural gas, it can sometimes not move with to the market where the gas is moving, creating overprovision.

When sold capacity is limited, overprovision leads to possible inefficient use of the network. The TSO must remain vigilant to these effects when allowing hydrogen blending, to ensure that the increased overprovision is limited. To avoid the negative effects, the TSO must therefore closely monitor the hydrogen production made for blending, to anticipate their needs, instead of solely going off the sold capacity, as the bought capacity might not give a full indication of the hydrogen producers need at that time. This would ensure that entry and exit capacity is not unnecessarily limited due to potential hydrogen blending.

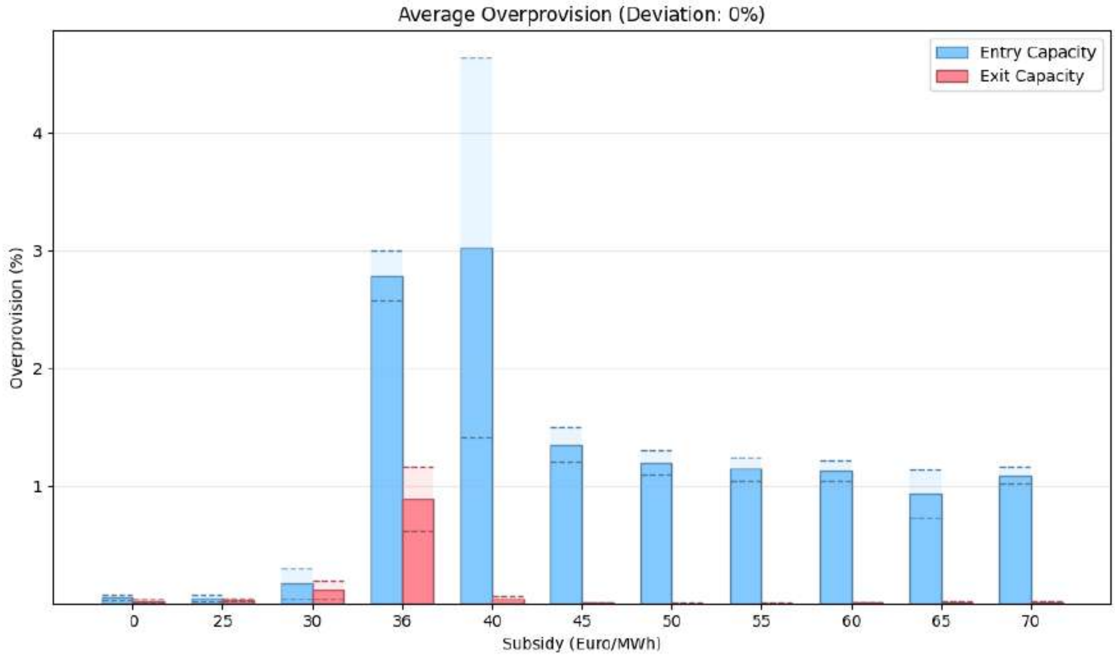

Figure 20: Overprovisions (%) for bought entry and exit capacity at different subsidy levels at a deviation of 0%. The amount of unused bought entry and exit capacity increases when subsidy is increased, but decreases again when hydrogen blending is always valuable.

In summary, an additional challenge of hydrogen blending is that bought entry-exit capacity can remain unused when hydrogen blending is subsidized, as hydrogen blending can is only feasible when prices are sufficiently high. Therefore, adding hydrogen producers to the traditional entry-exit capacity system should be taken under careful consideration.

5.2.4 Blending obligation

To limit the negative effects of a subsidy, the TSO can instead be obligated to allow a minimum amount of hydrogen blending on its network. The model can be adapted to account for this regulation in the form of a constraint. Namely, Equation (42) shows the additional requirement for the TSO, integrated into the model, where $\hat{F}_i$ represents the required hydrogen that is blended, for experiment $i \in I'$.

$$\sum_{n \in N_{h,g}} \sum_{a \in A_n^-} f_{a,m}^{H_2} - \sum_{a \in A_n^+} f_{a,m}^{H_2} \geq \hat{F}_i \quad \forall \quad m \in M_3 \tag{42}$$

The policy was examined for different levels of obligated blending, shown in Equation (43). As there exist market and technical restrictions on hydrogen blending, the model becomes infeasible at higher percentages of the total available production. Therefore, this range examines the full range of a possible blending obligation. The range was examined for both no deviation and full deviation, to gain an impression of the influence of the market restrictions on the policy. The experiments were carried out on four different seeds, to obtain statistical significance of the results.

$$\hat{F}_i = \phi_i \sum_{m \in M_3} \pi_{3,m} \sum_{n \in N_{h,g}} \alpha_n^{H2} G_{n,m} \quad \forall \quad \phi_i \in \{0\%, 1\%, \ldots, 20\%\} \tag{43}$$

As shown, hydrogen blending is not economically viable without a subsidy, such that the model always optimizes to meet the restriction, and will not exceed it, as the objective would become lower. Therefore, it is not of interest to examine the total hydrogen production. Instead, the effect on the impact on social welfare is measured directly. It should be noted that the social welfare of the policy changes, corresponding to Equation (44), where the subsidy cost is removed, however, the benefit of subsidy to the objective is also not considered.

$$W_i = \bar{O}_i + \sum_{m \in M_3} \pi_{3,m} (\sum_{n \in N_{h,g}} \sum_{a \in A_n^-} f_{a,m}^{H_2} - \sum_{a \in A_n^+} f_{a,m}^{H_2}) o^c \tag{44}$$

A comparison between the system welfare effect of both policy measures is plotted against the amount of blended hydrogen shown in Figure 21. The figure shows that a blending obligation yields a higher net welfare effect than subsidizing. This stems from the fact that no additional investment is needed which lowers the objective. Furthermore, the ability to blend hydrogen is higher for the subsidy experiment compared to the obligation. This is due to the restriction, where under a strict the model can become infeasible in a scenario due to demand obligation, where under the subsidy policy, the model can change the total hydrogen production between scenarios, enabling for a higher average hydrogen production across the scenarios, as well as an increased social welfare.

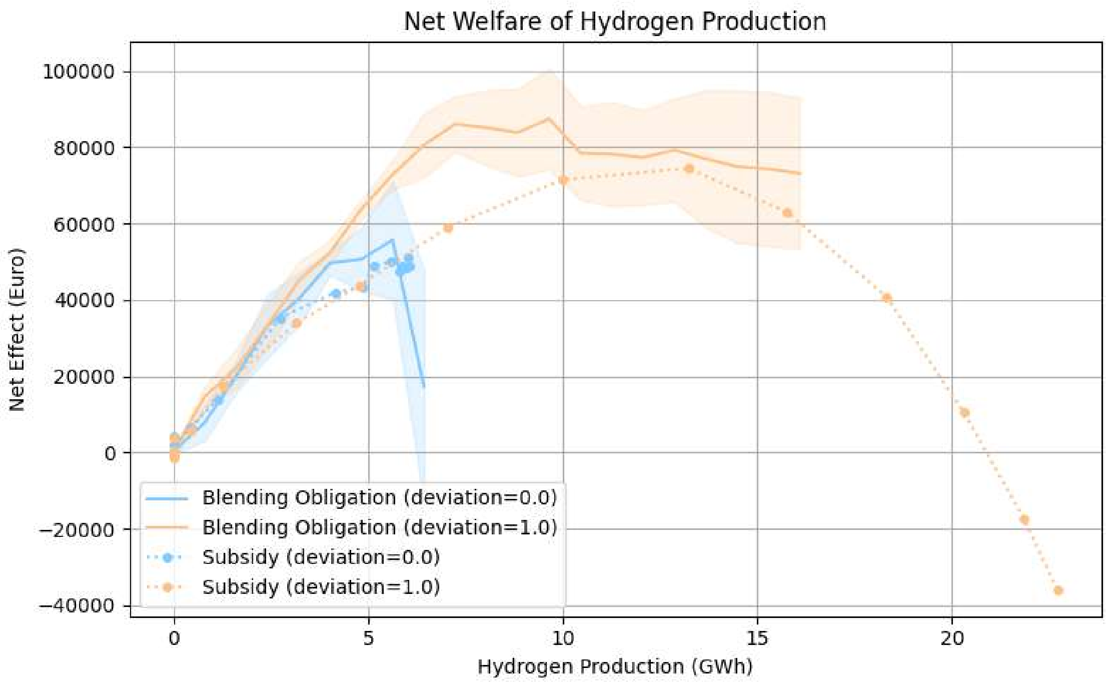

Figure 21: Net welfare effect against the amount of blended hydrogen

Therefore, a blending obligation can be considered as a policy measure to circumvent the need for subsidies, as it yields a potentially higher net welfare effect. However, the highest possible hydrogen production is lower under the obligation compared to a subsidy, such that for hydrogen blending, a subsidy should be preferred.

5.3 Technical Restrictions

Hydrogen blending is subject to several technical restrictions. The TSO has to ensure that the network remains operational, indicating the restrictions should be followed. The technical restrictions could in turn limit the hydrogen blending if they are chosen more strict, or changes in the network occur, which change the applicability of hydrogen blending. Therefore, this section examines changes in the technical restrictions in the model, and its impact on hydrogen blending.

5.3.1 Hydrogen Blending Percentage

Advancing the Norwegian Continental Shelf toward allowing the theoretical technical limit of 20% hydrogen through the pipelines is ambitious. Instead, the TSO could instead allow a lower percentage of allowed hydrogen blending, and still obtain the benefits of blending. To this aim, for three different subsidies (30, 45 and 70€/Mwh), the system was examined for different percentages of hydrogen within the pipelines, up to the theoretical technical limit.

For each of the subsidies and allowed hydrogen percentages, the hydrogen production is plotted, which is shown in Figure 22. The figure shows that the hydrogen production increases linearly with the percentage of allowed hydrogen production. Therefore, the allowed pipeline fraction creates a bottleneck on the system, and relaxing this constraint enables the benefits of hydrogen blending directly.

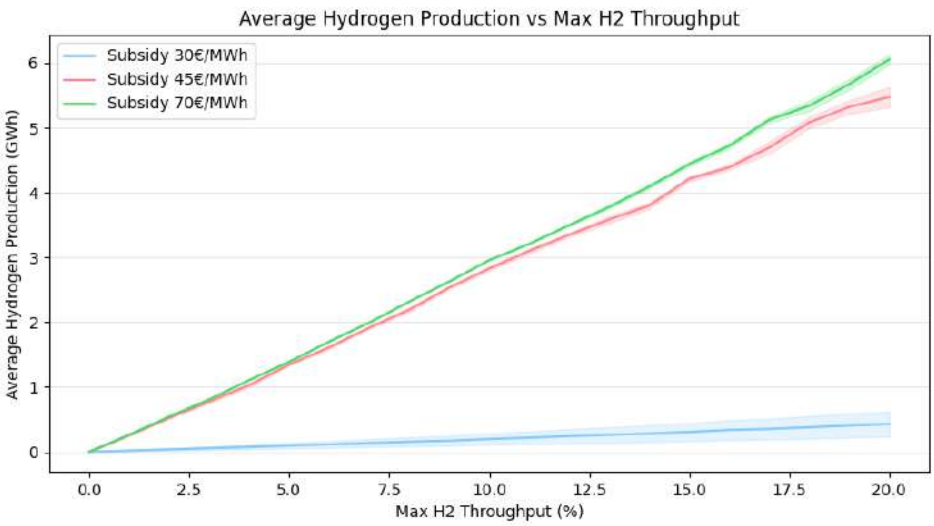

Figure 22: Hydrogen production (Gwh) under different percentages of allowed hydrogen throughput, at an allowed deviation of 0%. The increasing hydrogen production shows that pipe restrictions on hydrogen are a limiting factor for hydrogen production.

The net effect is also examined for different allowed percentage, which is shown in Figure 23. While the net effect is noisy, a linear trend does seem to prevail, where the net effect is approximately equal for each of the different percentages, which is similar to the net effect for the full 20% shown in Figure 16. This indicates that the net effect grows with the amount of hydrogen production when pipeline restrictions are universally eased.

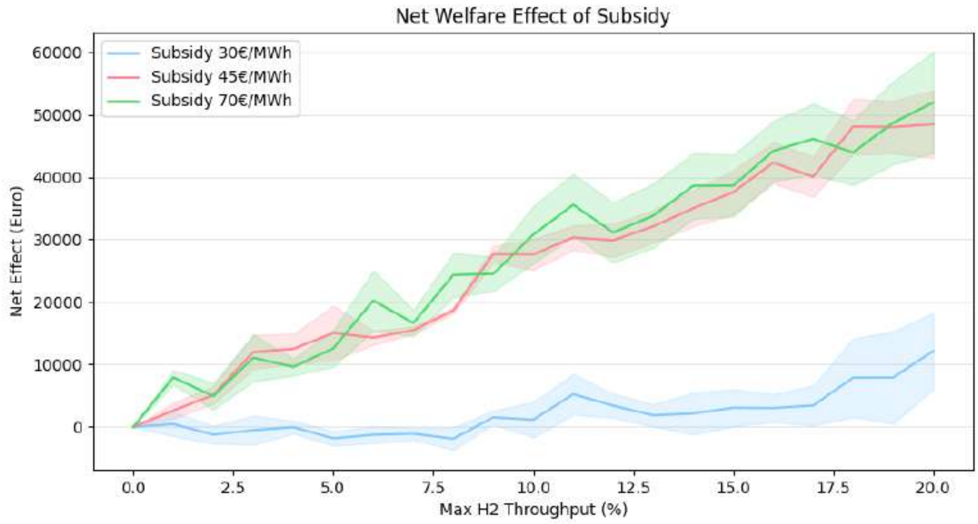

Figure 23: Welfare net effect (€) under different percentages allowed of throughput, at an allowed deviation of 0%. The increasing welfare shows that pipe restrictions on hydrogen are a limiting factor for the increase in welfare.

Therefore, tightening the allowed percentage on hydrogen can reduce the benefits of hydrogen blending. In turn, possible technical limits need to be weighed against the added benefits of hydrogen blending to obtain the full welfare effect of hydrogen blending.

5.3.2 Element Closure

In addition to the universal effect of not allowing hydrogen, the sensitivity of hydrogen blending to a (temporarily) closed natural gas generation point or a closed pipeline must be examined. Referring back to Figure 40 (See Appendix B.1 for the names of the nodes, B.2 and B.3 for the specifics per arc and node), it can be seen that the pipes from Kårstø to Draupner and Dornum are the most important under the current market restrictions, as well as the pipelines that follow from Draupner to the markets of Dunkerque and Emden. Furthermore, the generation nodes supplying Kårstø could be equally important for blending, to move hydrogen along the supplied gas. When those fields go dry, the impact on the system is substantial. Therefore, the fields of Gjøa and Norne are considered as they directly supply the hydrogen production plant in Kårstø, as well as one indirect connection which supplies to Draupner.

For each of the examined fields and pipelines, the remaining hydrogen production was examined. However, when pipelines or generation nodes are removed, the model can easily become infeasible to solve, as demand might not be met at market nodes. Therefore, to ensure feasibility, demand satisfaction constraints (shown in Equations (8) and (9)) are transformed to soft constraints, where any unmet demand is highly punished. To model the soft constraints, the symbols shown in Table 13 are introduced. Two shortage variables, $\eta^g_{h,m}$ and $\eta^d_{n,m}$, are introduced that are applied to the hard constraints to turn them into soft constraints. Second, penalty terms are introduced for any missed demand. These are manually tuned such that when demand is feasible, the model prioritizes satisfying it, and when infeasible, it still optimizes the rest of the system. Finally, a new objective is introduced that includes the penalties.

Table 13: Additional symbols for soft demand constraints.

Symbol	Type	Description	Range	Unit
$\eta^g_{h,m}$	Variable	Unmet demand for supplier h under scenario m	$\mathbb{R}^+$	Mwh
$\eta^d_{n,m}$	Variable	Unmet demand at market node n under scenario m	$\mathbb{R}^+$	Mwh
λ^g	Parameter	Penalty cost per unit unmet supplier demand	$\mathbb{R}^+$	€/Mwh
λ^d	Parameter	Penalty cost per unit unmet market demand	$\mathbb{R}^+$	€/ Mwh
O^λ	Objective	Objective function including missed demand penalty	$\mathbb{R}$	€

The adapted constraints are shown in Equations (45) and (46). The shortage variables allow respectively suppliers or markets to fall short on the required demand to the market, as the variable would take on the difference for the supplier or market. In addition, the objective is changed in Equation (47) to include the penalty terms for the soft constraints. The penalty value was taken at $\lambda^g = \lambda^d = 1000$€/Mwh, as the costs and opportunity costs of missing demand never exceed this number, such that the model always prefers to fulfill demand if possible. However, when it is impossible, the model can still optimize the other aspects of the objective without encountering numerical issues. In turn, this constraint is of a different nature than the missed demand penalty proposed by (Hasturk et al., 2025), as the missed penalty is an actual choice to miss demand in their model, while in the current model it is always beneficial to fulfill demand if possible.

$$\eta^g_{h,m} + \sum_{c \in C} r_c \sum_{n \in N_{h,g}} \Big(\sum_{a \in A_n^-} f^c_{a,m} - \sum_{a \in A_n^+} f^c_{a,m} \Big) \geq \sum_{n \in N_d} D_{h,n,m} \quad \forall h \in H,\ m \in M_3 \tag{45}$$

$$\eta^d_{n,m} + \sum_{a \in A_n^+} \sum_{c \in C} r_c f^c_{a,m} \geq \sum_{h \in H} D_{h,n,m} \quad \forall\, n \in N_d,\ m \in M_3 \tag{46}$$

$$\max O^\lambda = O - \sum_{m \in M_3} \Big(\sum_{h \in H} \lambda^g \eta^g_{h,m} + \sum_{n \in N_d} \lambda^d \eta^d_{n,m} \Big) \tag{47}$$

The model was again run four times under the standard setup for different subsidies (0,30, 45, 70 €/Mwh), under a deviation of 0%. This provides the ability to study the effects of subsidies under given market constraints, with the addition of the impact of a closed pipeline.

After solving, the missed demand is taken for each failed pipeline and generation plant. When there was no failed plant, all demand is delivered, which follows from the construction of the penalty, where if feasible, all demand must be delivered to reach optimality. However, for a closed generation node, there is a shortage to meet delivery from production, while if a pipeline to the market is closed, there is a shortage there. The magnitude of these events is shown in Figure 24, which shows that closing Gjøa causes production shortage. This stems from the fact that the only plant considered for Vår Energi is Gjøa, such that when this plant closes, all the demand taken on by the operator is left unsatisfied. Instead, when a pipeline is closed, a shortage in demand brought to market points arises. Namely, when the final pipeline to Dunkerque and Emden close, the full demand remains unsatisfied (see Table 10). This originates from the critical nature of these pipelines, which act as a single connection to the market. When the single connection fails, no gas can be brought to the market, and the demand is left unsatisfied. Therefore, modeling the unsatisfied demand as a soft constraint is necessary to avoid infeasibility when examining network element closure.

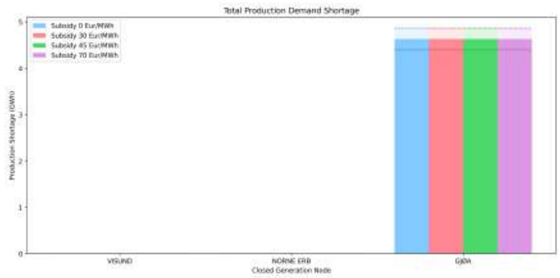

(a) Total shortage (Gwh) over suppliers averaged across scenarios due to closed Generation nodes, with shortage occurring when the Gjøa closes, stemming from the limited production by Vår Energi considered in the study.

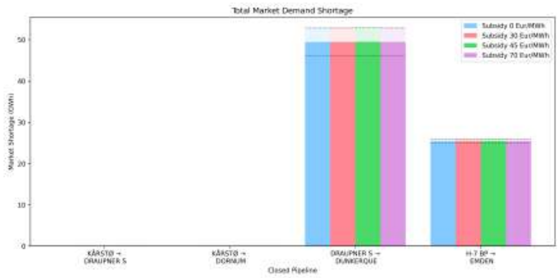

(b) Total shortage (Gwh) over market nodes, averaged across scenarios due to closed pipelines, with shortage occurring when the single pipeline connected to a market closes.

Figure 24: Demand shortages arising from closing network elements, no market demand shortages were found from closing generation nodes, and no production demand shortages from closing pipelines, which are therefore not shown.

Since a possible demand shortage is taken into account, the system effects for hydrogen blending of closing a pipeline or generation node can be examined. First, the change in hydrogen production is analyzed. Figure 25 shows that closing a plant can have a negative effect on hydrogen blending. Namely, when less natural gas flows to a hydrogen blending point, in this case Kårstø, less hydrogen gas can flow alongside it, enforced by the technical restriction on the pipelines. In addition, there exists a significant decrease at a subsidy of 70 for all three examined hydrogen generation plants. However, the impact of losing the Gjøa generation point reduces the amount of produced hydrogen drastically, and more than Visund and Norne ERB. This is because Gjøa is a substantially larger plant than Norne, while Visund only adds natural gas indirectly for hydrogen blending. Therefore, the direct supply of natural gas needs to be stable to enable the long-term possibilities of hydrogen blending.

For pipelines, Figure 25b shows that the effect of closing pipelines on hydrogen production is more complex than the effect that can be caused by closing a generation node. When the pipelines to Draupner and Emden close, the amount of hydrogen blended on the system does decrease significantly compared to the full system as the subsidy increases. However, for the pipelines to Dornum and Dunkerque the amount of blended hydrogen does not decrease, and even increases significantly at very high subsidies when the pipe to Dornum is closed. This pattern arises from the redirected flow of natural gas to different market points, due to the closures. For example, when the pipeline from Kårstø to Dornum is closed, the gas previously directed to Dornum flows to the central point at Draupner, where more hydrogen gas can be distributed over the remaining markets. Therefore, when a pipeline closes, hydrogen blending can still be possible, when gas can be rerouted to different markets.

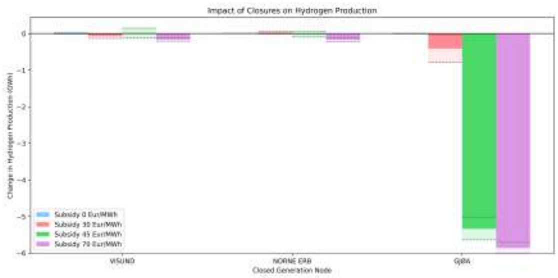

(a) Change in hydrogen production (Gwh) due to closure of production plant compared to the network without closures.

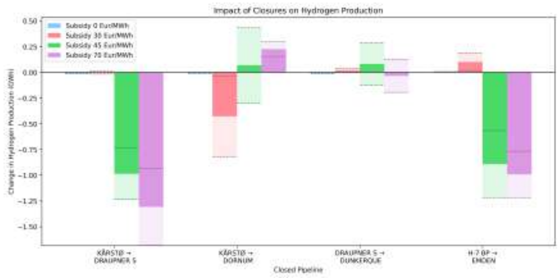

(b) Change in hydrogen production (Gwh) due to closure of pipeline compared to the network without closures.

Figure 25: Change in hydrogen production for the examined generation plants and pipelines.

Therefore, the closure of production plants and pipelines have significant effects on the system. Closing upstream production plants can greatly limit the possibilities of hydrogen blending. However, closing downstream pipelines has mostly negative effects on hydrogen blending, but can, for some pipelines, help reroute the gas to drive additional hydrogen gas to market points, circumventing chokepoints.

5.4 Market Volatility

In times of global unrest, supply shocks in the natural gas pipeline systems increase price volatility (Hailemariam and Smyth, 2019). The Norwegian network, as part of the international gas market, is subject to the possible increase in price volatility. The added volatility can change the direction of gas flows in scenarios, and influence decisions to blend natural gas. To examine this, the standard deviations were increased uniformly across the markets, thereby increasing price volatility between markets. Both the long and short-term price variation are examined, as the stage difference present distinct behaviors. In other terms, the $\sigma_{2,n}$ and $\sigma_{3,n}$ are multiplied by a constant factor for each node $n \in N_d$ to examine the changes in solution quality.

Besides volatility, price shocks are usually positively correlated (cointegrated) across markets (Kopytin et al., 2022). To model this more complex behavior, the correlation factor $r \in [-1, 1]$ is introduced, as well as the systematic variation $Z_r^d \sim N(1, 1)$. In the Equation $Z_{2,n}^d \sim N(1, \sigma_{2,n})$ and $Z_{3,n}^d \sim N(1, \sigma_{2,n})$ denote the long-term and day-ahead price shock respectively, using the standard deviations from Table 10, while $\mathbb{E}_{m \in M_3}[o_{n,m}^d]$ denotes the expected market price at node n for the base case study.

$$o_{n,m}^d = \begin{cases} \mathbb{E}_{m \in M_3}[o_{n,m}^d] \max\left((rZ_r^d \sigma_{2,n} + \sqrt{1-r^2} Z_{2,n}^d) Z_{3,n}^d, 0\right) & \text{if shock in } k = 2 \\ \mathbb{E}_{m \in M_3}[o_{n,m}^d] \max\left(Z_{2,n}^d (rZ_r^d \sigma_{3,n} + \sqrt{1-r^2} Z_{3,n}^d), 0\right) & \text{if shock in } k = 3 \end{cases} \tag{48}$$
$$\forall\, n \in N_d,\; m \in M_3$$

To gain a full overview of volatility, it is examined for different subsidies (30, 45 and 70€/Mwh). Furthermore, different correlation levels are examined, namely $r \in \{0, 20\%, 40\%, 60\%, 80\%, 100\%\}$. The price volatility in stage two and three are chosen at $\hat{\sigma}_{k,n} \in \{2^i \sigma_{k,n} \mid i = 0, \dots, 4\}$ and applied individually. Finally, each combination of these parameters was run four times to obtain a measure of statistical significance.

5.4.1 Objective and Conditional Value at Risk

Price volatility can affect the objective, as market revenue is the driver of the objective (see Figure 13). To examine this, the objective is plotted against the volatilities factors in Figure 26. In the figure, the runs across subsidies and the runs were averaged, but the differences for correlation levels are shown. The subsidies were averaged, as the relative change in objective value from subsidies is negligible compared to the increased volatility. The figure shows that for both long-term and day-ahead increased price volatility, the objective increases. Furthermore, the objective increases more when markets are not fully cointegrated. These patterns stand to reason. When market volatility increases, a market is more likely to become either really valuable or entirely worthless. When a market becomes really valuable, the suppliers aim to send as much gas to this market, while if a market price becomes uneconomical the suppliers will only fulfill their required demand. Furthermore, if all markets become uneconomical, no supplier delivers gas beside the required demand, saving costs. Averaging over the possibilities in the scenarios, the overall objective increases. In addition, this also explains that when markets are fully cointegrated the increase in objective is lower. Namely, when the markets are fully cointegrated, arbitrage opportunities between markets disappear, as the price moves together.

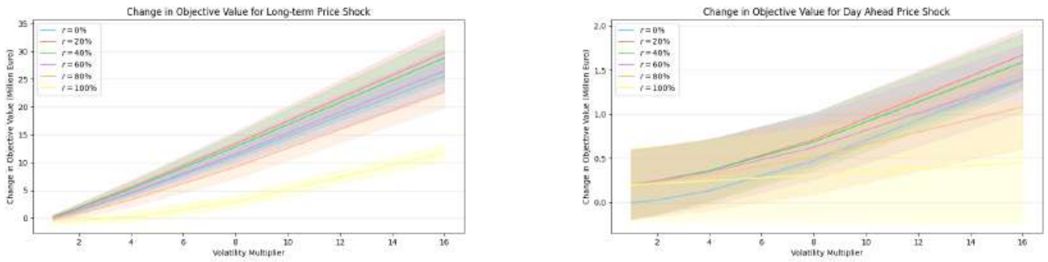

(a) Long-term price shock

(b) Day Ahead price shock

Figure 26: Change in objective values under price shocks in different stages, with a baseline without correlation or increased volatility. When markets are fully cointegrated ($r = 100\%$), the benefit to system welfare is reduced.

Although the overall objective function value increases, the objective values associated with low-end scenarios may deteriorate as a consequence of the heightened volatility. To examine this, the Conditional Value at Risk (CVaR) is computed at 5% for each experiment. To achieve this the objective value per scenario is computed and ordered, and the average over the worst 5% is taken as the CVaR at 5%. The values were then averaged per run and subsidy, and are shown in Figure 27. When markets are cointegrated, the CVaR declines, which is expected, as markets in some scenarios all have lower prices, reducing the objective. However, when markets are uncorrelated, the aforementioned arbitrage opportunities offset the possible lower prices, as gas can be in most scenarios be rerouted to higher priced markets. The effect is larger on long-term price shocks, while for short-term volatility, this effect is less pronounced. This is explained by the lower base volatility of short-term prices, such that other effects, such as possible increased costs from buying entry and exit capacity costs take over. This could also explain why increasing the correlation to 20% actually positively affects the CVaR.

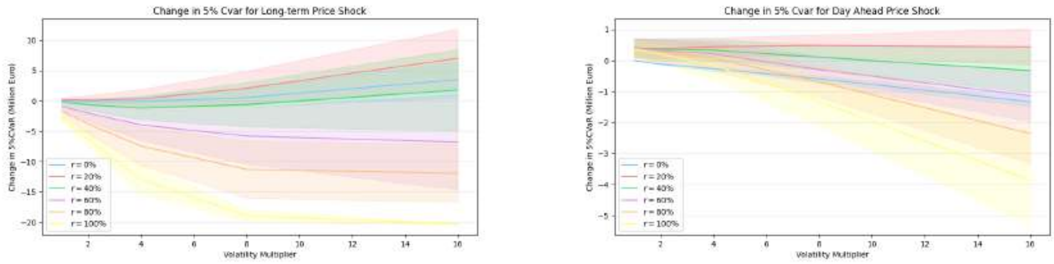

(a) Long-term price shock

(b) Day Ahead price shock

Figure 27: Change in Conditional Value at Risk values under price shocks in different stages, with a baseline without correlation or increased volatility. When markets become more cointegrated the CVaR becomes lower, while for uncorrelated markets arbitrage opportunities add to the CVaR.

5.4.2 Entry-Exit Capacity

In addition, the effect of acquired exit capacity can be examined. Capacity becomes more expensive in later stages, lowering the objective, while the increased uncertainty increases the benefit of waiting. This is because the determination of when a market attains economic significance can only be made ex post, once sufficient volatility has been observed.

This behavior is shown in Figure 28, which shows the change bought entry and exit capacity for both the long-term and day-ahead price shocks. The plot shows that when the price shock increases, the percentage of exit-capacity bought rises in the stage where this price is revealed. For exit-capacities, the percentage of bought capacity stabilizes for both stage two and three increased price volatility. This is because the capacity for contracted demand, which is revealed in stage two, can already be partly bought in stage one based on the distribution of the demand, regardless of the price volatility. Second, once demand is revealed, a second commitment can be made to exit-capacity, to account for the demand, and possibly increased market prices. However, when the day-ahead price shocks are introduced, it becomes increasingly valuable to delay buying exit capacity, to better align with arbitrage opportunities. However, because this occurs at the expense of the primary objective, overall system welfare is reduced relative to the case in which purchasing occurs in stage two. This also accounts for the lower Conditional Value at Risk (CVaR) associated with short-term price shocks.

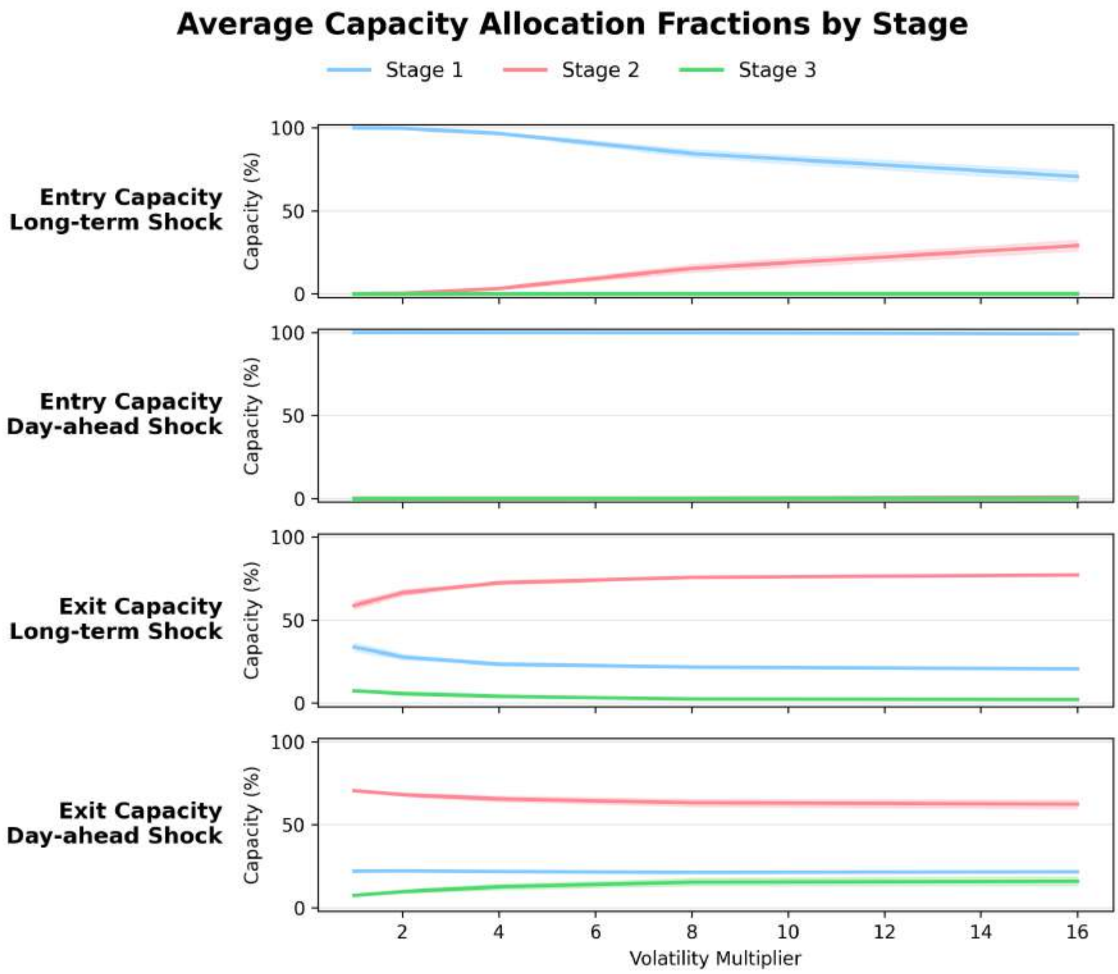

Figure 28: Percentage of bought entry and exit capacity bought per stage when volatility increases.

5.4.3 Hydrogen Production

Finally, average hydrogen production can be revisited. As price volatility increases, hydrogen production could change, as a market price might become economically viable in some scenarios, while others could become invaluable even at high subsidy levels. To examine this, the average hydrogen production across experiments can be examined, for different subsidy levels. The data is summarized in Figure 29, which shows that when price volatility increases, the influence of the subsidy decreases. The effect is less pronounced for day-ahead increased volatility, which stems from the lower base volatility associated with the stage three shocks. This can be explained by the fact that hydrogen production is not economically viable given the average price, but when prices fluctuate more, the price can rise to a level where hydrogen does become worth it. This increases the average hydrogen production when there was no subsidy, as the scenarios where prices decrease, still do not obtain hydrogen production, while those with higher prices suddenly do. Conversely, when there exists a high subsidy, when gas becomes economically nonviable to a market where hydrogen is allowed, there is no hydrogen blending, even though the hydrogen itself is worth to be blended. This can cause the average production to decrease, as high-priced scenarios were already valuable for hydrogen blending, such that the hydrogen production could only reduce. Therefore, when introducing subsidies, price volatility should be assessed to measure the impact of the subsidy on the hydrogen production.

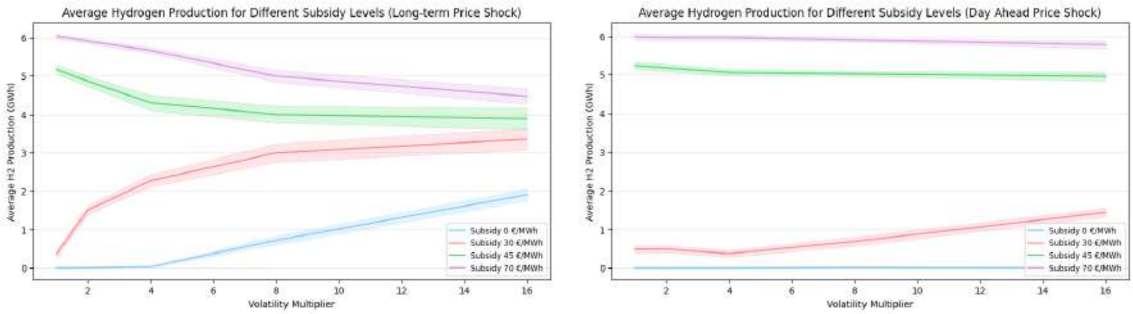

(a) Long-term shock

(b) Day Ahead shock

Figure 29: Average hydrogen production under different shock types

For different levels of correlation, the hydrogen production can also be assessed. As the effect on hydrogen production is more pronounced for long-term increased volatility, the average production for different correlation levels is shown, averaged across the different volatilities. Figure 30 shows that the average hydrogen production decreases as the correlation increases for all subsidies. Although very high and very low subsidies are the least affected, intermediate subsidy levels decrease more drastically. When long-term price correlation goes to one, the effect becomes the strongest, which indicates that when the long-term price variation is completely correlated, less hydrogen flow is economically viable across scenarios. Therefore, market correlation should be taken into account when determining the value of hydrogen production.

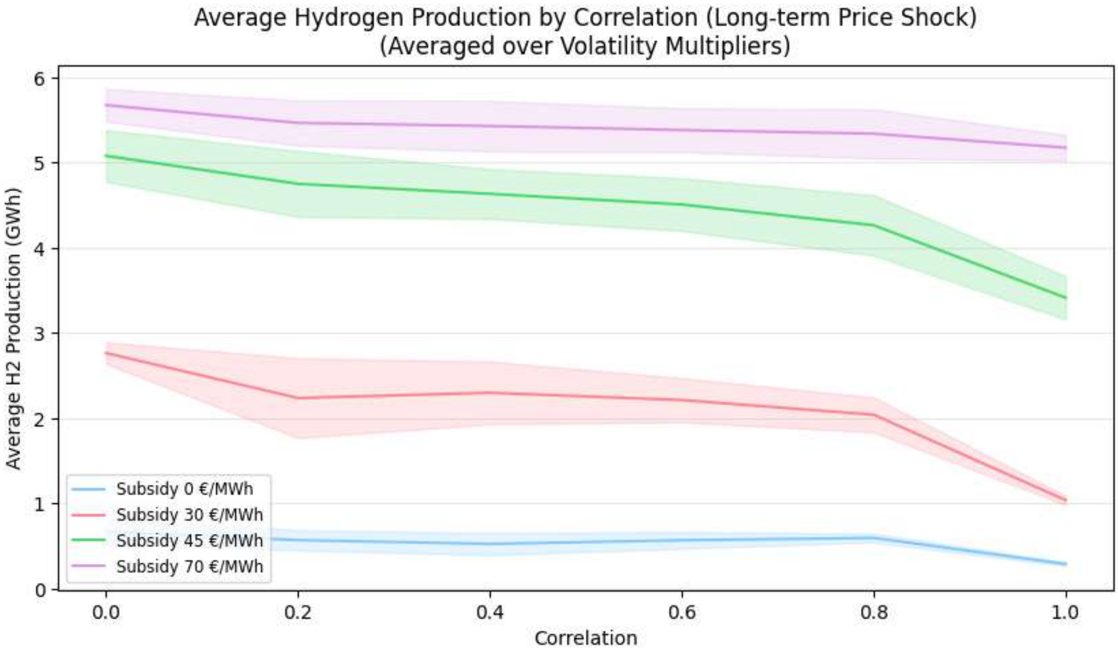

Figure 30: Average hydrogen production (Gwh) for different levels of correlations at different subsidy levels.

The influence of volatility on the hydrogen production can be formalized for special network structures. Suppose there exists a simple network, with one blending point and one market point, where the production cost of natural gas is lower than the hydrogen gas production cost, then, the decline of the influence of a subsidy can be proven. Suppose also for simplicity, that the contracted demand can be satisfied without hydrogen production for all scenarios. An example of such a network is given in Figure 31. Going forward, the blending node is denoted as node, B, whereas the market node is node C.

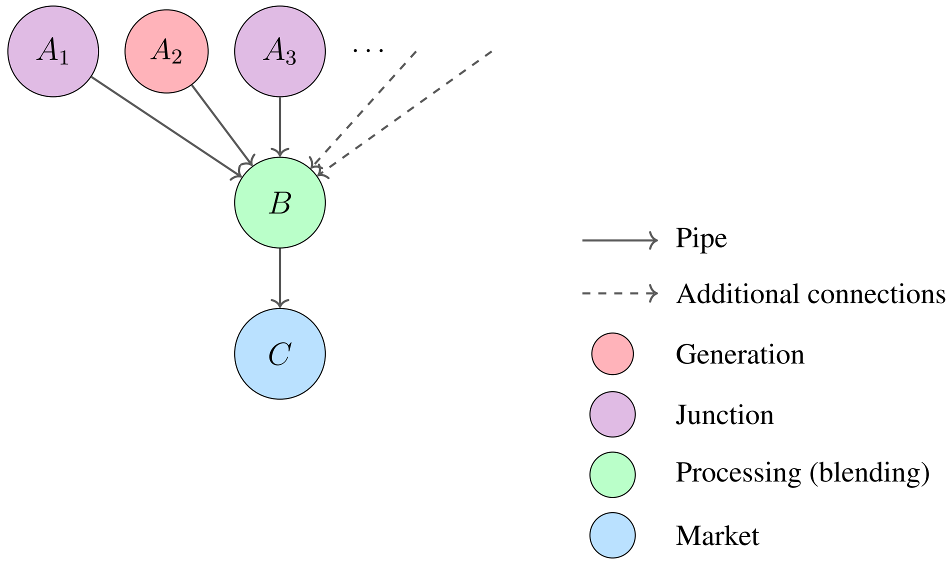

Figure 31: Simplified network with a single blending node and a single market node.

In this case, for each scenario, hydrogen production is either economically viable, and can be blended alongside the already valuable natural gas, or when the price is insufficient for hydrogen blending, any blending is omitted. More precisely, there is a price level, denoted by $\tilde{o}_i^d$, at which hydrogen blending becomes economically beneficial for subsidy level o_{s_i}. Suppose that, due to the tightest limit (e.g. pipeline, market, or generation limit), the maximum amount of blended hydrogen is denoted as $\tilde{f}_{B,C}^{H2}$ to the market node. Because blending is either fully or not economically viable, this limit is reached, or the amount of hydrogen blending is zero. In turn, the expected amount of hydrogen blending at a subsidy level o_{s_i} is given by Equation (49).

$$\mathbb{E}_{m \in M_3}[f_{B,C}^{H2} \mid o_{s_i}] = \tilde{f}_{B,C}^{H2} \mathbb{P}_{m \in M_3}(o_{C,m}^d \geq \tilde{o}_i^d) \tag{49}$$

Using this value, the difference between two subsidy levels can be computed. As the subsidy level does not influence the limit of hydrogen blending, the difference in hydrogen blending between two levels of subsidy, where $\infty \geq o_{s_a} \geq o_{s_b} \geq -\infty$ is given by Equation (50). The equation shows that when the probability that the price lies in between the two price levels declines, the added value of the subsidy declines.

$$\begin{aligned} \mathbb{E}_{m \in M_3}[f_{B,C}^{H2} \mid o_{s_a}] - \mathbb{E}_{m \in M_3}[f_{B,C}^{H2} \mid o_{s_b}] = \\ \tilde{f}_{B,C}^{H2} \left(\mathbb{P}_{m \in M_3}(o_{C,m}^d \geq \tilde{o}_a^d) - \mathbb{P}_{m \in M_3}(o_{C,m}^d \geq \tilde{o}_b^d) \right) = \\ \tilde{f}_{B,C}^{H2} \left(\mathbb{P}_{m \in M_3}(\tilde{o}_a^d \leq o_{C,m}^d \leq \tilde{o}_b^d) \right) \end{aligned} \tag{50}$$

As volatility of the price increases, the probability of lying in such a region becomes smaller. Namely, for an adjustable standard deviation $\hat{\sigma}_{k,C}$, the limit shown in Equation (51) can be obtained for the case study distribution. Furthermore, as this holds for any finite interval of price levels, the average produced hydrogen converges to a single value, regardless of the subsidy.

$$\lim_{\hat{\sigma}_{k,C} \to \infty} \tilde{f}_{B,C}^{H2} \left(\mathbb{P}_{m \in M_3}(\tilde{o}_a^d \leq o_{C,m}^d \leq \tilde{o}_b^d) \right) = \tilde{f}_{B,C}^{H2} \lim_{\hat{\sigma}_{k,C} \to \infty} \mathbb{P}_{m \in M_3}(\tilde{o}_a^d \leq o_{C,m}^d \leq \tilde{o}_b^d) = 0 \tag{51}$$

This does not necessarily hold for multiple markets, as different limits can exist for different markets, and gas can be rerouted to different markets to obtain extra flow. Nonetheless, this does illustrate why the influence of subsidies decrease as price volatility rises.

5.5 Stochastic Value Evaluation

As the model has been extended to include stochasticity, it should be extended to determine what the value of including these characteristics is. The value of extending the model to include stochastic scenarios can be determined by computing the Value of the Stochastic Solution (VSS) and the Expected Value of Perfect Information (EVPI). The VSS denotes the value of optimizing the long-term decisions for each scenario at the same time, instead of optimizing them for the average of the scenarios. Instead, the EVPI denotes the value of knowing which scenario will actualize, such that the long-term decisions can be coordinated (optimized) for each scenario individually.

To compute the VSS, the objective of the regular problem is calculated, as well as the objective given the long-term decisions are optimized by the average of the scenarios, such that the ad-hoc solution for each scenario is then computed with the fixed long-term decisions. In the current model, the long-term decisions that require fixing are the bought entry and exit capacity in stage one and two. Therefore, let $O(\boldsymbol{x}, m)$ be the optimized solution for scenario $m \in M_3$ and given bought capacities of $\boldsymbol{x}$ in stage one and two, as shown in Equation (52), such that the objective can be written as $O = \max_{\boldsymbol{x}} \mathbb{E}_{m \in M_3}[O(\boldsymbol{x}, m)]$.

$$\boldsymbol{x} := \left\{ x^{+}_{n,k',m'},\ x^{-}_{n,k',m'} \;\middle|\; n \in N,\ (k', m') \in M_3(m), m \in M_3 \right\} \tag{52}$$

This gives rise to the VSS formulation according to Equation (53), where $\hat{\boldsymbol{x}}$ represents the entry-exit capacities when the model is optimized for the average solution (EV), as shown in Equation (54), and taken as fixed. Note that when computing this quantity numerically, the average is computed over the scenarios instead of taking the expectation.

$$\text{VSS} = O - \mathbb{E}_{m \in M_3}\big[O(\hat{\boldsymbol{x}}, m) \mid \hat{\boldsymbol{x}}\big] \tag{53}$$

$$\hat{\boldsymbol{x}} := \left\{ \hat{x}^{+}_{n,1,\text{EV}},\ \hat{x}^{-}_{n,1,\text{EV}}\ \hat{x}^{+}_{n,2,\text{EV}},\ \hat{x}^{-}_{n,2,\text{EV}} \;\middle|\; n \in N \right\} \tag{54}$$

Similarly, the EVPI can be computed by computing the expectation of the objective where the stage one and two decisions are optimized individually. This is shown in Equation (55), where $\boldsymbol{x}^m$ refers to the capacity decisions in the earlier stages corresponding to scenario m. Again, note that the expectation for the case study is estimated numerically by taking the average over the optimized scenarios.

$$\text{EVPI} = \mathbb{E}_{m \in M_3}[\max_{\boldsymbol{x}^m} O(\boldsymbol{x}^m, m)] - O \tag{55}$$

$$\boldsymbol{x}^m := \left\{ \hat{x}^{+}_{n,k',m'},\ \hat{x}^{-}_{n,k',m'} \;\middle|\; n \in N,\ (k', m') \in M_3(m) \right\} \tag{56}$$

It should be noted that the scenario intersecting variable δ_m is omitted from these formulations. The variable is designed to model the rule relaxations that can be given by an extraordinary scenario to maintain flow when quality restrictions are not met, such as when there exist high prices, such that additional hydrogen gas can be allowed. However, when the deviation is a fraction, only part of the scenarios is allowed these relaxations. In turn, when computing the EVPI, the model would be able to cheat on each scenario, as the violation can be applied to each scenario individually. Otherwise, if the deviation is instead not allowed in a single scenario, as a fraction of a single scenario means no actual scenario can allow deviation, the EVPI is underestimated instead. Therefore, only the situation where no market deviation is allowed is examined here, as well as the situation where all scenarios are allowed deviation, as choosing the scenarios where deviation is allowed is of no concern for both. However, for the other examined deviation levels, Appendix D.2 can be consulted.

Besides deviation (0%, 5%, 10%. 20% and 100%), the statistics are gathered for different subsidy levels (0, 30, 45 and 70€/Mwh), as well as different scenario tree branches to stage two and three (2, 4 and 8 for both stages). To gain some statistical significance over the results, each combination of parameters was run ten times.

For a deviation of 0% the VSS and EVPI for each combination of parameters are given in Figure 32, alongside the standard error. For all combinations of parameters, the VSS and EVPI are quite small as a percentage of the objective, indicating respectively that the effect of accounting for uncertainty is relatively small, and obtaining knowledge about the uncertainty in advance yields only a small benefit. However, in absolute terms, these effects can still be considered substantial, as the objective is in the millions per day (see Figure 13). Namely, the VSS is approximately 77-92 thousand Euro, while the EVPI values are around 15-26 thousand euro, which translates to large sums on a yearly basis. Therefore, the price and demand uncertainty should be considered when making decisions on entry-exit capacity.

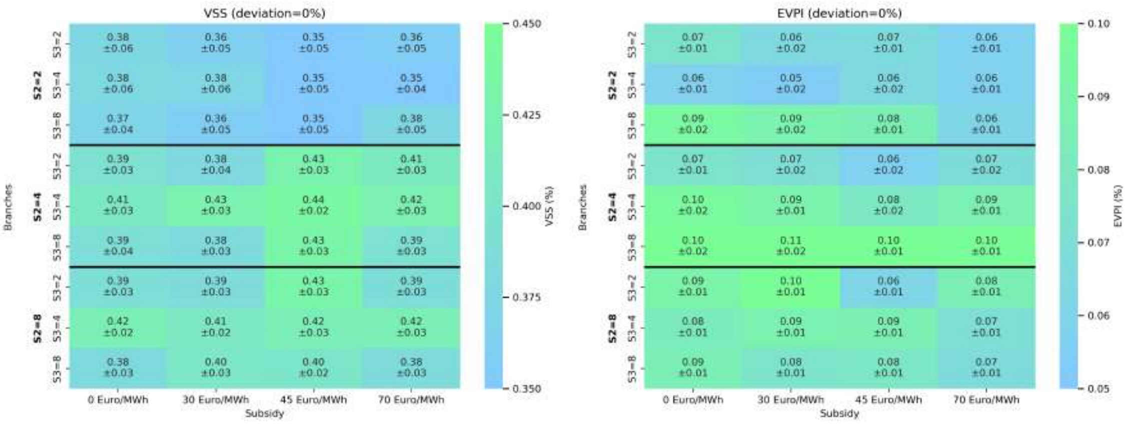

Figure 32: VSS and EVPI as a percentage of the objective value at 0% deviation for different amount of branches and subsidies.

Otherwise, the results where market deviation is allowed can also be examined. For each examined combination of parameters, the values are shown in Figure 33, alongside the standard error. The figure shows that the VSS is not notably different when market constraints are alleviated. Similarly, the EVPI does not show many differences as well, indicating that market constraints do not influence the effectiveness of incorporating multiple scenarios for long-term entry-exit capacity decisions.

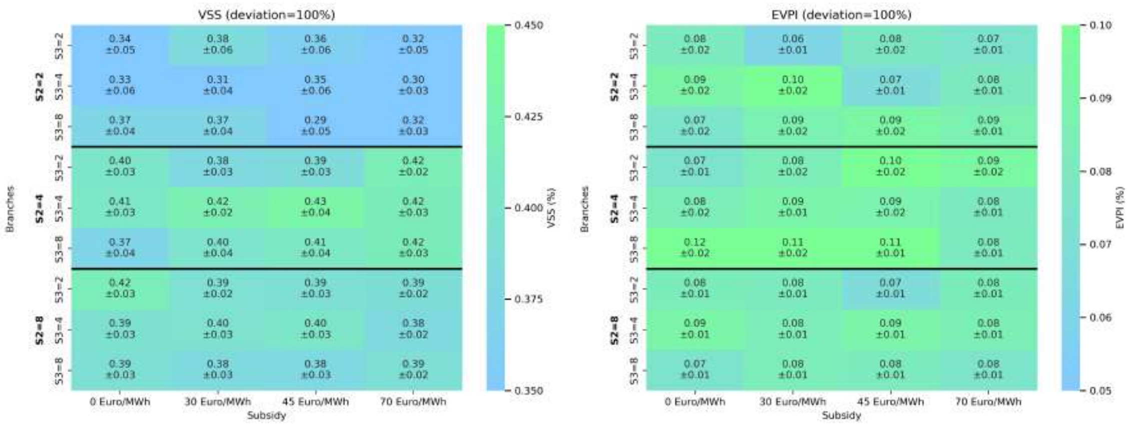

Figure 33: VSS and EVPI as a percentage of the objective value at 100% deviation for different amount of branches and subsidies.

Besides general significance, no pair of VSS and EVPI significantly differ from each other, indicating that the difference in VSS and EVPI do not differ substantially between subsidy levels. However, a superficial view shows that both the VSS and EVPI are lower when only two stage branches are considered for both 0% and 100% deviation. To test this, the non-parametric Mann-Whitney U-test is employed (Chicco et al., 2025). An explanation of the details of the tests can be found in Appendix D.2.1.

The results of the tests are shown in Table 14. The table shows that all groups have significantly different VSS values, while the EVPI is only different between two branches and four branches in stage two. Likely, the lower VSS in stage two can be explained by the lower chance that extreme scenarios appear, in turn making the averaged optimized decisions a better fit than when a lot of uncertainty exist in the model. However, when optimizing fewer scenarios, these extremes can be overlooked, and therefore the amount of scenarios should be set sufficiently high to account for these extreme scenarios.

Table 14: Pairwise Mann-Whitney U test results for different stages (percentages)

Metric	Comparison (average %)	U-stat	Bonferoni p_{value}	Reject Equality
VSS	2 (0.35) vs 4 (0.41)	22690	0.000	Yes
VSS	2 (0.35) vs 8 (0.40)	24539	0.015	Yes
VSS	4 (0.41) vs 8 (0.40)	32742	0.028	Yes
EVPI	2 (0.08) vs 4 (0.09)	24174	0.007	Yes
EVPI	2 (0.08) vs 8 (0.08)	25756	0.136	No
EVPI	4 (0.09) vs 8 (0.08)	30968	0.461	No

5.6 Model Scalability

To apply the model in a practical, the model needs to be scalable. To examine this, the model is run for a different number of scenarios, as well as different networks. Together, this provides an indication on how the model would scale to other case studies.

5.6.1 Scenario Tree Structure

For the amount of scenarios, different combinations are examined. The resulting solve times including the standard deviation is shown in Figure 34. The figure shows that branching in either stage two or stage three yields an increase in solve times, but are not necessarily distinct in the increased solve time. Therefore, the amount of scenarios is a driving factor in the solve time and should be limited to obtain optimal solutions.

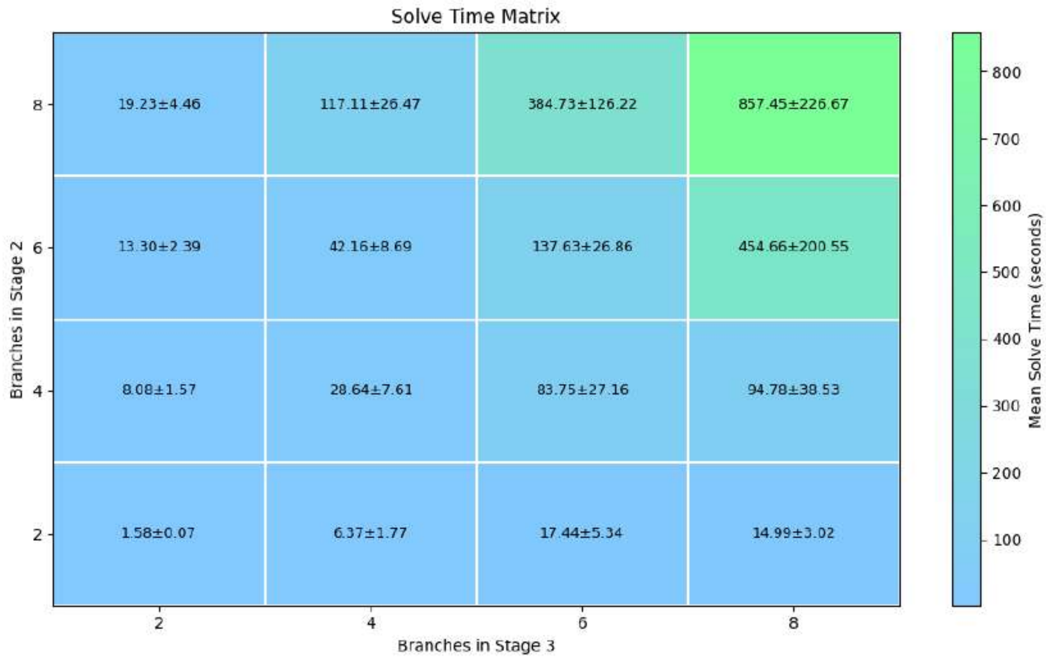

Figure 34: Solve time matrix for different number of scenarios.

5.6.2 Network Structure

Instead, to test the influence of the network structure, networks are generated procedurally, according to the process described in Appendix B.4, where the networks are reflected to obtain in part the aspects of the case study network, while remaining distinct from each other. A correlation matrix between the features can be found in Appendix D.3. The networks are solved at a smaller scenario size, branching four times in stage 2 and 3 respectively (16 scenarios total), to reduce the chance of the model breaking at outliers. The model was solved under the soft missed demand constraint shown in Equation (45) and (46), to ensure the model remained feasible for each sampled network. Each network was run 20 times, to obtain statistically significant results.

A histogram of the natural logarithm of the solve times is shown in Figure 35. The logarithm of the solve time is displayed, to account for the severe right skewed distribution of the solve times. Even with the log scaling, the distribution of the solve time is still right skewed, indicating that the complexity of the network can severely slow down model performance. Therefore, it is of importance to examine how the network structure impacts performance.

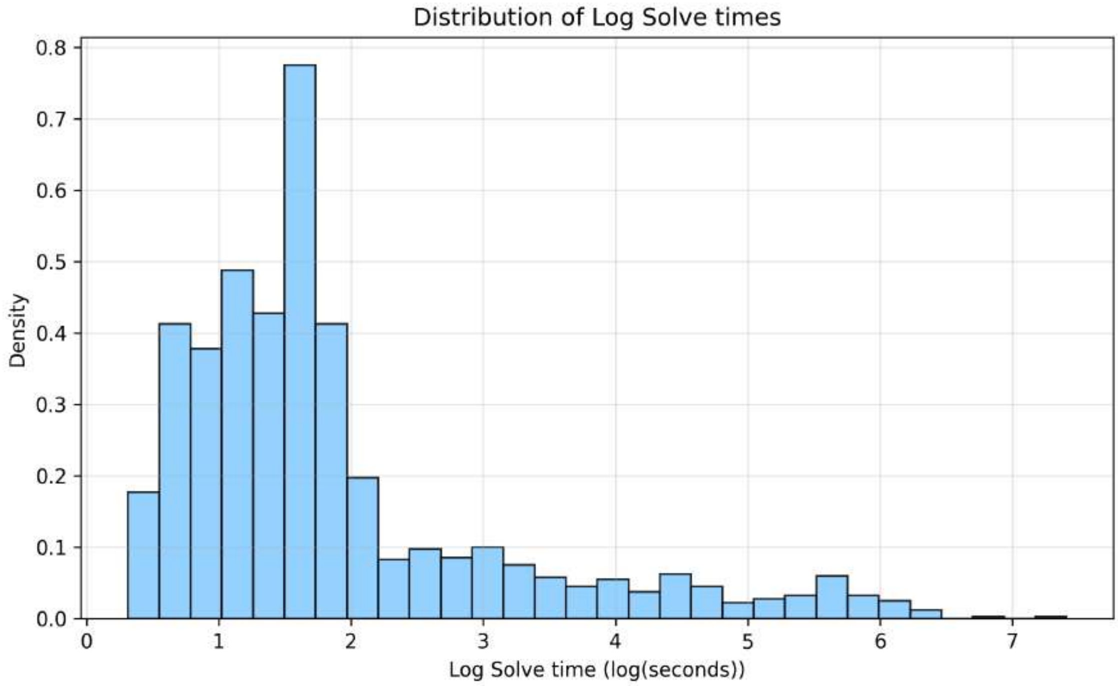

Figure 35: Distribution of the natural logarithm of the solve times for different networks. The figure shows that the original solve time is heavily right skewed.

First, the influence of network size was examined by training a linear regression model on the solve time. Namely, the natural logarithm of the solve time (t), in terms of the amount of the natural logarithm of the nodes $\mid N \mid$ and arcs $\mid A \mid$ is estimated, shown in Equation 57 to reflect the multiplicative nature of the network size, while fitting a linear model. The model was trained on 80% on the generated networks, while 20% was kept hidden to measure performance.

$$\log(t) = \beta_0 + \beta_1 \log(\mid N \mid) + \beta_2 \log(\mid A \mid) + \epsilon \tag{57}$$

The trained regressor provides estimations on the coefficients of the exponent of the nodes and edges. The model obtains the coefficients, significance levels and scores shown in Table 15. The tables show that while the influence of nodes is positive and significant, the influences of the number of edges is negative. This can be explained by the manner of network creation, as the number of nodes and edges are collinear to each other, such that these coefficients cannot be examined on their own. By contrast, the performance of the linear model does show that the network size impacts the solve time of the model, and can explain at least thirty percent of the variance. However, the RMSE shows that the model can still get the solve time wrong by a full magnitude.

(a) Regression coefficients

Variable	Coefficient	p-value
Intercept	-2.399	0.000
Nodes	3.013	0.000
Edges	-1.484	1.97×10^{-7}

(b) Model performance

Metric	Train	Test
R^2	0.332	0.462
RMSE	1.064	0.840

Table 15: Linear regression results for predicting log solve time from network size characteristics.

Besides the network size, the network structure can also influence the solve time. For the current problem, the network structure constitutes network aspects (see (Newman, 2018) for an explanation of the aspects), as well as the percentage of each node type in the network. As the fractions sum to one, the fraction of compression nodes was omitted to avoid overfitting. A list of the features considered for the network structure is shown in Table 16.

Table 16: Network features considered for the random forest regressor.

Features		
Avg In-Deg.	Avg Out-Deg.	Generation %
Cyclomatic	Density	Junction %
Market %	Max In-Deg.	Max Out-Deg.
Processing %	Redundancy	

To examine whether the structure influences the solve time, a random forest regressor (RF) was trained on the residuals (ϵ) of the linear regressor, to determine whether the network structure can provide additional insight into the solve time. A random forest regressor was chosen, as it can incorporate non-linear behavior of the structure into the prediction of the solve time. The RF is trained with 500 trees, at max depth of 3 for each tree, and a minimum of 40 samples per leaf, to avoid overfitting. Nonetheless, the model still overfitted, as shown by the performance of the algorithm shown in Table 17. This can be explained by the limited number of networks in the training data. However, the RF did reduce the MSE, indicating that some of the residuals can be explained by the structure of the network.

Table 17: Model performance metrics.

Metric	Train	Test
R^2	0.359	0.074
RMSE	0.852	0.806

As the regressor was trained on several features, it is important to know which features are drivers of the solve time. Therefore, the feature importance in terms of mean decrease in impurity (*Mean Decrease Impurity (MDI) in Tree Models* 2025) is extracted, as well the slope of the partial dependence (Gupta, 2024).

Figure 36 displays the results for the model characteristics. The figure shows that the percentage of junction node presents the highest influence in the model, and shows that the slope is also positive, indicating that the solve time increases with the number of junction nodes. This is expected, as junction nodes introduce binary variables into the model, which make it harder to solve. In addition, density presents an important factor, although the influence is mixed, as the slope is close to zero. Furthermore, the percentage of market nodes also present a positive influence. This is also expected, as balancing the gas between a higher number of market nodes causes upstream effects, which influences the pressure flow relationship, and differs per scenario. Otherwise, the features provide only a marginal influence, and suggest that besides the size, many aspects of the network structure might not be relevant to predict the solve time.

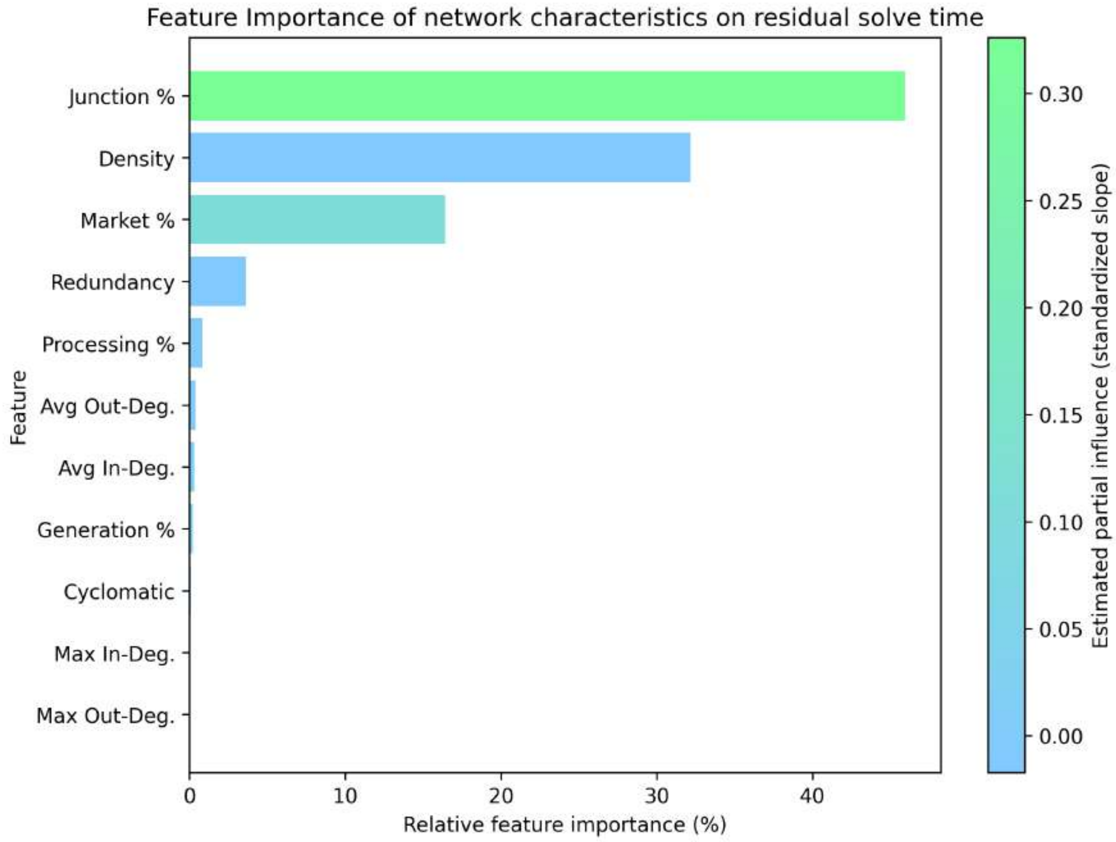

Figure 36: Feature importance of the features with partial dependence slope as color.

Therefore, the influence size of the scenario tree and the network are significant and superlinear. Furthermore, the percentage of junction and market nodes provide a positive influence, while the influence of density is relevant but not necessarily positive. In turn, the size of the scenario tree and the network structure need to be carefully considered when applying the model to a gas network.

"If a man will begin with certainties, he shall end in doubts; but if he will be content to begin with doubts, he shall end in certainties."

— Francis Bacon

6 Conclusion

This thesis examined the integration of non-linear pressure and gas quality constraints in a stochastic linear program to examine the benefits of hydrogen blending in a pipeline network. The model was then applied to a stylized case study, to examine the impact of policy measures on hydrogen blending, sensitivity analysis on the policy measures, and the influence of modeling aspects on the solve time and value of stochasticity. Together, the experiments give rise to policy insights as well as methodological guidance for future applications of the modeling framework in hydrogen infrastructure planning.

6.1 Policy Measures

It was found that hydrogen blending can be stimulated by a subsidy, which, given sufficient production capacity, needs to be sufficiently high to make hydrogen blending economically viable. For the case study, the subsidy needed to be at least 30€/Mwh to have an impact and 45€/Mwh to obtain the highest net welfare effect. In addition, a positive net welfare effect can be generated when introducing a subsidy, when considering the cost of carbon. Instead, putting an obligation on the TSO to inject a minimum amount of hydrogen blending creates a slightly net welfare effect, but greatly limits the amount of possible hydrogen blending. The effect is smaller because the measure must be uniformly applied to each scenario, which limits the flexibility of hydrogen blending between scenarios.

There are also limitations to the possibilities of hydrogen blending. Increasing the subsidy beyond a threshold can reduce the added welfare effect, as natural gas is instead routed to markets where a higher percentage of hydrogen blending is allowed. Furthermore, the possibility of hydrogen blending is limited under market restrictions, as the strictest market connected to an upstream junction determines the fraction of allowed hydrogen to be blended for all other connections to the junction. Cross-collaboration between markets is therefore necessary. In addition, a limitation can be found in the entry-exit booking, where uncertain gas routing can limit hydrogen production, resulting in overbooking of capacity for hydrogen blending.

6.2 Sensitivity Analysis

In addition, for the investigated policy measures, sensitivity analysis was executed on several parameters. Stricter technical limitations were examined, which showed that pipe limitations are binding on the possibilities of hydrogen blending. Closing a pipeline can in specific instances increase hydrogen production, although the influence is usually negative. Increased price volatility increases the objective, but lowers the CVaR. In addition, the increased volatility reduces the influence of hydrogen subsidy, and postpones the amount of bought entry and exit capacity to later stages.

6.3 Scalability and Stochastic Value

Finally, the scalability and stochastic value of the model was examined. It was found that the solve time scales superlinearly in the number of scenarios, while there exists no difference in solve time between branching in the second and third stage of the stochastic program. The network structure also presents influence on the solve time of the model. A trained regression model showed that the network size has a positive influence on the solve times. In addition, the network structure provides additional influence on the model, where the ratio of junction and market nodes increase the solve time, while density has a mixed influence, noted that the trained model had weak performance.

It was found that the VSS is generally low at 0.3%-0.5% of the objective, but not negligible. Furthermore, increasing the scenario tree has a positive effect on the value of the stochastic solution, indicating that sufficient scenarios are needed to capture the full uncertainty. Equivalently, the EVPI is also low at 0.06%-0.12%, indicating that the stochastic program is able to optimize for most of the considered uncertainty. Therefore, extending the model to a stochastic formulation is beneficial in optimizing gas network with entry-exit capacities.

"Sensation furnishes the mind with ideas; reflection gives us ideas of its own operations."

— John Locke

7 Discussion

The conclusions of the thesis demonstrate that hydrogen blending can provide a substantial impact on the Norwegian Continental Shelf, as well as the applicability of the underlying stochastic model. To ground these findings, this section will relate them to existing literature. In addition, this section deliberates on the limitations of the model, case study and experiments respectively. Finally, possibilities for further research are discussed.

7.1 Relation to existing literature

The conclusion gave rise to several findings that are substantiated by literature. The stimulation of hydrogen blending with a subsidy has also been examined by Kanellopoulos et al. (2022, p. 19), who state that a subsidy between 33-45€/Mwh makes hydrogen blending competitive with the natural gas market. This is completely in line with current results, where a similar range results in the highest welfare effect. Sodwatana et al. (2023, p. 1234) show similar findings, where after a conversion of units, a minimum of approximately 31€/Mwh is required to stimulate hydrogen blending, which also corresponds to the current findings. In addition, they examine a hydrogen obligation, which also showed that hydrogen is exactly blended at the limit, as it is not economically viable. In addition, the positive net welfare effect from subsidies is substantiated by (Klatzer et al., 2024), who observed a decreased system cost when including carbon pricing.

Limitations of hydrogen blending are less articulated in the academic literature; rather, they are embedded within policy documents. Namely, overprovision could become a serious issue, as hydrogen producers could lose their nominations (Gassco, 2026a, p. 15). In addition, Fleming (2024, p. 22) notes the fact that cross-market harmonization is required to reach the full benefits of hydrogen blending, which relates to the limitation that arises from junction nodes.

Kanellopoulos et al. (2022, p. 18) matches the findings of the sensitivity analysis, who summarize that technical limits on pipelines can severely limit hydrogen blending. In addition, the increase in objective due to an increase in price sensitivity is also measured by Saliba and Dimitrakopolous (2019) and Mitrai et al. (2024), who both note the increased arbitrage possibilities.

Finally, the current model uses aspects of the model of Markhorst et al. (2026), such that the scalability of both models can be compared. In terms of scenario tree size, the current model is notably slower than Markhorst et al. (2026), likely due to the inclusion of binary variables in the operational stage. The VSS is present, and the EVPI is lower in the current problem than in Markhorst et al. (2026), because storage is not taken into account. To compare the scalability in network size, the problem can be compared against multi-commodity flow problems (Gendron and Gouveia, 2017; F. Zhang and Boyd, 2025), which are easier to solve as they are not stochastic problems. The current problem is notably more complex and has a slower base solve time, but scales better in the number of nodes compared to the multi-commodity flow problems.

7.2 Limitations

This thesis has explicated how to construct a stochastic linear program that incorporates technical pressure and quality constraints, which was then applied to a stylized case study to illuminate the benefits of hydrogen blending. However, there are limitations on the research that should be noted to contextualize the findings. Namely, the developed model has made design choices that limits the accuracy of the underlying system. In addition, the formulation of the case study might not fully reflect the conditions on the Norwegian Continental Shelf. Finally, the boundary confines under which the experiments hold are explained.

7.2.1 Model Limitations

Most modeling choices are substantiated by their existence in previous models. Nonetheless, some choices might not reflect the decisions of the TSO precisely. An example of this can be found in the operating pressure increases at compression nodes. The compressibility factor was determined to be fixed for every compression node, to compute the fuel consumption constants associated with compression. Although this choice is also made by Tomasgard et al. (2007), it does not reflect the decisions of the TSO, where compression factors can be chosen day by day (Wong and Larson, 1968; Das et al., 2025). Therefore, the compression constraints in the model could be improved upon.

In the model, it is also assumed that booking in an earlier stage is beneficial. This can be artificially modeled by increasing the cost of booking in later stages, to encourage booking in earlier stages. In actuality, booking does not become expensive closer to the delivery date, but instead, less capacity is available in later stages, which encourages suppliers to book earlier. Therefore, the current model can only simulate this behavior by tuning the price increases of the booking cost in later stages, but might not reflect actual behavior, due to the difference between formulation and actual booking process.

In addition, the booking market was viewed solely from the perspective of the TSO, while suppliers actually book capacity. This introduces limitations, as the decisions by suppliers might not align with the social welfare driven goals of the TSO. Under full competition, it was stated that the absence of strategic behavior could be assumed between suppliers on the booking market, taken directly from Markhorst et al. (2026). However, in natural gas networks, suppliers might have substantial market power (Grimm et al., 2019). Strategic behavior arises from this. With market power, the market price is not merely stochastic, but also influenced by the booking decisions of the supplier, as they can drive up the price of some markets by delivering less. As this effect is marginal for interconnected natural gas markets, it can be disregarded for modeling. However, when hydrogen blending is introduced, the violation plays a larger role. For example, suppose a supplier controls a large share of the natural gas supply to the market, such that it has market power, and starts hydrogen production for blending. In this case, the supplier might limit the flow of gas to certain markets, to make hydrogen blending for those markets financially attractive. Naturally, this has to balance with the allowed blending rate, yielding possibly interesting dynamics. Therefore, the applicability of the model in a system with strategic suppliers is limited.

Finally, the model itself does not scale very well in some aspects. Namely, the model does not scale very well in the number of scenarios. This can become a problem for graphs with a substantial number of market nodes, where a limited number of scenarios might not capture sufficient patterns of market behavior, and in turn miss relations between markets. The high computational complexity likely stems from the integer variables in the model, which can slow down the solve process. For example, homogeneous splitting introduces integers in the model, which can slow down model performance, especially when more components get introduced. Therefore, the model size is limited through its use of integer variables.

7.2.2 Case Study Limitations

The case study derives its characteristics from true to life data on the network and gas markets. However, through the implementation of the case study, some aspects of the underlying network in the Norwegian Continental Shelf might be lost. In general, the availability of public data was limited, as some characteristics of the network are withheld from the public to protect commercially sensitive information and ensure operational security. The most notable examples of this arise in the production, market and compression node characteristics. For example, the presented generation costs might not represent the marginal production costs, such that the subsidy thresholds are sensitive to these costs. Therefore, as the data might not reflect the actual network, the direct actionability of the findings for the Norwegian Continental Shelf remains limited.

In addition to the limited data, the case study is also stylized. In the construction of the network, only pipelines owned by Gassled are considered, which is the largest part of the network operated by Gassco. This restricts the scope, but allows hydrogen blending to not flow to pipeline owners who might not be interested in blending. However, in the actual network, there might be connections between the pipeline owners, which could restrict hydrogen blending further. The model does already allow for these constraints, however, the implementation might show that hydrogen blending becomes impossible on the Norwegian Continental Shelf. Moreover, compression nodes were constructed solely based on their position in the network, which might not reflect their actual function. Therefore, the applicability of the case study in its stylized form is limited.

Besides the limited representability, the position of the Norwegian Continental Shelf in the European gas market might not lend itself for hydrogen blending. As shown in the thesis, hydrogen blending requires cross-collaboration between exit points in the system to achieve the highest benefit. As the Norwegian grid is placed at the starting point for a substantial amount of European gas, this requires a lot of coordination. In addition, the considered hydrogen production plants are currently not in development and would therefore have to be reconsidered for hydrogen blending to take fruition. Furthermore, the possibility of liquefying gas for higher transport efficiency vanishes with blending, as the temperature and pressure required to liquefy blended gas is nearly unattainable (Peletiri et al., 2019). Any downstream market that wants to use LNG can therefore not use the blended gas from Norway. The Norwegian Continental Shelf might therefore not be an ideal target, and selecting a different network characterized by fewer and less interconnected downstream markets could yield a less complex optimization problem which offers more straightforward opportunities for blending.

In addition to the design of the case study network, the surrounding hyperparameters can produce limitations on the findings. Namely, while the choice of cutting plane points provide accurate values for the relationship between pressure and flow, the choice of homogeneous splitting points was limited, to maintain a reasonable solve time. However, a discrete choice between flows can limit the objective, such that with more finetuned bounds, the objective, can be increased (for a more detailed explanation, see Appendix C.3). In addition, the discretization of density bounds was limited to one bound for the case study, as the influence on solve time is large. Nonetheless, because these parameters affected the obtained solutions while not being directly attributable to the case study itself, they constrain the overall accuracy of the model.

Finally, the scenario tree was sampled rather than constructed manually. As the scenario tree size is limited, this can lead to asymmetries in the scenario tree, where for example, a market node only obtains low prices by coincidence due to the sampling, without a counterbalanced scenario with a high price. These asymmetries could in turn lead to unrealistic first stage booking decisions, which might resemble actual booking patterns. Another limitation of the current sampling method is that in its basic form, there exists no correlation between price shocks at markets. However, for example, the UK market points are likely to be highly correlated, as they serve the same market. Nonetheless, this choice was made to enable measuring results with some statistical significance as well as gain more flexibility in the sensitivity analysis, but does come with these added drawbacks.

7.2.3 Experiment Limitations

The experiments are executed with care, and for the most part subsist in changing only a few aspects of the model. However, some experiments are limited in their scope. Namely, when a subsidy is implemented, the TSO does not actually benefit, as they do not have a profit motive. Instead, the subsidy should go to the hydrogen supplier, who benefits from the lower costs. However, the TSO might not be inclined to allow hydrogen on their network. Therefore, while the two policy measures of a subsidy and a blending obligation are examined separately in the thesis, in practice, they might need to be implemented simultaneously in some form to enable hydrogen blending.

In addition, the current examination of the impact of solve time on the scalability of the model has some limitations. Namely, for the examination of the influence of the network size, the collinearity between nodes and edges might have caused edges to have a negative exponent, while this might not accurately reflect solve time behavior. In addition, the Random Forest exhibits pronounced overfitting, which limits the applicability of the results. In fact, when running the model on different test sets, while the importance and direction of coefficients remain the same, the test set performances were not significantly larger than zero, indicating that the random forest does not necessarily explain the solve time behavior from the network structure. Therefore, the implications of the influence of the network structure are limited.

7.3 Further Research

Both the findings and limitations of the current thesis show room for further research. Possible model extensions and adaptations are explored first. Second, additional experiments are illuminated. Finally, other possible case studies are provided that could further drive insight into hydrogen blending.

7.3.1 Model Extensions & Adaptations

To increase the applicability of the model, several extensions can be implemented to model different aspects of the gas network. First, the inclusion of bidirectional pipelines can be included in the model, as shown in Appendix A.1, which would allow to examine networks where gas flows from two directions, such as the Dutch (GTS, 2026b) or Italian (SNAM, 2018) gas network. Second, although not currently necessary, quality constraints on the overall gas mix can be implemented instead of per component, as shown in Appendix A.2, which could allow for additional blending. Third, storage can be implemented into the model, following Appendix A.3. However, this would require an additional time index, which could hinder model performance further.

Instead, the model can also be adapted, to increase model performance or to better reflect the decisions of the TSO. First, the discretization of the homogeneous splits may be replaced by McCormick envelopes (Urban, 2021), which could speed up computation, at a possible loss of accuracy in splitting. To obtain a high accuracy and avoid binary variables, tight bounds must be set on the outgoing flows, which is possible when tight demand exists and is known per scenario, as gas must flow to fulfill demand. In turn, McCormick envelopes could result in quicker solve times at high accuracy. The model can also be adapted to circumvent the limitation of fixed pressure increases at compressors. Namely, a stage 2 variable can be introduced that fixes the pressure increases for the next day based on a discrete choice, connected with the fuel constants. Although it may increase solve times, it models an extra TSO decision, better reflecting their decision process.

7.3.2 Additional Experiments

Besides possible additions to the model, the model can also be utilized in its current form to discover additional findings. To this aim, several experiments can be developed. The sensitivity analyses can be extended to account for more changes in the model. Namely, for the closure of pipelines, only the closure of some pipelines related to hydrogen blending were examined. This can be extended to any number of pipelines breaking in the system, to measure the resiliency of the Norwegian gas network. In addition, only complete pipeline closure was examined, though the impact of hydrogen blending could also be assessed when some pipelines are closed only for hydrogen. Furthermore, when correlation between prices at market nodes was examined, correlation was given by only one systematic component. However, this can be extended to a correlation matrix, to identify patterns in gas delivery between the markets on the Norwegian Continental Shelf.

Moreover, The analysis of how network structure affects solve time can be further extended. The easiest solution to overfitting is to generate additional networks and solve these, to gain extra datapoints for in the training and test set, allowing the model to better fit to the actual distribution. Furthermore, training networks with more variability would also reduce the collinearity between the nodes and edges of the network, allowing for a better examination of the influence of the size of the network. Together, these improvements could drive further insights into the scalability of the model.

Finally, in the case study, the production of natural gas and hydrogen gas is fixed between scenarios. However, problems at natural gas plants could reduce production, and hydrogen production is dependent on electricity availability and prices, and therefore has an added degree of uncertainty. The model already allows the production limit $G_{n,m}$ to be distinct between scenarios, and can therefore be directly be applied to the model. Uncertain production amounts can produce additional system instability, which in turn could further illuminate the limitations of hydrogen blending. It could therefore be relevant to examine uncertain production in hydrogen blending.

7.3.3 Additional Case studies

In addition to changes in the model and the execution of more experiments, other case studies can also be considered to further substantiate and contextualize the findings. Three additional case studies should be considered. First, the current case study can likely be restructured to account for all owners of pipelines on the Norwegian Continental Shelf. This would allow to examine the full system, which can in turn yield additional insights into the system. However, to limit the network size, the system can be simplified elsewhere. Namely, the example usage showed that it was nearly always beneficial to produce up to the maximum amount, therefore, the upstream parts of the network can be taken as a given instead, until a routing decision to a market is made. In turn this would save computation time, without loss to the findings on hydrogen blending.

Second, while the UK currently allows very little hydrogen blending on its network (IEA, 2025), it could present a prime candidate. Specifically, as the UK is primarily a consumer of natural gas, it is not required to engage in cross-collaboration between markets that Norway is exposed to. In addition, they employ an entry-exit system that fits directly into the model formulation (Gas, 2022). Therefore, the UK can become an example on how the shown limitations on hydrogen blending can be overcome.

Finally, the network in France can be used to determine whether the model reflects reality, as hydrogen blending is already allowed up to 6% in their network and are examining the feasibility of scaling to 10% (IEA, 2025). In addition, while this would require the implementation of bidirectional pipelines (see Appendix A.1), the model is again fit to deal with their entry-exit system (CRE, 2024).

Together, these case studies would further pinpoint the advantages and drawbacks of hydrogen blending within European gas transmission system. In addition, the supplementary model additions and experiments can provide accuracy and depth to the findings shown in the thesis. However, this thesis has already suggested that hydrogen gas can provide a substantial impact for the energy transition. Therefore, the further research can alongside this thesis show that hydrogen blending is not merely a bonus to the existing energy system, but a meaningful step towards carbon neutrality.

References

Aastad, Aurora (Apr. 2025). *Annual Report 2024*. en-GB. URL: https://gassco.eu/en/annual-report-2024/ (visited on 01/16/2026).

Adomaitis, Nerijus and Nora Buli (Jan. 2025). "Norway gas exports expected to stay close to last year's record levels". en. In: *Reuters*. URL: https://www.reuters.com/business/energy/norway-gas-output-hit-record-2024-seen-slightly-lower-2025-2025-01-09/ (visited on 01/23/2026).

Ajinkya, Bipin B. and Prem C. Jain (Nov. 1989). "The behavior of daily stock market trading volume". In: *Journal of Accounting and Economics* 11.4, pp. 331–359. ISSN: 0165-4101. DOI: 10.1016/0165-4101(89)90018-9. URL: https://www.sciencedirect.com/science/article/pii/0165410189900189 (visited on 04/24/2026).

Amoiralis, Eleftherios I. and Kostas Andriosopoulos (Nov. 2017). "Challenges for a compliance officer in the liberalized EU energy market: A case study on the Greek gas transmission system operator". In: *Energy Policy* 110, pp. 117–125. ISSN: 0301-4215. DOI: 10.1016/j.enpol.2017.08.011. URL: https://www.sciencedirect.com/science/article/pii/S0301421517305050 (visited on 01/23/2026).

Aristotle (2026). *Posterior Analytics*. en-US. URL: https://iep.utm.edu/aristotle/ (visited on 06/28/2026).

Babonneau, Frederic, Yuri Nesterov, and Jean-Philippe Vial (Aug. 2009). "Design and Operations of Gas Transmission Networks". en. In: *Operations Research*. URL: https://pubsonline.informs.org/doi/abs/10.1287/opre.1110.1001 (visited on 05/05/2026).

Beemster, Larson (June 2026). *LarsonVU/hydrogen_gas*. original-date: 2026-01-14T17:00:56Z. URL: https://github.com/LarsonVU/hydrogen_gas (visited on 06/30/2026).

Bødal, Espen Flo, Dharik Mallapragada, Audun Botterud, and Magnus Korpås (Nov. 2020). "Decarbonization synergies from joint planning of electricity and hydrogen production: A Texas case study". In: *International Journal of Hydrogen Energy* 45.58, pp. 32899–32915. ISSN: 0360-3199. DOI: 10.1016/j.ijhydene.2020.09.127. URL: https://www.sciencedirect.com/science/article/pii/S0360319920335679 (visited on 11/06/2025).

Brandão, António, Isabel Soares, Paula Sarmento, Joana Resende, and Joana Pinho (May 2014). "Regulating international gas transport: Welfare effects of postage stamp and entry–exit systems". In: *Energy* 69, pp. 86–95. ISSN: 0360-5442. DOI: 10.1016/j.energy.2014.01.006. URL: https://www.sciencedirect.com/science/article/pii/S0360544214000139 (visited on 01/16/2026).

Bynum, Michael L., Gabriel A. Hackebeil, William E. Hart, Carl D. Laird, Bethany L. Nicholson, John D. Siirola, Jean-Paul Watson, and David L. Woodruff (2021). *Pyomo — Optimization Modeling in Python*. en. Vol. 67. Springer Optimization and Its Applications. Cham: Springer International Publishing. DOI: 10.1007/978-3-030-68928-5. URL: http://link.springer.com/10.1007/978-3-030-68928-5 (visited on 03/25/2026).

Callen, Jeffrey L. (1978). "Production, Efficiency, and Welfare in the Natural Gas Transmission Industry". In: *The American Economic Review* 68.3, pp. 311–323. ISSN: 0002-8282. URL: https://www.jstor.org/stable/1805263 (visited on 01/16/2026).

Cheng, C., K. van Greevenbroek, and I. Viole (Oct. 2024). "The competitive edge of Norway's hydrogen by 2030: Socio-environmental considerations". In: *International Journal of Hydrogen Energy* 85, pp. 962–975. ISSN: 0360-3199. DOI: 10.1016/j.ijhydene.2024.08.377. URL: https://www.sciencedirect.com/science/article/pii/S0360319924035468 (visited on 01/23/2026).

Chicco, Davide, Andrea Sichenze, and Giuseppe Jurman (Aug. 2025). "A simple guide to the use of Student's t-test, Mann-Whitney U test, Chi-squared test, and Kruskal-Wallis test in biostatistics". In: *BioData Mining* 18, p. 56. ISSN: 1756-0381. DOI: 10.1186/s13040-025-00465-6. URL: https://pmc.ncbi.nlm.nih.gov/articles/PMC12366075/ (visited on 05/06/2026).

Clever Markets (Oct. 2025). *National Balancing Point (NBP) Explained for Gas Traders*. en-US. Section: Uncategorized. URL: https://clevermarkets.com/blog/national-balancing-point-a-strategic-guide/ (visited on 02/23/2026).

CRE (2024). "Deliberation of the French Energy Regulatory Commission of 30 January 2024 on the decision on the tariff for the use of the natural gas transmission networks of GRTgaz and Teréga". en. In: 2024.

Dahl, Hans Jørgen (2001). "Norwegian natural gas transportation systems: Operations in a liberalized European gas market". en. In: URL: https://nva.sikt.no/registration/0198cc467162-8e44f7e1-7713-49e4-b28e-56f1250356ad (visited on 01/16/2026).

Dale, Sigbjørn (Jan. 2025). *Rørledninger - Kartkatalogen*. URL: https://kartkatalog.geonorge.no/metadata/pipelines/3a31a1f1-f836-4565-937f-731286fb8baa (visited on 11/13/2025).

Das, Pronob, Andrew Rowe, Peter Wild, and Chiradeep Majumdar (May 2025). "Modeling and optimization of a hydrogen blended natural gas transmission network: Effect of compressor electrification". In: *International Journal of Hydrogen Energy* 127, pp. 497–510. ISSN: 0360-3199. DOI: 10.1016/j.ijhydene.2025.03.380. URL: https://www.sciencedirect.com/science/article/pii/S0360319925015320 (visited on 01/30/2026).

Dralle, Tilman Michael (2018). "The Unbundling and Unbundling-Related Measures in the EU Energy Sector". en. In: *Ownership Unbundling and Related Measures in the EU Energy Sector: Foundations, the Impact of WTO Law and Investment Protection*. Ed. by Tilman Michael Dralle. Cham: Springer International Publishing, pp. 21–63. ISBN: 978-3-319-77797-9. DOI: 10.1007/978-3-319-77797-9_2. URL: https://doi.org/10.1007/978-3-319-77797-9_2 (visited on 01/27/2026).

Egging, Rudolf Gerardus (2010). "Multi-period natural gas market modeling Applications, stochastic extensions and solution approaches". English. Publication Title: ProQuest Dissertations and Theses. Ph.D. United States – Maryland: University of Maryland, College Park. ISBN: 978-1-124-48658-1. URL: https://www.proquest.com/docview/855613535/abstract/BCF1CC4591FF4F9DPQ/1 (visited on 01/23/2026).

Egging, Ruud, Alois Pichler, Øyvind Iversen Kalvø, and Thomas Meyer Walle–Hansen (May 2017). "Risk aversion in imperfect natural gas markets". In: *European Journal of Operational Research* 259.1, pp. 367–383. ISSN: 0377-2217. DOI: 10.1016/j.ejor.2016.10.020. URL: https://www.sciencedirect.com/science/article/pii/S0377221716308530 (visited on 01/23/2026).

Egging, Ruud and Asgeir Tomasgard (Apr. 2018). "Norway's role in the European energy transition". In: *Energy Strategy Reviews* 20, pp. 99–101. ISSN: 2211-467X. DOI: 10.1016/j.esr.2018.02.004. URL: https://www.sciencedirect.com/science/article/pii/S2211467X18300075 (visited on 01/23/2026).

Egging-Bratseth, Ruud, Anne Neumann, and Kjetil Midthun (Jan. 2025). "Natural gas networks". In: pp. 101–114. ISBN: 978-0-323-91407-9. DOI: 10.1016/B978-0-323-91013-2.00016-2.

Emissieautoriteit, Nederlandse (Oct. 2025). *Tarieven CO2-heffing*. nl. webpagina. Last Modified: 2026-01-21T13:14:58.963Z. URL: https://www.emissieautoriteit.nl/regelgeving/co2-heffing/tarieven-co2-heffing (visited on 06/22/2026).

EngineersToolbox (2003a). *Air - Composition and Molecular Weight*. en. URL: https://www.engineeringtoolbox.com/air-composition-d_212.html (visited on 02/02/2026).
— (2003b). *Density of Gases*. en. URL: https://www.engineeringtoolbox.com/gas-density-d_158.html (visited on 02/24/2026).
— (2003c). *Gases - Ratios of Specific Heat*. en. URL: https://www.engineeringtoolbox.com/specific-heat-ratio-d_608.html (visited on 01/30/2026).
— (2003d). *Higher Calorific Values of Common Fuels: Reference & Data*. en. URL: https://www.engineeringtoolbox.com/fuels-higher-calorific-values-d_169.html (visited on 02/23/2026).
Entsog (May 2018). *Position Paper on Gas Quality*.
— (Dec. 2024). "Gas Quality Monitoring Report – First Edition". en. In.
Evangelopoulou, Stavroula, Alessia De Vita, Georgios Zazias, Pantelis Capros, Stavroula Evangelopoulou, Alessia De Vita, Georgios Zazias, and Pantelis Capros (July 2019). "Energy System Modelling of Carbon-Neutral Hydrogen as an Enabler of Sectoral Integration within a Decarbonization Pathway". en. In: *Energies* 12.13. ISSN: 1996-1073. DOI: 10.3390/en12132551. URL: https://www.mdpi.com/1996-1073/12/13/2551 (visited on 01/19/2026).
Fleming, Ruven, ed. (2024). *The Cambridge Handbook of Hydrogen and the Law*. Cambridge Law Handbooks. Cambridge: Cambridge University Press. ISBN: 978-1-009-45923-5. DOI: 10.1017/9781009459259. URL: https://www.cambridge.org/core/books/cambridge-handbook-of-hydrogen-and-the-law/C5CC681490CA41DD6AF906666BC3C0BB (visited on 06/23/2026).
Fodstad, Marte, Pedro Crespo del Granado, Lars Hellemo, Brage Rugstad Knudsen, Paolo Pisciella, Antti Silvast, Chiara Bordin, Sarah Schmidt, and Julian Straus (May 2022). "Next frontiers in energy system modelling: A review on challenges and the state of the art". In: *Renewable and Sustainable Energy Reviews* 160, p. 112246. ISSN: 1364-0321. DOI: 10.1016/j.rser.2022.112246. URL: https://www.sciencedirect.com/science/article/pii/S136403212200168X (visited on 01/16/2026).
Fodstad, Marte, Ruud Egging, Kjetil Midthun, and Asgeir Tomasgard (Dec. 2016). "Stochastic Modeling of Natural Gas Infrastructure Development in Europe under Demand Uncertainty". EN. In: *The Energy Journal* 37.3_suppl, pp. 5–32. ISSN: 0195-6574. DOI: 10.5547/01956574.37.SI3.mfod. URL: https://doi.org/10.5547/01956574.37.SI3.mfod (visited on 01/16/2026).
Francis Bacon (Jan. 2004). *The Advancement of Learning*. URL: https://www.gutenberg.org/files/5500/5500-h/5500-h.htm (visited on 06/29/2026).
Gas, National (June 2022). *Capacity Guidelines June 2022*. en-gb. URL: https://www.nationalgas.com/our-businesses/system-operation/our-regulatory-documents (visited on 06/24/2026).
Gassco (Apr. 2023). *Millions of Europeans put their trust in Gassco every single day.*
— (Jan. 2024). *BOOKING MANUAL*. URL: https://gassco.eu/wp-content/uploads/2024/10/Booking-Manual-01.10.2024-.pdf.
— (Jan. 2026a). *Gassled Terms and Conditions*. URL: https://gassco.eu/wp-content/uploads/2026/01/Gassled-Terms-and-Conditions-01.01.2026-with-Appendices.pdf.
— (2026b). *Tariffs and areas*. en-GB. URL: https://gassco.eu/en/shippers/tariffs-and-areas/ (visited on 02/23/2026).
— (2026c). *Gassco Map*. no. URL: https://map.gassco.eu/rorledninger/zeepipe (visited on 02/23/2026).

Gendron, Bernard and Luis Gouveia (May 2017). “Reformulations by Discretization for Piecewise Linear Integer Multicommodity Network Flow Problems”. In: *Transportation Science* 51.2, pp. 629–649. ISSN: 0041-1655. DOI: 10.1287/trsc.2015.0634. URL: https://pubsonline.informs.org/doi/abs/10.1287/trsc.2015.0634 (visited on 12/11/2025).

Gillessen, Bastian, Hans-Josef Allelein, Joachim Müller-Kirchenbauer, and Detlef Stolten (2020). *Auswirkungen der Energiewende auf das deutsche Gastransportsystem*. German. Schriften des Forschungszentrums Jülich. Reihe Energie & Umwelt/Energy & environment 502. Jülich: Forschungszentrum Jülich GmbH, Zentralbibliothek, Verlag. ISBN: 978-3-95806-487-4.

GreenH (2026). *Projects*. en-GB. URL: https://greenh.no/en/projects/ (visited on 01/20/2026).

Grimm, Veronika, Lars Schewe, Martin Schmidt, and Gregor Zöttl (Apr. 2019). “A multilevel model of the European entry-exit gas market”. en. In: *Mathematical Methods of Operations Research* 89.2, pp. 223–255. ISSN: 1432-5217. DOI: 10.1007/s00186-018-0647-z. URL: https://doi.org/10.1007/s00186-018-0647-z (visited on 01/20/2026).

Growitsch, Christian and Marcus Stronzik (Oct. 2014). “Ownership unbundling of natural gas transmission networks: empirical evidence”. en. In: *Journal of Regulatory Economics* 46.2, pp. 207–225. ISSN: 1573-0468. DOI: 10.1007/s11149-014-9252-0. URL: https://doi.org/10.1007/s11149-014-9252-0 (visited on 01/16/2026).

GTS (2023). *Entry and exit capacity*. en. URL: https://www.gasunietransportservices.nl/en/shipper-trader/capacity-booking/entry-and-exit-capacity (visited on 02/09/2026).

— (2026a). *Entry and exit capacity*. en. URL: https://www.gasunietransportservices.nl/en/shipper-trader/capacity-booking/entry-and-exit-capacity (visited on 02/09/2026).

— (2026b). *The transmission network*. en. URL: https://www.gasunietransportservices.nl/en/network-operations/the-transmission-network (visited on 06/24/2026).

Gupta, Mehul (Feb. 2024). *Understanding Partial Dependence Plots (PDPs)*. en. URL: https://medium.com/data-science-in-your-pocket/understanding-partial-dependence-plots-pdps-415346b7e7f1 (visited on 06/16/2026).

Gurobi (Mar. 2026). *Gurobi Optimizer Reference Manual*. URL: https://docs.gurobi.com/projects/optimizer/en/current/ (visited on 03/25/2026).

Hailemariam, Abebe and Russell Smyth (May 2019). “What drives volatility in natural gas prices?” In: *Energy Economics* 80, pp. 731–742. ISSN: 0140-9883. DOI: 10.1016/j.eneco.2019.02.011. URL: https://www.sciencedirect.com/science/article/pii/S0140988319300623 (visited on 05/12/2026).

Hasturk, Umur, Albert H. Schrotenboer, Kees Jan Roodbergen, and Evrim Ursavas (Dec. 2025). *Multi-period Stochastic Network Design for Combined Natural Gas and Hydrogen Distribution*. arXiv:2312.13388 [math] version: 1. DOI: 10.48550/arXiv.2312.13388. URL: http://arxiv.org/abs/2312.13388 (visited on 01/20/2026).

Hellemo, Lars, Kjetil Midthun, Asgeir Tomasgard, and Adrian Werner (May 2012). “Multi-Stage Stochastic Programming for Natural Gas Infrastructure Design with a Production Perspective”. In: *Stochastic Programming*. Vol. Volume 4. World Scientific Series in Finance Volume 4. WORLD SCIENTIFIC, pp. 259–288. ISBN: 978-981-4407-50-2. DOI: 10.1142/9789814407519_0010. URL: https://www.worldscientific.com/doi/abs/10.1142/9789814407519_0010 (visited on 01/27/2026).

Hoeven, Tom van der (2004). *Math in gas and the art of linearization*. Groningen: Energy Delta Institute. ISBN: 978-90-367-1990-2.

HYDS (2026). *Ongoing projects*. en-US. URL: https://hydrogensolutions.no/about/ongoing-projects/ (visited on 01/20/2026).

ICE (Oct. 2025). *Open Interest across ICE's Global Futures and Options Markets Reaches a Record 107 Million Contracts*. en-US. URL: https://ir.theice.com/press/news-details/2025/Open-Interest-across-ICEs-Global-Futures-and-Options-Markets-Reaches-a-Record-107-Million-Contracts/default.aspx (visited on 02/24/2026).

— (2026a). *Dutch TTF Natural Gas Options (Futures Style Margin)*. URL: https://www.ice.com/products/71085679/Dutch-TTF-Natural-Gas-Options-Futures-Style-Margin (visited on 02/24/2026).

— (2026b). *UK NBP Natural Gas Daily Future*. URL: https://www.ice.com/products/20774967/UK-NBP-Natural-Gas-Daily-Future (visited on 02/23/2026).

IEA (Sept. 2005). "A review of natural CO2 occurrences and their relevance to CO2 storage." In.

— (May 2025). *Northwest European Hydrogen Monitor 2025 – Analysis*. en-GB. URL: https://www.iea.org/reports/northwest-european-hydrogen-monitor-2025 (visited on 01/21/2026).

Jia, Guanwei, Mingyu Lei, Mengya Li, Weiqing Xu, Rui Li, Yanghui Lu, and Maolin Cai (Sept. 2023). "Hydrogen embrittlement in hydrogen-blended natural gas transportation systems: A review". In: *International Journal of Hydrogen Energy* 48.82, pp. 32137–32157. ISSN: 0360-3199. DOI: 10.1016/j.ijhydene.2023.04.266. URL: https://www.sciencedirect.com/science/article/pii/S0360319923020967 (visited on 11/06/2025).

John Locke (2004). "An Essay Concerning Human Understanding Book II: Ideas". en. In.

Kanellopoulos, Konstantinos, Sebastian Busch, FELICE Matteo De, Sergio Giaccaria, and Anca Costescu (2022). *Blending hydrogen from electrolysis into the European gas grid*. en. ISBN: 9789276463467 ISSN: 1831-9424. DOI: 10.2760/908387. URL: https://publications.jrc.ec.europa.eu/repository/handle/JRC126763 (visited on 06/17/2026).

Klatzer, T., U. Bachhiesl, S. Wogrin, and A. Tomasgard (Feb. 2024). "Ramping up the hydrogen sector: An energy system modeling framework". In: *Applied Energy* 355, p. 122264. ISSN: 0306-2619. DOI: 10.1016/j.apenergy.2023.122264. URL: https://www.sciencedirect.com/science/article/pii/S0306261923016288 (visited on 01/23/2026).

Kopytin, Ivan Aleksandrovich, Alexander Oskarovich Maslennikov, and Stanislav Vyacheslavovich Zhukov (May 2022). "Europe in World Natural Gas Market: International Transmission of European Price Shocks". en. In: *International Journal of Energy Economics and Policy* 12.3, pp. 8–15. ISSN: 2146-4553. DOI: 10.32479/ijeep.12941. URL: https://econjournals.com/index.php/ijeep/article/view/12941 (visited on 05/16/2026).

Kotek, Peter, Pedro Crespo del Granado, Ruud Egging, and Borbala T. Toth (Sept. 2019). "European Natural Gas Infrastructure in the Energy Transition". In: *2019 16th International Conference on the European Energy Market (EEM)*. ISSN: 2165-4093, pp. 1–6. DOI: 10.1109/EEM.2019.8916432. URL: https://ieeexplore.ieee.org/document/8916432 (visited on 01/16/2026).

Lakeit, Kim Malin, Gassco, and Dena (Nov. 2023). *GER-NOR Joint feasibility study report - Hydrogen*.

Lea, Aidan (Sept. 2024). *Equinor halts Norway-Germany H2 pipeline planning | Latest Market News*. en. URL: https://www.argusmedia.com/en/news-and-insights/latest-market-news/2610545-equinor-halts-norway-germany-h2-pipeline-planning (visited on 01/20/2026).

Levinsky, Howard, Sander Gersen, and Bert Kiewiet (Oct. 2015). *Requirements for gas quality and gas appliances*. DNV-GL.

Li, Ji-Chao, Yong Fan, Dan Pang, Tong Wu, Ying Zhang, and Ke Zhou (Dec. 2024). “Investigation on the Compressibility Factor of Hydrogen-Doped Natural Gas Using GERG-2008 Equation of State”. en. In: *Energies* 18.1. ISSN: 1996-1073. DOI: 10.3390/en18010053. URL: https://www.mdpi.com/1996-1073/18/1/53 (visited on 02/19/2026).

Mahajan, Devinder, Kun Tan, T. Venkatesh, Pradheep Kileti, and Clive R. Clayton (Jan. 2022). “Hydrogen Blending in Gas Pipeline Networks—A Review”. en. In: *Energies* 15.10, p. 3582. ISSN: 1996-1073. DOI: 10.3390/en15103582. URL: https://www.mdpi.com/1996-1073/15/10/3582 (visited on 11/03/2025).

Marcus Aurelius (Apr. 2006). *Meditations*. nl-NL. URL: https://www.bol.com/nl/nl/f/meditations/9200000023783714/ (visited on 06/29/2026).

Markhorst, Berend, Ruurd Buijs, Ruud Egging-Bratseth, and Rob van der Mei (Jan. 2026). “Optimizing gas entry–exit capacity utilization under uncertainty”. en. In: *Computational Management Science* 23.1, p. 9. ISSN: 1619-6988. DOI: 10.1007/s10287-025-00552-3. URL: https://doi.org/10.1007/s10287-025-00552-3 (visited on 01/25/2026).

Mary Hesse (2026). *Wikiquote*. en. URL: https://en.wikiquote.org/wiki/Mary_Hesse (visited on 06/29/2026).

Mean Decrease Impurity (MDI) in Tree Models (Sept. 2025). URL: https://www.emergentmind.com/topics/mean-decrease-impurity-mdi (visited on 06/16/2026).

Menon, E. Shashi (2005). *Gas Pipeline Hydraulics (ebook), E. Shashi Menon | 9781040061725 | Boeken | bol*. nl-NL. URL: https://www.bol.com/nl/nl/p/gas-pipeline-hydraulics/9300000197846662/ (visited on 02/24/2026).

Midthun, Kjetil T., Mette Bjørndal, and Asgeir Tomasgard (2009). “Modeling Optimal Economic Dispatch and System Effects in Natural Gas Networks”. In: *The Energy Journal* 30.4, pp. 155–180. ISSN: 0195-6574. URL: https://www.jstor.org/stable/41323248 (visited on 01/22/2026).

Millieu Centraal (2025). *CO2 Emissiefactoren*. nl. URL: https://co2emissiefactoren.nl/ (visited on 03/27/2026).

Mitrai, Ilias, Matthew J. Palys, and Prodromos Daoutidis (Feb. 2024). “A Two-Stage Stochastic Programming Approach for the Design of Renewable Ammonia Supply Chain Networks”. en. In: *Processes* 12.2, p. 325. ISSN: 2227-9717. DOI: 10.3390/pr12020325. URL: https://www.mdpi.com/2227-9717/12/2/325 (visited on 06/23/2026).

N. Riddick, Stuart and Denise L. Mauzerall (2023). “Likely substantial underestimation of reported methane emissions from United Kingdom upstream oil and gas activities”. en. In: *Energy & Environmental Science* 16.1, pp. 295–304. DOI: 10.1039/D2EE03072A. URL: https://pubs.rsc.org/en/content/articlelanding/2023/ee/d2ee03072a (visited on 02/03/2026).

Newman, Mark (July 2018). *Networks*. en. Google-Books-ID: YdZjDwAAQBAJ. Oxford University Press. ISBN: 978-0-19-252749-3.

NOD (June 2024). *Regulations relating to the stipulation of tariffs etc. for certain facilities*. en. URL: https://www.sodir.no/en/regulations/regulations/regulations-relating-to-the-stipulation-of-tariffs-etc.-for-certain-facilities (visited on 01/19/2026).

Nørstebø, Vibeke Stærkebye, Frode Rømo, and Lars Hellemo (Sept. 2010). “Using operations research to optimise operation of the Norwegian natural gas system”. In: *Journal of Natural Gas Science and Engineering* 2.4, pp. 153–162. ISSN: 1875-5100. DOI: 10.1016/j.jngse.2010.05.004. URL: https://www.sciencedirect.com/science/article/pii/S1875510010000351 (visited on 01/23/2026).

Norwegian Petroleum (2025). *Fields on the Norwegian continental shelf*. en. URL: https://www.norskpetroleum.no/en/facts/field/ (visited on 02/20/2026).

Peletiri, Suoton Philip, Iqbal M. Mujtaba, and Nejat Rahmanian (Dec. 2019). "Process simulation of impurity impacts on CO2 fluids flowing in pipelines". In: *Journal of Cleaner Production* 240, p. 118145. ISSN: 0959-6526. DOI: 10.1016/j.jclepro.2019.118145. URL: https://www.sciencedirect.com/science/article/pii/S095965261933015X (visited on 06/24/2026).

Petroleum, Norwegian (Nov. 2025). *The oil and gas pipeline system*. en. URL: https://www.norskpetroleum.no/en/production-and-exports/the-oil-and-gas-pipeline-system/ (visited on 01/16/2026).

Plato (Jan. 2013). *Phaedrus,* URL: https://www.gutenberg.org/files/1636/1636-h/1636-h.htm (visited on 06/29/2026).

Poe, William and Saeid Mokhatab (2012). *Handbook of Natural Gas Transmission and Processing*. en. ISBN: 9780123869142. URL: http://p5070-www.sciencedirect.com/book/monograph/9780123869142/handbook-of-natural-gas-transmission-and-processing (visited on 02/22/2026).

Pollitt, Michael G. (Aug. 2012). "Lessons from the history of independent system operators in the energy sector". In: *Energy Policy* 47, pp. 32–48. ISSN: 0301-4215. DOI: 10.1016/j.enpol.2012.04.007. URL: https://www.sciencedirect.com/science/article/pii/S0301421512002923 (visited on 01/15/2026).

Postek, Krzysztof, Alessandro Zocca, and Joaquim A. S. Gromicho (2025). *Hands-On Mathematical Optimization with Python*. English. Cambridge, United Kingdom ; New York, NY, USA: Cambridge University Press. ISBN: 978-1-009-49350-5.

Pustišek, Andrej and Michael Karasz (Mar. 2017). *Natural Gas: A Commercial Perspective*. en. Google-Books-ID: wNpyDgAAQBAJ. Springer. ISBN: 978-3-319-53249-3.

Python (July 2024). *Python Release Python 3.13.0*. en. URL: https://www.python.org/downloads/release/python-3130/ (visited on 03/25/2026).

Quintino, Filipe M., Nuno Nascimento, and Edgar C. Fernandes (Sept. 2021). "Aspects of Hydrogen and Biomethane Introduction in Natural Gas Infrastructure and Equipment". en. In: *Hydrogen* 2.3, pp. 301–318. ISSN: 2673-4141. DOI: 10.3390/hydrogen2030016. URL: https://www.mdpi.com/2673-4141/2/3/16 (visited on 01/19/2026).

Raj, Aashna, I. A. Sofia Larsson, Anna-Lena Ljung, Tobias Forslund, Robin Andersson, Joel Sundström, and T. Staffan Lundström (May 2024). "Evaluating hydrogen gas transport in pipelines: Current state of numerical and experimental methodologies". In: *International Journal of Hydrogen Energy* 67, pp. 136–149. ISSN: 0360-3199. DOI: 10.1016/j.ijhydene.2024.04.140. URL: https://www.sciencedirect.com/science/article/pii/S0360319924014137 (visited on 11/09/2025).

Rennert, Kevin, Frank Errickson, Brian C. Prest, Lisa Rennels, Richard G. Newell, William Pizer, Cora Kingdon, Jordan Wingenroth, Roger Cooke, Bryan Parthum, David Smith, Kevin Cromar, Delavane Diaz, Frances C. Moore, Ulrich K. Müller, Richard J. Plevin, Adrian E. Raftery, Hana Ševčíková, Hannah Sheets, James H. Stock, Tammy Tan, Mark Watson, Tony E. Wong, and David Anthoff (Oct. 2022). "Comprehensive evidence implies a higher social cost of CO2". en. In: *Nature* 610.7933, pp. 687–692. ISSN: 1476-4687. DOI: 10.1038/s41586-022-05224-9. URL: https://www.nature.com/articles/s41586-022-05224-9 (visited on 03/27/2026).

Rømo, Frode, Asgeir Tomasgard, Lars Hellemo, Marte Fodstad, Bjørgulf Haukelidsæter Eidesen, and Birger Pedersen (Feb. 2009). "Optimizing the Norwegian Natural Gas Production and Transport". en. In: *Interfaces*. DOI: 10.1287/inte.1080.0414. URL: https://pubsonline.informs.org/doi/abs/10.1287/inte.1080.0414 (visited on 01/15/2026).

S&P Global (Sept. 2024). *Shell pulls plug on Norwegian blue hydrogen project citing lack of demand*. en. URL: https://www.spglobal.com/commodity-insights/en/news-research/latest-news/energy-transition/092424-shell-pulls-plug-on-norwegian-blue-hydrogen-project-citing-lack-of-demand (visited on 11/14/2025).

Saliba, Zaid and Roussos Dimitrakopolous (Jan. 2019). "Simultaneous stochastic optimization of an open pit gold mining complex with supply and market uncertainty". en. In: ISSN: 2572-6668. DOI: https://doi-org.vu-nl.idm.oclc.org/10.1080/25726668.2019.1626169. URL: https://journals.sagepub.com/doi/epub/10.1080/25726668.2019.1626169 (visited on 06/23/2026).

SNAM (2018). *SNAM Annual Report 2017 - Snam presence in transport in Italy*. en. URL: https://reports.snam.it/2017/annual-report/directors-report/business-segment-operating-performance/natural-gas-transportation/snam-presence-in-transport-in-italy.html (visited on 06/24/2026).

Sodwatana, Mo, Saif R. Kazi, Kaarthik Sundar, and Anatoly Zlotnik (May 2023). "Optimization of Hydrogen Blending in Natural Gas Networks for Carbon Emissions Reduction". In: *2023 American Control Conference (ACC)*. ISSN: 2378-5861, pp. 1229–1236. DOI: 10.23919/ACC55779.2023.10156202. URL: https://ieeexplore.ieee.org/abstract/document/10156202 (visited on 06/23/2026).

Starreveld, J. S. (2026). "Mathematical optimization under uncertainty: With application to hydrogen deployment in the Netherlands". en. In: URL: https://dare.uva.nl/search?field1=keyword;value1=lukszo;docsPerPage=1;startDoc=1 (visited on 02/05/2026).

THE (2026a). *Trading Hub Europe > Publications > Balancing gas > Contracted capacity*. URL: https://www.tradinghub.eu/en-gb/Publications/Balancing-gas/Contracted-capacity (visited on 02/10/2026).

— (2026b). *Trading Hub Europe > Publications > Prices > Price monitor*. URL: https://www.tradinghub.eu/en-gb/Publications/Prices/Price-monitor# (visited on 02/23/2026).

Tomasgard, Asgeir, Frode Rømo, Marte Fodstad, and Kjetil Midthun (2007). "Optimization Models for the Natural Gas Value Chain". en. In: *Geometric Modelling, Numerical Simulation, and Optimization: Applied Mathematics at SINTEF*. Ed. by Geir Hasle, Knut-Andreas Lie, and Ewald Quak. Berlin, Heidelberg: Springer, pp. 521–558. ISBN: 978-3-540-68783-2. DOI: 10.1007/978-3-540-68783-2_16. URL: https://doi.org/10.1007/978-3-540-68783-2_16 (visited on 01/15/2026).

Ulstein, Nina Linn, Bjørn Nygreen, and Jan Richard Sagli (Jan. 2007). "Tactical planning of offshore petroleum production". en. In: *European Journal of Operational Research* 176.1, pp. 550–564. ISSN: 03772217. DOI: 10.1016/j.ejor.2005.06.060. URL: https://linkinghub.elsevier.com/retrieve/pii/S0377221705006363 (visited on 01/16/2026).

Urban, Susan (2021). *McCormick envelopes*. en. URL: https://optimization.cbe.cornell.edu/index.php?title=McCormick_envelopes (visited on 06/24/2026).

Wang, Siyang (Jan. 2026). "Blending hydrogen in urban gas pipeline system: Investigation of the hydrogen compatibility of PE pipeline material". In: *Journal of Pipeline Science and Engineering* 6.1, p. 100297. ISSN: 2667-1433. DOI: 10.1016/j.jpse.2025.100297. URL: https://www.sciencedirect.com/science/article/pii/S2667143325000447 (visited on 01/30/2026).

Weisstein, Eric W. (2026a). *Bonferroni Correction*. en. Text. URL: https://mathworld.wolfram.com/BonferroniCorrection.html (visited on 05/07/2026).

Weisstein, Eric W. (2026b). *Euler's Homogeneous Function Theorem*. en. Text. URL: https://mathworld.wolfram.com/EulersHomogeneousFunctionTheorem.html (visited on 05/01/2026).

Wolsey, Laurence A. (Sept. 2020). *Integer Programming*. en. Google-Books-ID: knH8DwAAQBAJ. John Wiley & Sons. ISBN: 978-1-119-60652-9.

Wong, P. and R. Larson (Oct. 1968). "Optimization of natural-gas pipeline systems via dynamic programming". In: *IEEE Transactions on Automatic Control* 13.5, pp. 475–481. ISSN: 1558-2523. DOI: 10.1109/TAC.1968.1098990. URL: https://ieeexplore.ieee.org/document/1098990 (visited on 01/20/2026).

Xie, Zongao, Qihang Jin, Guanli Su, Wei Lu, Zongao Xie, Qihang Jin, Guanli Su, and Wei Lu (Aug. 2024). "A Review of Hydrogen Storage and Transportation: Progresses and Challenges". en. In: *Energies* 17.16. ISSN: 1996-1073. DOI: 10.3390/en17164070. URL: https://www.mdpi.com/1996-1073/17/16/4070 (visited on 01/19/2026).

Zhang, Fangzhao and Stephen Boyd (Jan. 2025). *Solving Large Multicommodity Network Flow Problems on GPUs*. arXiv:2501.17996 [math] version: 1. DOI: 10.48550/arXiv.2501.17996. URL: http://arxiv.org/abs/2501.17996 (visited on 11/13/2025).

Zhang, Hongyu, Ignacio E. Grossmann, Ken McKinnon, Brage Rugstad Knudsen, Rodrigo Garcia Nava, and Asgeir Tomasgard (Sept. 2025). "Integrated investment, retrofit and abandonment energy system planning with multi-timescale uncertainty using stabilised adaptive Benders decomposition". In: *European Journal of Operational Research* 325.2, pp. 261–280. ISSN: 0377-2217. DOI: 10.1016/j.ejor.2025.04.005. URL: https://www.sciencedirect.com/science/article/pii/S0377221725002553 (visited on 11/03/2025).

Zhao, Yan, Vince McDonell, and Scott Samuelsen (Apr. 2020). "Assessment of the combustion performance of a room furnace operating on pipeline natural gas mixed with simulated biogas or hydrogen". In: *International Journal of Hydrogen Energy* 45.19, pp. 11368–11379. ISSN: 0360-3199. DOI: 10.1016/j.ijhydene.2020.02.071. URL: https://www.sciencedirect.com/science/article/pii/S0360319920306340 (visited on 01/19/2026).

Zou, Caineng, Bo Xiong, Huaqing Xue, Dewen Zheng, Zhixin Ge, Ying Wang, Luyang Jiang, Songqi Pan, and Songtao Wu (Apr. 2021). "The role of new energy in carbon neutral". In: *Petroleum Exploration and Development* 48.2, pp. 480–491. ISSN: 1876-3804. DOI: 10.1016/S1876-3804(21)60039-3. URL: https://www.sciencedirect.com/science/article/pii/S1876380421600393 (visited on 01/19/2026).

A Model Extensions

The following appendices refer to possible model extensions. First, the possibility of introducing bidirectional arcs is introduced, alongside the needed constraints. Second, possible additional constraints on the quality of the gas composition are discussed. Finally, the possibilities of the model surrounding storage are discussed.

A.1 Bidirectional pipelines

On the Norwegian Continental Shelf, the pipelines are only one directional. However, other pipeline networks, such as the Dutch and Italian network, gas can flow in both directions. Two problems arise here. First, the components of the gas all have to flow in the same direction, instead of the alignment of the sum. Second, the Weymouth flow does not account for bi-directional pipelines. To account for these problems, the solution by Tomasgard et al. (2007) can be considered. They introduce a binary variable, that allows the flow to go in either, but not both directions. This can be integrated into the current model. First, for a bidirectional arc, the network is extended into two directional arcs, of which a depiction is shown in Figure 37. The figure shows that when the variable $\xi_{A,B} = 1$ flow can go through that arc, but that the variable that indicates flow in the opposite direction is therefore zero.

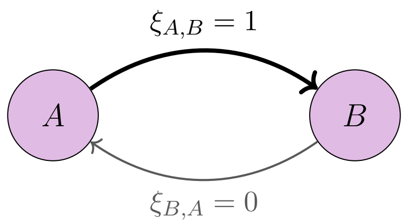

Figure 37: Bidirectional pipelines between junction nodes. In this case, $\xi_{A,B} = 1$, which indicates that flow is allowed from A to B.

This can be formalized in the model. For each bidirectional pair of arcs, let $a, a' \in A^{\circ}$ denote the set of bidirectional arcs. Let $\xi_{a,m}$ denote the variable that denotes whether flow is allowed for arc a and scenario m. A summary of the added symbols is given in Table 18.

Table 18: Notation for bidirectional arc modeling.

Symbol	Description	Index	Range
A°	Pair of bidirectional arcs	a, a'	N/A
$\xi_{a,m}$	Binary variable indicating whether flow is allowed on arc a in mode m	N/A	$\{0, 1\}$

Having defined the variable, it is related between the two directional arcs by Equation (58). Second, for all bidirectional arc pairs and each component, at most one direction of flow is allowed, which is Ensured by Equation (59). This ensures that components flow together, instead of the sum of flows where one component flows in the opposite direction.

$$\xi_a = 1 - \xi_{a'} \quad \forall \quad a, a' \in A^{\circ} \tag{58}$$

$$\left.\begin{aligned} f^c_{a,m} &\leq \bar{F}_a \xi_a \\ f^c_{a',m} &\leq \bar{F}_{a'} \xi_{a'} \end{aligned}\right\} \quad \forall\, c \in C\ a, a' \in A^{\circ}\ m \in M_3 \tag{59}$$

Second, the constraint between pressures arcs into and out of nodes (Equation (18)) needs to be relaxed when one of the two bidirectional arcs remains unused. Therefore, for each bidirectional arc, Equation (60), the restriction is lifted if the direction of the edge is unused. With this restriction lifted, the model becomes feasible again, while accounting for bidirectional pipelines. However, it should be noted that with the introduction of additional binary variables solving the model can become slower.

$$\left.\begin{array}{r} p_{a,\text{in},m} \leq p_{a',\text{out},m} + \bar{P}_a \xi_{a'} \\ p_{a,\text{in},m} \leq p_{a',\text{out},m} + \bar{P}'_a \xi_a \end{array}\right\} \quad \forall\, c \in C\ a, a^* \in A^\circ\ a' \in A_n^+,\ n \in N \setminus N_\gamma,\ m \in M_3 \tag{60}$$

A.2 Additional Quality Constraints

The model currently only considers restrictions on individual components of the gas mix. However, when modeling multiple energy components, such as splitting out methane from other carbon fuels in natural gas, it might be beneficial to put restrictions on the overall composition instead. To this end, new parameters are introduced, which are shown in Table 19.

Table 19: Add quality parameters.

Variable	Description
B	set of quality measures indexed by b
$q^{c,b}$	Value per unit of flow of component c of quality measure b
Q_n^{b+}	Maximum value of quality measure b per unit of flow arriving at node n
Q_n^{b-}	Minimum value of quality measure b per unit of flow arriving at node n

These parameters can be used to model other quality requirements, such as the GCV and the relative density, which can be represented as a linear combination of the components. This constraint is formulated in Equations (61) and (62). However, for the chosen components, the gas mix is piecewise sufficiently constraint, so these constraints are neglected.

$$\sum_{a \in A_n^+} \sum_{c \in C} q^{c,b} f_{a,m}^c \leq\ Q_n^{b+} \sum_{a \in A_n^+} \sum_{c \in C} f_{a,m}^c \quad \forall\, n \in N_d,\ m \in M_3 \tag{61}$$

$$\sum_{a \in A_n^+} \sum_{c \in C} q^{c,b} f_{a,m}^c \geq\ Q_n^{b-} \sum_{a \in A_n^+} \sum_{c \in C} f_{a,m}^c \quad \forall\, n \in N_d,\ m \in M_3, \tag{62}$$

A.3 Storage Extension

To account for fluctuating demands and prices, a supplier can book storage capacity to store gas in storage for later use when demand is high. Storage can occur in two places. First, storage can be placed at the nodes, where the silos store gas for later dates (R. G. Egging, 2010; Xie et al., 2024). Second, storage is possible by storing in arcs, via a process called linepacking (Grimm et al., 2019; Klatzer et al., 2024), by maintaining a high pressure at both the inlet and outlet of the pipe, to keep gas stored in a pipe. However, both Grimm et al. (2019) and Klatzer et al. (2024) remark that linepacking cannot be achieved with a stationary formulation of gas physics, such as the model presented here. Therefore, the presented model formulation can only be applied to stationary storage in silos.

For both cases, the benefits of storage only present themselves if a time index is introduced, such that the model can be optimized for the storage over time periods. Note that this would further increase the computation time, as the model has to optimize over all scenarios in multiple periods. However, besides the added time index, the model is already fit to include storage in the model, utilizing existing constraints.

To illustrate this, Figure 38 shows the modeling of storage, where an artificial node B_{store} is introduced, which can take on storage for a later date, while B_{flow} handles the regular flow for the current time period. In this case, the flow is required to be balanced over all time periods for B_{store}, while for B_{flow} the balance must occur at each time period. The pressure at the storage node functions as a compressor, where the outward pressure is determined by the incoming pressure and the flow. Finally, it should be noted that here, node A is a homogeneous splitting node when the storage happens without processing, and a heterogeneous splitting node otherwise.

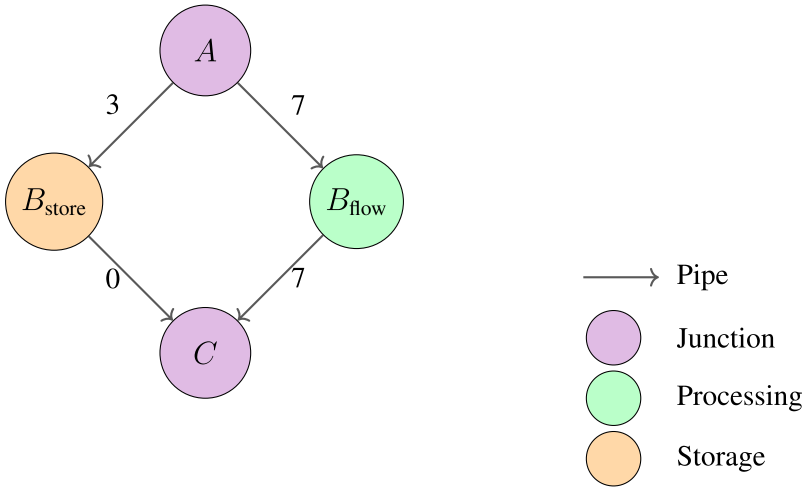

Figure 38: Inclusion of storage nodes into the network.

B Additional Case Study Information

This section contains additional information on the choices made for the case study. First, a hierarchal view of the network is given from sources to sinks. Second, the parameters on booking costs and pipeline limits are given for each node and arc respectively. Third, the additional networks are given that are used for generating the sampled networks.

B.1 Hierarchical Layout of the Network

Figure 39 provides a hierarchical view of the network. The network shows that the market nodes are at various degrees removed from the market node. Furthermore, in this simplified version, a high amount of the junction nodes do not have a function, due to the fact that they only link to one other node. Nonetheless, the representation does give insight into the complexity of the network.

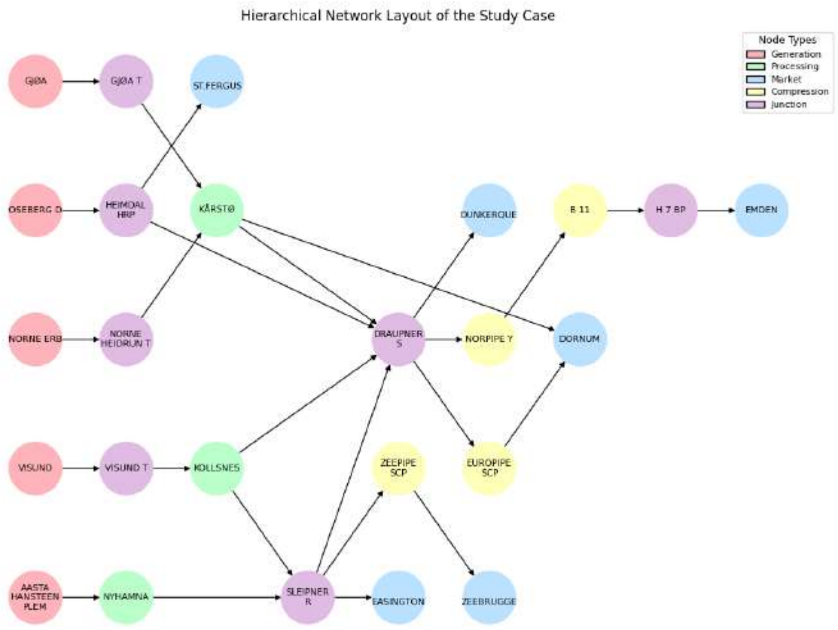

Figure 39: Hierarchical representation of the network.

B.2 Arc Parameters

Table 20 describes the flow of all the used pipelines (arcs). The first three represent names of the columns, including the name in the dataset, the name in the interactive map (Gassco, 2026c), as well as the unique id, while the last column represents the capacity limit.

Table 20: Network arcs with capacities and updated Weymouth constants.

Pipeline	Segment name	ID	Capacity	Weymouth const.	Closure analysis
Åsgard Transport	42" Gas ÅSGARD ERB, KÅRSTØ	307674	40.0	0.293	
Europipe I	40" Gas DRAUPNER E, EUROPIPE-SCP	326340	45.7	0.381	yes
Europipe I	40" Gas EUROPIPE-SCP, EMDEN	327394	45.7	0.378	Yes
Europipe II	42" Gas KÅRSTØ, EMDEN	323212	73.5	0.295	Yes
Franpipe	42" Gas DRAUPNER E, DUNKERQUE	326374	54.2	0.265	Yes
Gjøa Gassrør	28" Gas GJØA, GJØA-T	406790	18.2	0.236	
Kvitebjørn Gassrør	30" Gas KVITEBJØRN, KOLLSNES	357492	33.5	0.258	
Langeled	42" Gas NYHAMNA, SLEIPNER R	369461	74.4	0.313	
Langeled	44" Gas SLEIPNER R, EASINGTON	369498	73.8	0.365	
Norne Gasstransport	16" Gas NORNE ERB, NORNE/HEIDRUN T	319132	11.0	0.052	
Norpipe Gassledning	36" Gas NORPIPE Y, B-11	319166	44.4	0.419	
Norpipe Gassledning	36" Gas B-11, H-7 BP	324844	44.4	0.415	
Norpipe Gassledning	36" Gas H-7 BP, EMDEN	321784	44.4	0.404	
Oseberg Gasstransport	36" Gas OSEBERG D, HEIMDAL HRP	319676	35.0	0.479	
Polarled	36" Gas AASTA HANSTEEN PLEM, NYHAMNA	444927	57.6	0.229	
Statpipe	28" Gas KÅRSTØ, DRAUPNER S	323042	44.4	0.177	Yes
Statpipe	30" Gas STAT-SSTC, KÅRSTØ	313556	21.1	0.182	
Statpipe	36" Gas HEIMDAL, DRAUPNER S	322464	30.7	0.398	
Statpipe	36" Gas DRAUPNER S, NORPIPE Y	326408	30.7	0.355	
Vesterled	32" Gas HEIMDAL HRP, ST.FERGUS	322532	36.9	0.201	
VISUND	20" Gas VISUND, VISUND T	364645	40.0	0.179	
Zeepipe I	40" Gas ZEEPIPE-SCP, ZEEBRUGGE	310326	42.2	0.335	
Zeepipe I	40" Gas SLEIPNER R, ZEEPIPE-SCP	321002	55.0	0.325	
Zeepipe I	30" Gas SLEIPNER R, DRAUPNER S	321036	42.2	0.493	
Zeepipe II A	40" Gas KOLLSNES, SLEIPNER R	323076	40.0	0.383	
Zeepipe II B	40" Gas KOLLSNES, DRAUPNER E	323110	40.0	0.382	

B.3 Node Parameters

Table 21 represents the entry and exit costs that apply to each node. It should be noted that costs are only incurred when gas is put into or taken off the network, so only generation nodes, market nodes and the hydrogen production nodes have relevant tariff costs.

Table 21: Network nodes with booking tariffs.

Name	ID	Lon	Lat	Type	Area	Tariff (€/Mscm)	Closure analysis
AASTA HANSTEEN PLEM	459032	7.107227	67.055610	Generation	O	1731	
B-11	277265	4.551625	55.462302	Compression	D	3278	
DORNUM	286141A	7.326420	53.679700	Market	D	3278	
DRAUPNER S	271945	2.469756	58.190288	Junction	D	3278	
DUNKERQUE	286757	2.252709	51.046406	Market	D	3278	
EASINGTON	369424	0.116031	53.659231	Market	D	3278	
EMDEN	286141	7.189290	53.346200	Market	D	3278	
EUROPIPE-SCP	286841	4.222622	55.706969	Compression	D	3278	
GJØA	406672	3.904990	61.330194	Generation	I	893	Yes
GJØA-T	406731	1.791105	61.136872	Junction	I	893	
H-7 BP	377218	6.035305	54.509016	Junction	D	3278	
HEIMDAL HRP	280569	2.227316	59.576233	Junction	D	3278	
KOLLSNES	286729	4.838084	60.545747	Processing	E	5718	
KÅRSTØ	286169	5.268005	59.318135	Processing	C	0	
NORNE ERB	282221	8.078544	66.029331	Generation	H	29623	Yes
NORNE/HEIDRUN T	287261	6.800257	65.095601	Junction	H	29623	
NORPIPE Y	287065	3.305096	56.504978	Compression	D	3278	
NYHAMNA	364693	6.947441	62.852606	Processing	P	11109	
OSEBERG D	280541	2.824046	60.486900	Generation	D	3278	
SLEIPNER R	277797	1.913921	58.368034	Junction	D	3278	
ST.FERGUS	286225	-1.825319	57.578706	Market	D	3278	
VISUND	277685	2.467809	61.368775	Generation	G	1731	Yes
VISUND T	364607	2.520206	61.072124	Junction	G	1731	
ZEEBRUGGE	286281	3.229797	51.350508	Market	D	3278	
ZEEPIPE-SCP	286533	3.299816	54.789494	Compression	D	3278	

B.4 Additional Networks

Two additional networks are created to determine the scalability of the linear program. First, a simplified version of the network is created by merging nodes when they are 150 km away from each other. Furthermore, features were merged to maintain a representation of the original network. Namely, supply capacities and demands were summed when nodes were merged. For each of the cost components, the average was taken. For the production and allowed market ratio of hydrogen, natural and CO_2 the dominant (highest production or demand) was taken, which was also applied to the standard deviations and variance on the market. However, the possibility exists that market demands cannot be met, due to suppliers disappearing. Therefore, the demand burden was put fully on Equinor for every node. For the edges, the sum was taken over the maximum flow, while the other parameters were kept the equal to the case study, as they are the same across all edges. This resulted in the smaller network shown in Figure 40 (a).

Second, a larger network is created by including the arcs managed by all operators, given that the arc is currently used. The same method was applied to create the network as for the case study. In the network, if a node or edge already existed, the parameters were copied over from the case study. If a node did not exist, the needed parameters from the node type were sampled randomly, to provide the network with the required characteristics. Otherwise, if an arc did not exist, it was given a max flow of 40, and the other parameters were taken over from the other nodes. This resulted in the network shown in Figure 40 (b).

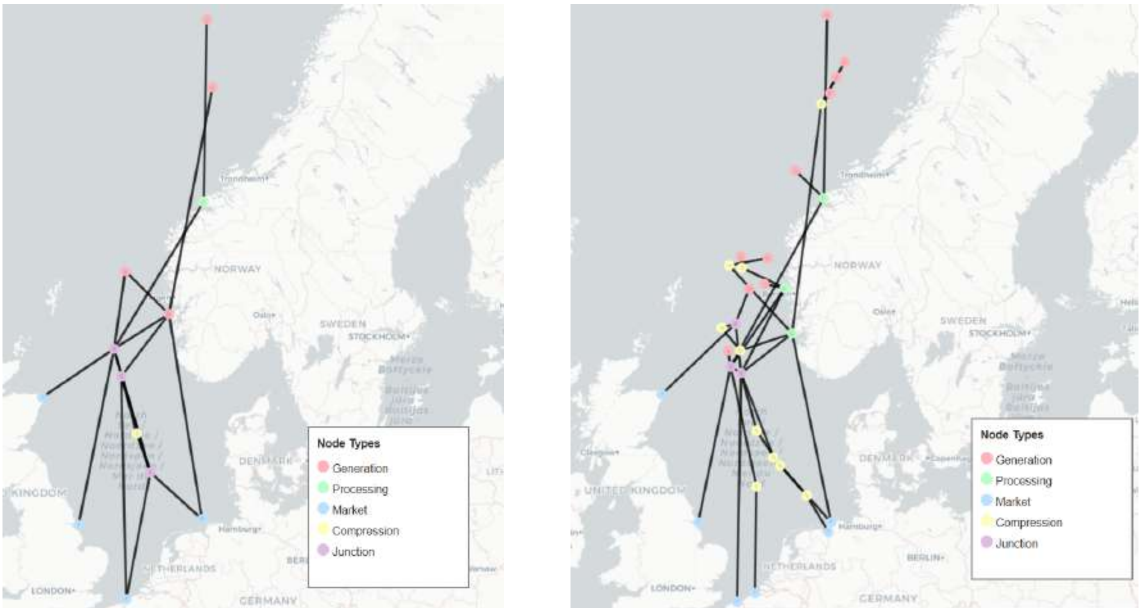

(a) Simplified Network (b) Extended Network

Figure 40: Simplified and extended case study network

Besides the two additional variations on the case study network, a hundred networks were also procedurally generated. First, a number of nodes for the network is decided between five and forty, to obtain networks of different sizes. Second, the node types are decided. The number of generation and market nodes is decided first, where it should be at least one, and between 15%-30% of the total number of nodes, to reflect the three variations of networks corresponding to the case study. Of the remaining nodes, they are sampled randomly among the remaining types (Junction, Processing and Compression). Third, network edges are decided by splitting the nodes into layers, where a layer can only obtain edges from previous nodes. Then, edges are added and removed, such that the generated network corresponds closely to the case study networks (33 to each type) in terms of the amount of redundant paths (such that gas can flow from a single point in different ways to the same market), as well as the average path length. At each iteration, after edges are changed, it was checked whether compression nodes only have one outgoing edge, and are adjusted otherwise. This resulted in 100 generated networks. Examples of the generated networks are given in Figure 41.

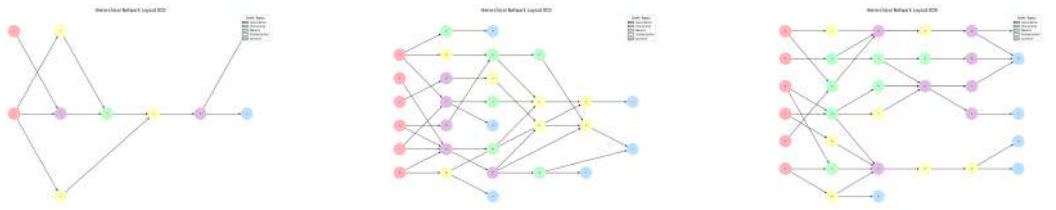

(a) Hierarchical graph representation of the second network.

(b) Hierarchical graph representation of the third network.

(c) Hierarchical graph representation of the eighth network.

Figure 41: Examples of hierarchical graph structures for three generated network instances: 002, 003, and 008. The figures illustrate differences in network topology and node organization.

C Modeling Constants

In this section, the hyperparameters are calculated or derived to be used to generate the results. First, the trade-offs on hyperparameters are discussed and values decided for the study case for the Weymouth cutting plane constants, relative density upperbounds and homogeneous splits. In addition, based on given literature the method to determine the Weymouth constant and Fuel consumption constants are further discussed.

C.1 Cutting Planes

The number of cutting planes and in turn computation time can be reduced by choosing the taylor approximation points effectively. To this aim, the cutting plane points on the set L are chosen using Equation (63). Here, $(P_{\text{in}}, P_{\text{out}})$ represents a point in the cutting plane, $N_{\text{out}}, N_{\text{in}}$ the number of cutting planes both outlet and inlet pressure individually, and $P_{\text{out}}^{\min}, P_{\text{out}}^{\max}$ and $P_{\text{in}}^{\max}$ represent bounds derived from pipeline pressures. This function ensures that the cutting plane points are chosen to diminish the deviation of the function from the upperbound. The exponent (x) was manually tuned and set to $x = 10$ to ensure that the most steep part of the function has the best coverage, thereby minimizing deviation.

$$
\begin{aligned}
L = \Big\{ (P_{\text{in}}, P_{\text{out}}) \;\Big|\; & P_{\text{out}} = P_{\text{out}}^{\min} + \frac{k}{N_{\text{out}} - 1}\big(P_{\text{out}}^{\max} - P_{\text{out}}^{\min}\big), && k \in \{0, \dots, N_{\text{out}} - 1\}, \\
& P_{\text{in}} = P_{\text{out}} + \big(P_{\text{in}}^{\max} - P_{\text{out}}\big)\, t_m^x, && m \in \{0, \dots, N_{\text{in}} - 1\}, \\
& P_{\text{in}} > P_{\text{out}}, \quad t_m = \frac{m}{N_{\text{in}} - 1} \in [0, 1] \Big\}
\end{aligned} \tag{63}
$$

Figure 42 shows how the cutting plane points are distributed across the relevant pressure range. For $P_{\text{in},l}$ and $P_{\text{out},l}$ there are ten points each, resulting in total a hundred points. The points $P_{\text{out},l}$ and provide the baseline over the possible pressure. However, as the function obtains the highest curvature when $P_{\text{in},l}$ is only slightly larger than $P_{\text{out},l}$, the points of $P_{\text{in},l}$ are chosen more frequent around $P_{\text{out},l}$ and are more scarce when $P_{\text{in},l}$ is large. Furthermore, note that the points are denser when $P_{\text{out},l}$ is high. This was chosen as when the output pressure is high, a slight increase in input pressure above that value can increase the amount of flow drastically, increasing the need for a more accurate approximation.

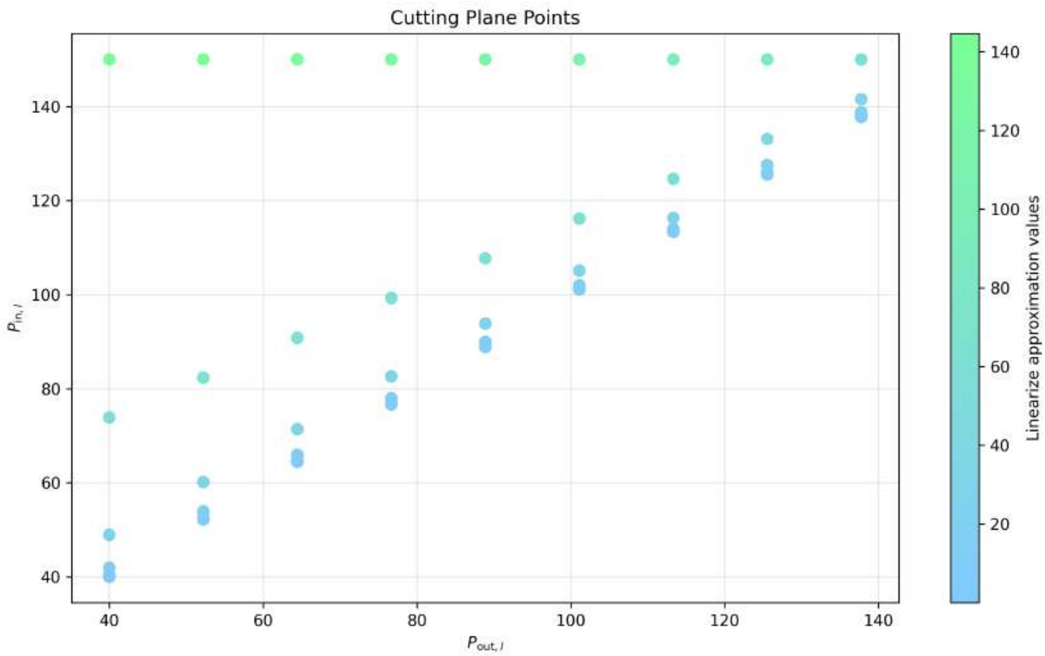

Figure 42: Grid of cutting plane points and associated values, all pressures are in bar.

Together, these choices allow the model to more accurately approximate the Weymouth equation, given a fixed number of points. For the base run of the model, the deviations are given in Figure 43, which shows that the deviations are very often zero, and otherwise very low. Therefore, creating the cutting plane points with the current method yields an accurate approximation.

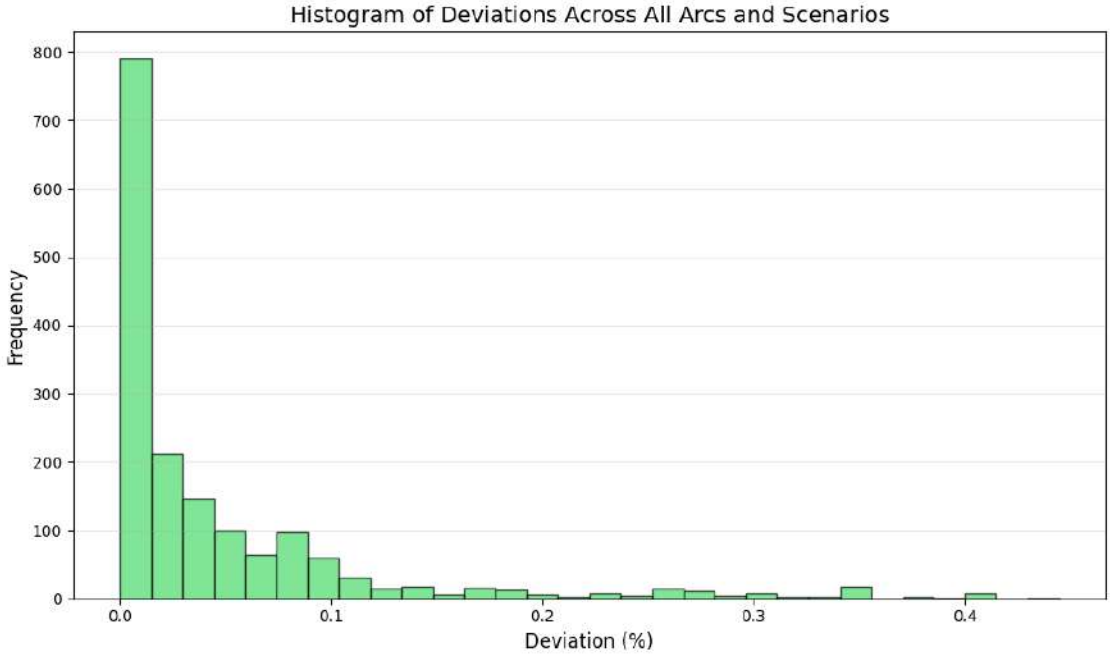

Figure 43: Distribution of flow deviation (%) from Weymouth flow. All deviations are small at less than 0.5%.

C.2 Relative Density Upperbounds

The relative density upperbounds shown in Equation (14) enable to model the impact of different gas compositions on the flow-pressure relationship, to more accurately represent the pressure costs. In addition, as hydrogen gas has a lower relative density, the flow increases with a higher percentage of hydrogen gas given the same pressure difference, which could reduce pressure costs. However, increasing the number of upper bounds multiplies the number of constraints per arc by that amount, and introduces additional binary variables to each arc, exploding model size.

Therefore, the amount of density upperbounds needs to be carefully chosen to balance between model accuracy and tractability. For this thesis, the bounds were chosen in the range given by EASEE $\rho_z \in [0.555, 0.700]$. Besides, the market restrictions by EASEE, these bounds are further reinforced by technical restrictions of the network. Hydrogen could only be safely blended up to 20% on pipelines, which restricts possible densities within the range $\rho \in [0.534, 0.67]$. Therefore, bounds within the EASEE range provide meaningful upperbounds.

Within this range, density bounds $z \in Z_\theta$ were uniformly divided throughout the range. This means that there exists a bound on every $\frac{20}{|Z_\theta|}\%$ interval of hydrogen gas blended with natural gas.

To examine the impact of density bounds on the effectivity of modeling gas blends deterministic variants of the model were run on the case study. Namely, a single scenario in stage two and three were sampled 50 times, and solved for different density bounds respectively. The deterministic variant was chosen, as incorporating stochasticity significantly slows down solution times, while being largely unrelated to the operational difficulties, such that it can be disregarded. As hydrogen remains unused when there is no subsidy in place for hydrogen producers, the impact was studied for different subsidy values, to show the effect of different density bounds on hydrogen production and pressure costs. As the effect is largest when deviation is allowed, the model is ran at 100% market deviation. To reduce the variance between results, common random numbers

(CRN) was used across subsidies and density bounds. The resulting averages over the runs were plotted, with error bars depicting the standard error.

Figure 44 shows that for no subsidy and a subsidy that makes production free, there exists virtually no difference between the density bounds, as hydrogen gas is not produced when there is no subsidy, and always produced when it is free. The difference arises for subsidies that make hydrogen production economically competitive. Here, when the number density bounds increase to 2, the average hydrogen production increases. This shows that the number of density bounds reduces the needed subsidy to make hydrogen production viable. Therefore, if the number of density bounds is kept low, the model provides a conservative estimate of the actual possibilities of hydrogen blending. However, when the amount of density bounds are increased to 4 or 8, the average amount of hydrogen does not increase anymore. This is because the upper bounds are more fine grained, resulting in less exploitation of sudden jumps of bounds. Nonetheless, there is still an increase in hydrogen production relative to only having one upperbound per arc.

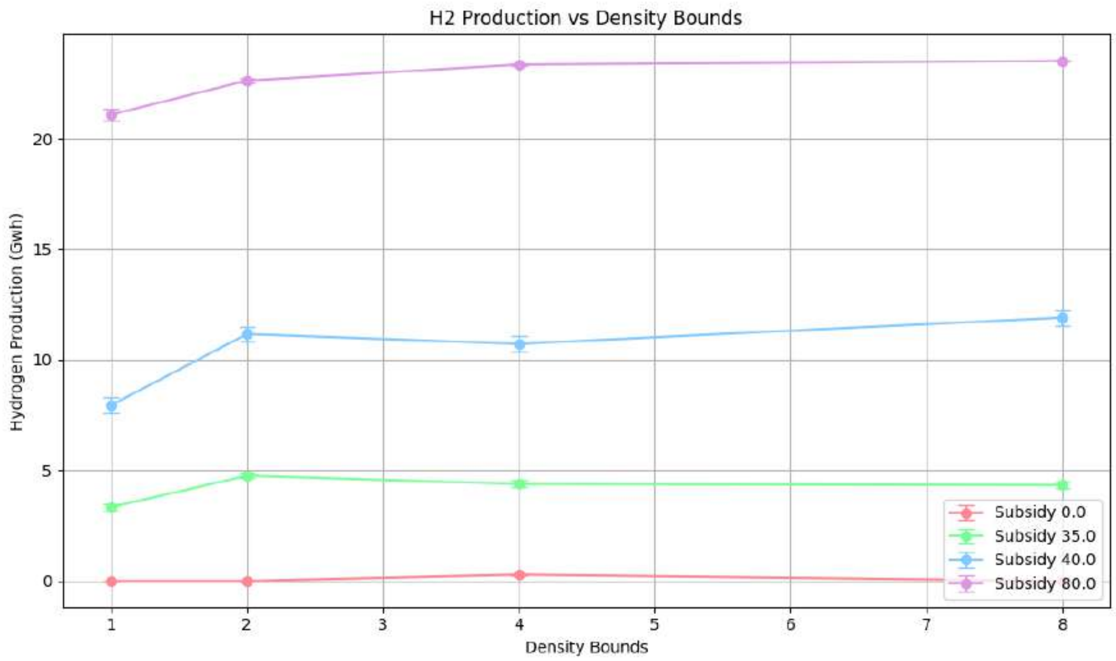

Figure 44: Hydrogen production for different number of density bounds and subsidies at 100% deviation.

Finally, Figure 45 shows that pressure costs do not necessarily decrease, indicating that the model opts for similar pressure costs, but at a higher total flow due to hydrogen production, as pipe limits might not have been reached.

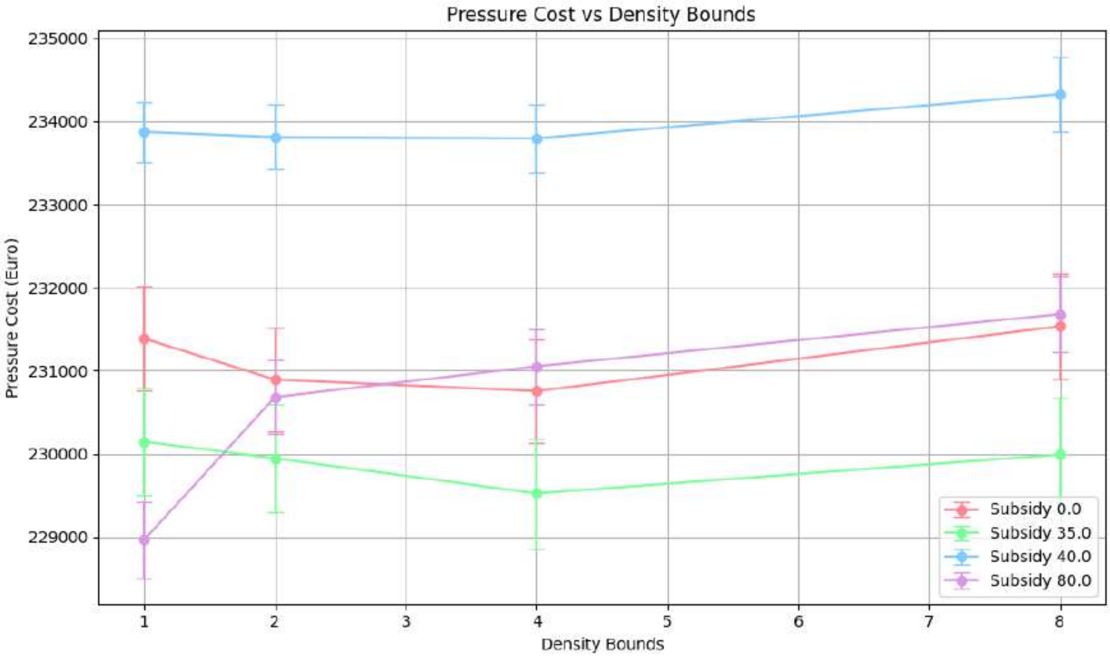

Figure 45: Pressure costs for different number of density bounds and subsidies

The solve times were also examined. As the solve time is interdependent with the number of scenarios, the model was run on sixteen scenarios sampled from the case study, and this was executed 10 times to reduce the error in the results. The model was not run on the full 64 scenarios, as the computing power was insufficient to run that experiment on different density bounds. Instead it was run with the deterministic variant discussed before. The resulting solve times are shown in Figure 46, which depicts the amount of upperbounds on the x-axis and the solve times on the y-axis, and shows that the solve times increase exponentially with the amount of upper-bounds. Together with the fact that the number of scenarios also increase solve times exponentially, a choice has to be made between a higher number of density bounds, or more scenarios.

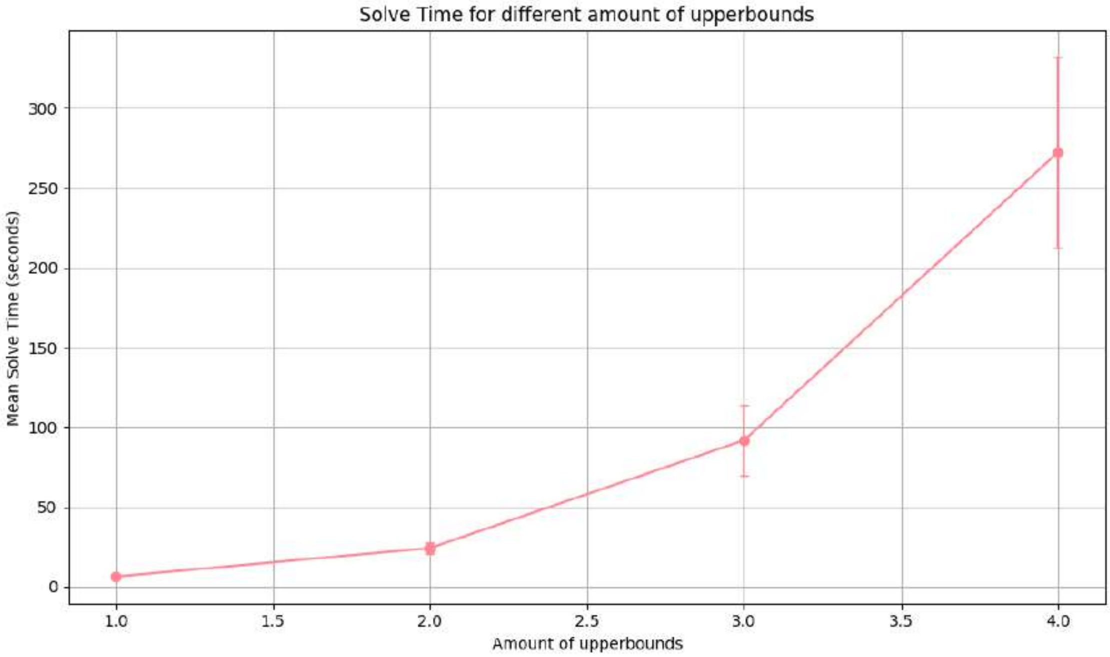

Figure 46: Solve times for different number of upperbounds on the case study network for sixteen scenarios, with the error bars depicting standard error over 20 runs.

For the main experiments, only one density bound was chosen at $\rho_z = 0.7$, to allow for a larger amount of scenarios, and in turn, a more stable model. Therefore, the amount of produced hydrogen is slightly underestimated for a given subsidy, but has increased accuracy through the number of scenarios.

C.3 Homogeneous Splits

The amount of allowed homogeneous fractional splits, used in Equation (30) per arc allows the model to better divide the incoming flow across outgoing arcs more easily. The more fine-grained the division, i.e. the amount of allowed splits, the higher the objective can become, as gas can better be split among arcs. However, the amount of splits also increases computation time, as binary variables are introduced for each split, making the model more difficult to solve. To show this behavior, the model was run for 6 allowed fractions (for each arc the possibility $\{0, 0.2., \ldots, 1\}$) up to 26 allowed fractions on the case study model, each with 16 scenarios branched four times in both stages. The model objective and solve times are shown in Figure 47 and 48 where the error bars describe the standard errors for the respective figures. Figure 48 shows that the solve time increases exponentially with the amount of splits, and should therefore be restricted. However, the figure on the left shows that with 11 splits per arc, the objective does not notably increase anymore. Therefore, the amount of splits was chosen at 11, and divided homogeneously from [0,1] for each arc, such that the fractions always sum to 1 for each choice of division.

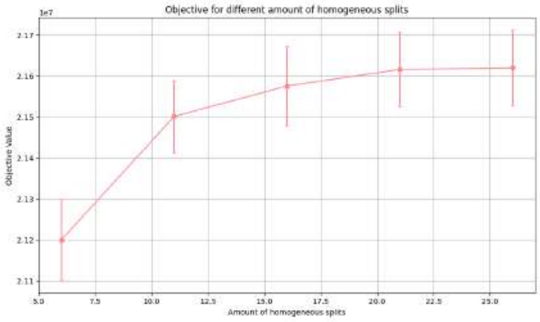

Figure 47: Objective values for different numbers of splits on the case study network for sixteen scenarios on a personal machine. 20 runs were executed per value

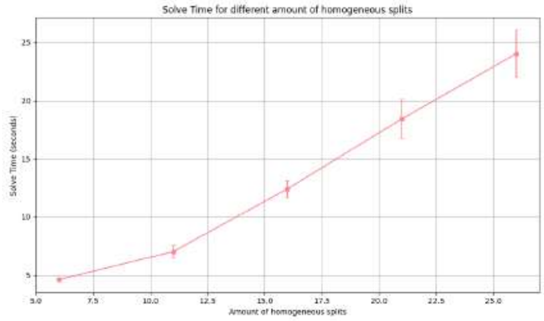

Figure 48: Solve times for different numbers of splits on the case study network for sixteen scenarios on a personal machine. 20 runs were executed per value

C.4 Weymouth Constant

The Weymouth constant, as obtained in Equation 1, is determined by several factors. Table 22 denotes the symbols that make up the Weymouth constant, while Equation (64) shows how to derive the constant, both derived from Egging-Bratseth et al. (2025). In the model, C is a constant found in observation and E_a denotes how efficient the pipeline is, with a perfect pipeline obtaining a factor of 1, and is derived from the case study from examples of Menon (2005, p. 62). The diameter of the pipe D_a is multiplied by an empirical exponent of $2\frac{2}{3}$, as the flow is positively influenced by the diameter. In contrast, the temperature of the gas reduces the flow. This is expected, because hot gas contains more volatile particles that exude more pressure at the same mass. In addition, the gas composition denotes the relative density and the gas compressibility factor, and a higher value reduces the flow. The relative density indicates less mass at the same pressure level by definition, and is taken into account for gas compositions due to the differences between natural gas and hydrogen gas. The gas compressibility factor also depends on the gas composition, but for low percentages of hydrogen shows little impact on the factor (Li et al., 2024). Therefore, it was assumed fixed, also derived from examples of Menon (2005, p. 62). Finally, as the pipe gets longer the flow is reduced, which is expected as more distance has to be crossed with the same amount of gas, requiring more energy (pressure). Since the diameter and length of the pipe influence the constant, they were derived per pipe. The full list of Weymouth constants K'_a are given in Appendix B.2.

Table 22: Symbols and parameter definition for the standard volumetric flow formulation. *Value converted from Menon (2005) to measure flow in Mscm. ** Compressibility factor is the ease to compress gas, not the pressure increase at compressors.

Symbol	Description	Unit	Value
C	Empirical constant	–	3.7435×10^{-9} *
E_a	Pipe efficiency factor	–	0.95
D_a	Pipe diameter	mm	–
T_{std}	Standard temperature	K	288.15
p_{std}	Standard air pressure	bar	1.01325
T	Ambient gas temperature	K	288.15
ρ_z	Gas relative density (chosen upperbound)	m^3/m^3	–
L_a	Pipeline length	km	–
Z	Gas compressibility factor**	–	0.9
n	Empirical exponent	–	$2\frac{2}{3}$

$$K_a = \frac{T_{\text{std}} C E_a (D_a)^n}{p_{\text{std}} \sqrt{T Z L_a}} \tag{64}$$

$$K_{a,z} = \frac{K_a}{\sqrt{\rho_z}} \tag{65}$$

In addition to the Weymouth equation, there exists a more recent equation, the Panhandle Equation (Menon, 2005; Das et al., 2025), which uses slightly different exponents than square root and sets $n = 2.61$. However, for the current estimation model, the Weymouth equation works sufficient.

C.5 Fuel Consumption Constants

Hoeven (2004) proposed a method to linearize the fuel consumption of a compressor. They found that for any compressor, the nonlinear relationship with κ (see Equation (2)) can be omitted. The linearization requires the normal operatorship (average over time) of the pressure coming from the arcs to the node $\bar{p}_{a,\text{out}}$, into the outgoing arc $\bar{p}_{a',\text{in}}$ (discharge pressure) and the flow $\bar{f}^c_a$. These constants provide the relationship between flow and pressure and allow for the linearization in the input pressure, the outlet pressure, and the flow. The relationship is defined in Equation (66). The equation shows that the effect of the discharge pressure and the flow is positive. This is expected, as the amount of gas being pressurized and the amount of pressure it increases is increase the fuel consumption. A higher pressure into the compressor affects the fuel consumption negatively. Together, these equations form the fuel consumption for each compressor in the network. For each of the compression nodes in the case study, the normal operatorship of the outlet, inlet and flow values, the first scenario from Nørstebø et al. (2010) was used to determine the inlet pressure and the normal flow. The values for each compression node are respectively $\bar{p}_{a,\text{out}} = 100$ bar, $\bar{p}_{a',\text{in}} = \bar{p}_{a,\text{out}}\hat{P}_n$ bar and $\sum_{c\in C} \bar{f}^c_{a'} = 25$. As the flow for hydrogen gas and CO_2 are not considered in Nørstebø et al. (2010), the fractions were chosen using the mode of the fractions in the gas composition of generation nodes, such that $\bar{f}^{H_2}_{a'} = 0$ while $\bar{f}^{\text{NG}}_{a'} = 25 \cdot 0.98$ and $\bar{f}^{CO_2}_{a'} = 25 \cdot 0.02 = 0.5$ (see Table 8).

However, Hoeven (2004) and Nørstebø et al. (2010) both mention a constant that is multiplied (k), but does not provide their used parameter values or definitions. For the current problem, the compressibility factor, standard pressure, ambient and standard temperature are kept consistent with the values used for the Weymouth constant (Table 22). Furthermore, the compressor adheres to an efficiency η, which was chosen at $\eta = 0.72$, following the case study of Das et al. (2025). This yields the values shown in Table 9.

$$k = \frac{p_{std} T z}{3600 \eta T_{std}} \tag{66a}$$

$$K^c_{p_{a'},\text{in}} = k \frac{\bar{p}_{a,\text{out}} \cdot \bar{f}^c_{a'}}{\left(\frac{2}{3}\bar{p}_{a,\text{out}} + \frac{1}{3}\bar{p}_{a',\text{in}}\right)^2} \tag{66b}$$

$$K^c_{p_a,\text{out}} = k \frac{\bar{p}_{a,\text{in}} \cdot \bar{f}^c_{a'}}{\left(\frac{2}{3}\bar{p}_{a,\text{out}} + \frac{1}{3}\bar{p}_{a',\text{in}}\right)^2} \tag{66c}$$

$$K_{f^c_a} = k \frac{\bar{p}_{a,\text{in}} - \bar{p}_{a',\text{out}}}{\frac{2}{3}\bar{p}_{a,\text{out}} + \frac{1}{3}\bar{p}_{a',\text{in}}} \tag{66d}$$

D Additional Results

In the following section, additional results on the executed experiments are given. First, the example usage on the results is shown for a manually created scenario tree. Second, the VSS and EVPI are explored further. Finally, additional results of the solve time matrix are shown.

D.1 Fixed scenario tree

In the formulated case study, scenarios are sampled based on random distributions, and ran multiple times to account for more unbiased randomness. However, as the scenarios are not sampled symmetrically, some of the non-anticipativity is lost, as prices in one part of the scenario tree can coincidentally rise together, yielding the model to superficially know that part of the scenario tree. To measure the impact of this behavior, an alternative fixed scenario was created and applied to the main results.

The creation of the scenario tree follows a similar structure to Markhorst et al. (2026). In stage two, the contracted demand at German markets and UK markets can either go up or down by twice the respective standard deviation (see Table 10), such that it represents the realistic edges of possible demands. As there are two markets that can deviate up or down, this yields four possible scenarios for the demands, such that $\mid M_2 \mid= 4$.

Second, instead of the movement of all prices, the price movement was limited to deviation within each country. Namely, the markets are divided based on the country of origin shown in Table 10, and the price can either rise or decline by twice the long-term standard deviation. The short-term standard deviation is neglected in this case. In turn, the third stage obtains $\mid M_3 \mid= 64$. Together, this yields the possible demands and prices shown in Table 23. Note that in this case, only the extreme scenarios are examined, and standard occurring intermediate scenarios are neglected, yielding a large part of the uncertainty unexplored. Nonetheless, it can be used to generate some example results.

Table 23: Demand and price realizations by market

Market	Demand Realizations (Gwh)	Price Realizations (€/Mwh)
Emden	25 ± 15	28 ± 5.6
Dornum	25 ± 15	28 ± 5.6
St. Fergus	12.5 ± 7.5	26 ± 7.8
Easington	12.5 ± 7.5	26 ± 7.8
Zeebrugge	25	29 ± 5.8
Dunkerque	50	30 ± 6.0

D.1.1 Example Usage

To give an idea of the similarity between the results with random sampling, the example usage is repeated here. First, the entry and exit distributions are examined. Figure 49 shows that the entry flows are still fixed, while the outflows are again unstable. Most markets have the same outflows, however, the edges are more varied, corresponding to the fact that only the extreme scenarios are considered.

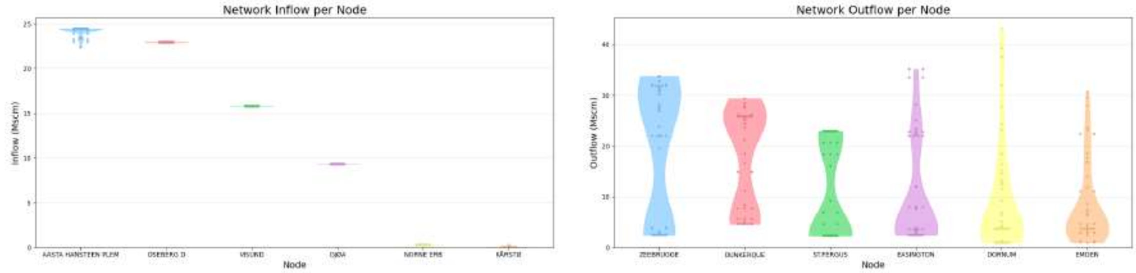

(a) Net inflow (Mscm) into the network from generation nodes. Inflow is again stable.

(b) Net outflow (Mscm) out of the network to market nodes. Outflow is again unstable.

Figure 49: Net inflow and outflow distributions for fixed scenario trees

Second, a comparison of entry and exit capacity bought per stage and node is shown in Figure 50. As price is only revealed in the third stage, but bears no relation with the stage two branch, most of the exit capacity is now only bought in stage three as the prices are more variable between scenarios, even though it is the day-ahead, and the change between intra-day and day-ahead prices are usually not large. Therefore, the sampling technique presented in the main section results in a more accurate depiction of booking behavior.

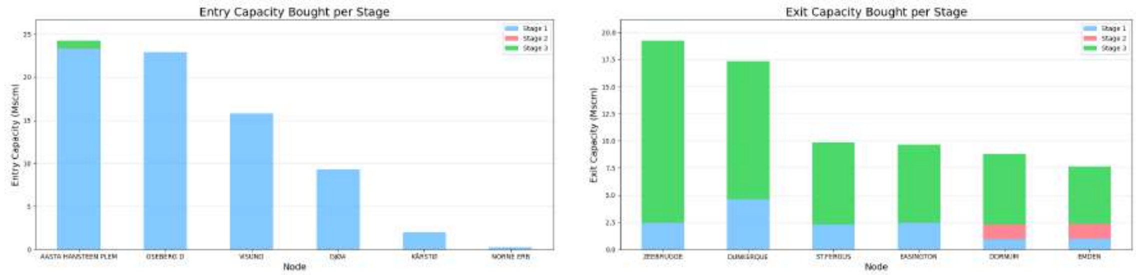

(a) Entry capacity per node (Mscm). The entry capacity is bought in the first stage mostly, which is related to the stable inflow.

(b) Exit capacity per node (Mscm). The exit capacity is bought mostly in stage three, corresponding to the high price fluctuation

Figure 50: Comparison of entry and exit capacity per node for the fixed scenario tree

In addition, the pressure distribution for the example arcs can be compared against the randomized sampling. The corresponding distribution is shown in Figure 51. Again, the results are nearly identical, although the outermost tail to the compression point (H7) obtains a more right skewed distribution here, instead of the bi-modal distribution.

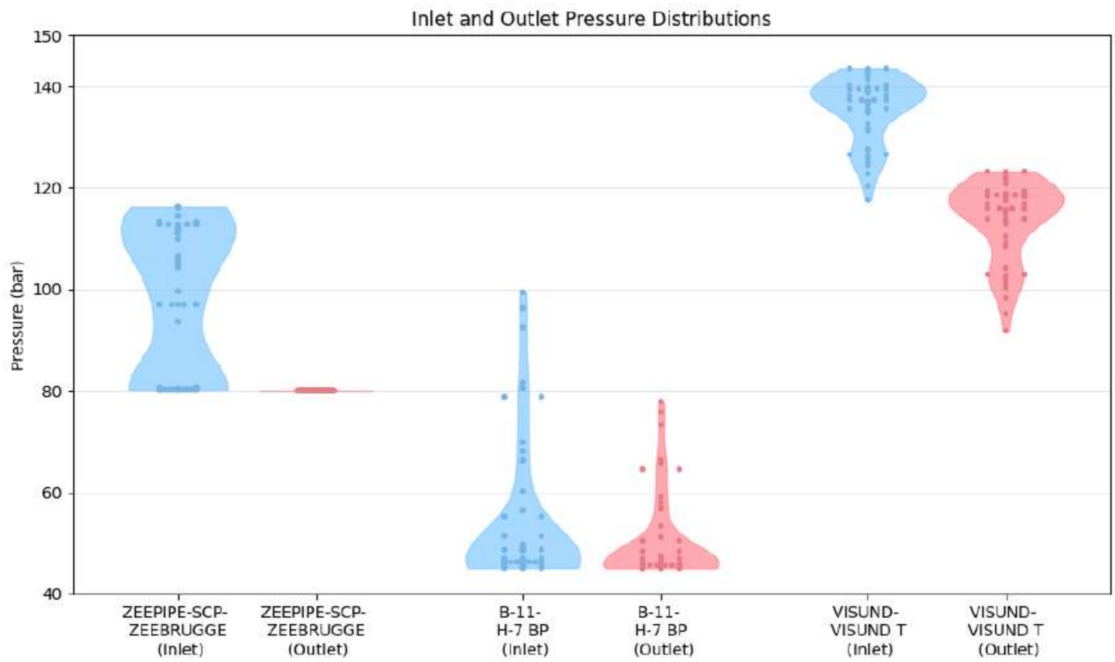

Figure 51: Distribution of inlet and outlet pressures (Bar) for 3 example arcs for a fixed scenario tree.

Finally, the distributions of the revenue and costs can be examined, which is shown in Figure 52. The figure shows that the spread between the scenarios becomes larger, resulting from the extreme scenarios pulling the objective apart between scenarios.

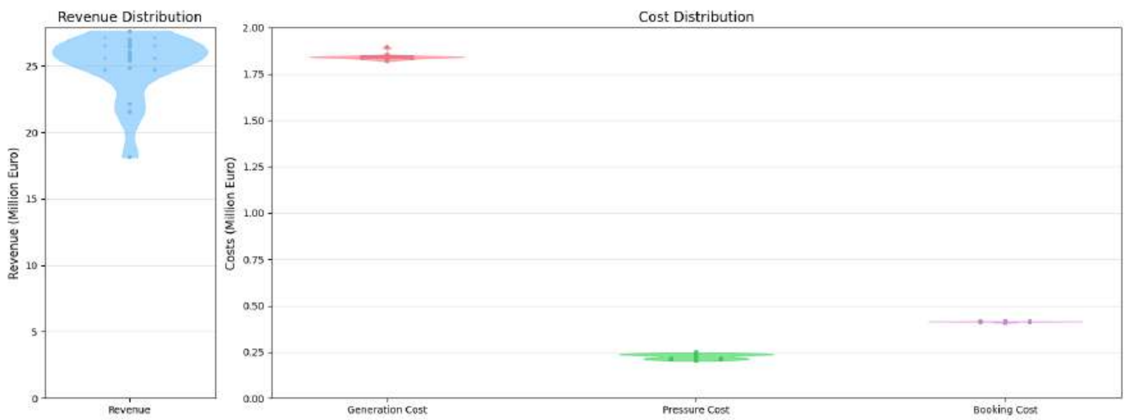

Figure 52: Distributions over the scenario of revenue and costs (Million €). The revenue is a degree higher than the cost, but is also more varied across scenarios.

Therefore, this choice of uncertainty results in more varied scenarios, due to the inclusion of solely extreme possibilities. In addition, the uncertainty on price yields the most consideration, as demand is only changed in four different ways.

D.2 Stochasticity Results

As discussed, computing the EVPI for fractional percentages of deviations is uninformative as it shows the benefit of deviation in each scenario, rather than the benefit of deciding based on the knowledge of the scenario. To avoid this behavior, the Conditional Expected Value of Perfect Information (CEVPI) is employed. The CEVPI uses a partial wait and see on chosen long-term decisions, while the remaining are given a conditional value. In this case, the entry-exit decisions remain under wait and see for each scenario, but the scenarios with deviation are conditioned upon, based on whether the main stochastic solution chose that scenario to allow deviation, denoted by the decision variable δ^*_m. The CEVPI for the current problem is formulated in Equation 67.

$$\text{CEVPI} = \mathbb{E}_{m \in M_3} \left[\max_{\boldsymbol{x}^m} O(\boldsymbol{x}^m, m) \mid \delta^*_m \right] - O \tag{67}$$

Using this equation, the VSS, EVPI and CEVPI were calculated for each of the explored fractional deviations. This results in Figure 53. The figure shows that the EVPI grows exponentially in the subsidy, as it becomes more worth deviating from the quality restrictions. Instead, when the deviation is fixed per scenario, the CEVPI actually decreases slightly when the subsidy becomes larger. This could be from the construction of fixing the scenarios, instead of optimizing separately. However, fixing the deviation yields a CEVPI value similar to those found when the deviation is 0% or 100%. This indicates that the CEVPI can more accurately depict the value of perfect information for capacity booking.

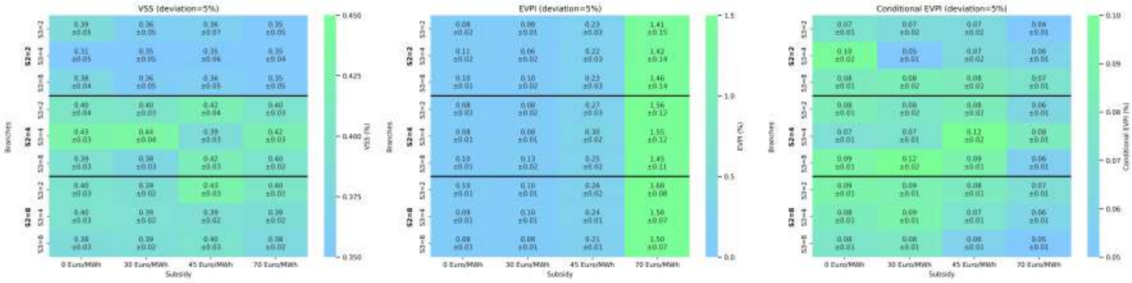

(a) Deviation 5%

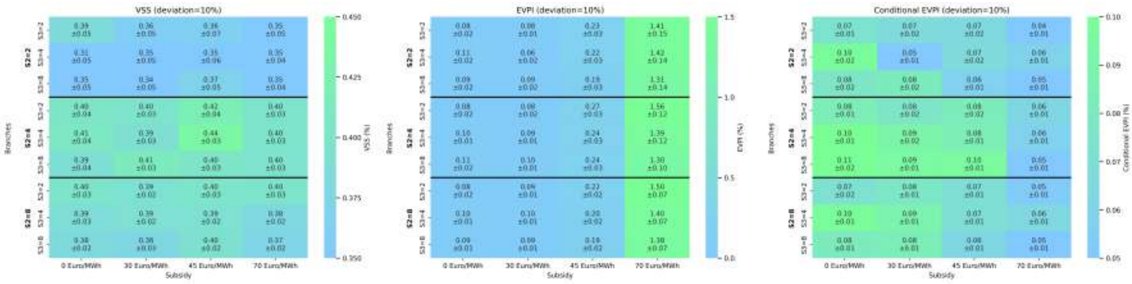

(b) Deviation 10%

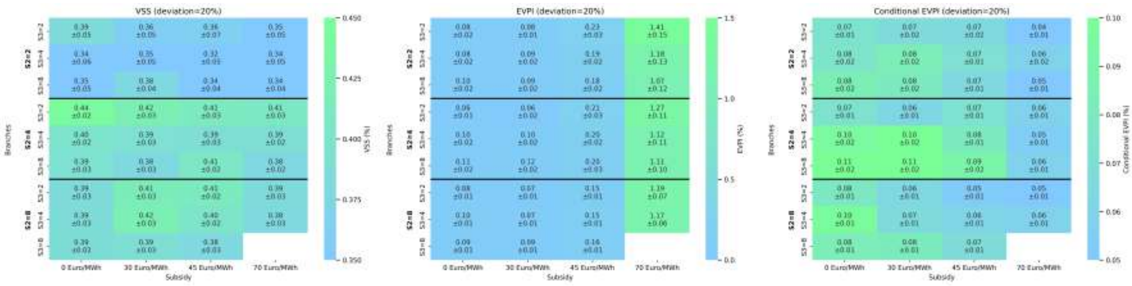

(c) Deviation 20%. The results for the €70/MWh subsidy case with 64 scenarios are not included, as one of the runs could not be solved within the allotted experiment time due to solver convergence issues. Consequently, the corresponding outcomes could not be reported.

Figure 53: Comparison of VSS, EVPI and CEVPI under different levels of allowed deviation.

D.2.1 VSS and EVPI Test explanation

The Mann-Whitney U-test can compare different groups, without a requirement on the underlying distribution of the sample. As the VSS and EVPI are non-negative quantities, normality cannot be assumed, which makes this test the appropriate choice. The test statistic U is calculated by Equation 68, where n_i resembles the sample size of group i, and R_i is the sum of ranks for group i. The current test is to determine whether different amount of branches in stage 2 yield unequal VSS and EVPI values. The different amount of branches that are tested are compared against each other.

$$U = \min\left(n_1 n_2 + \frac{n_1(n_1+1)}{2} - R_1, n_1 n_2 + \frac{n_2(n_2+1)}{2} - R_2\right) \tag{68}$$

Since multiple groups are compared, the p-values have to be corrected to reduce the family wide type one error rate. To be conservative, Bonferroni correction is applied (Weisstein, 2026a), which divides the significance level by the number of tests (m), which equivalently gives, for a family wide p-value (p_{value}), the experiment p-value mp_{value}. Together, this gives the results shown in Table 14.

D.3 Solve Time Results

Figure 54 displays a correlation heatmap of the features. The heatmap shows that nodes and edges provide the highest correlation with the log solve time. Instead, the density has a very negative correlation with the solve time.

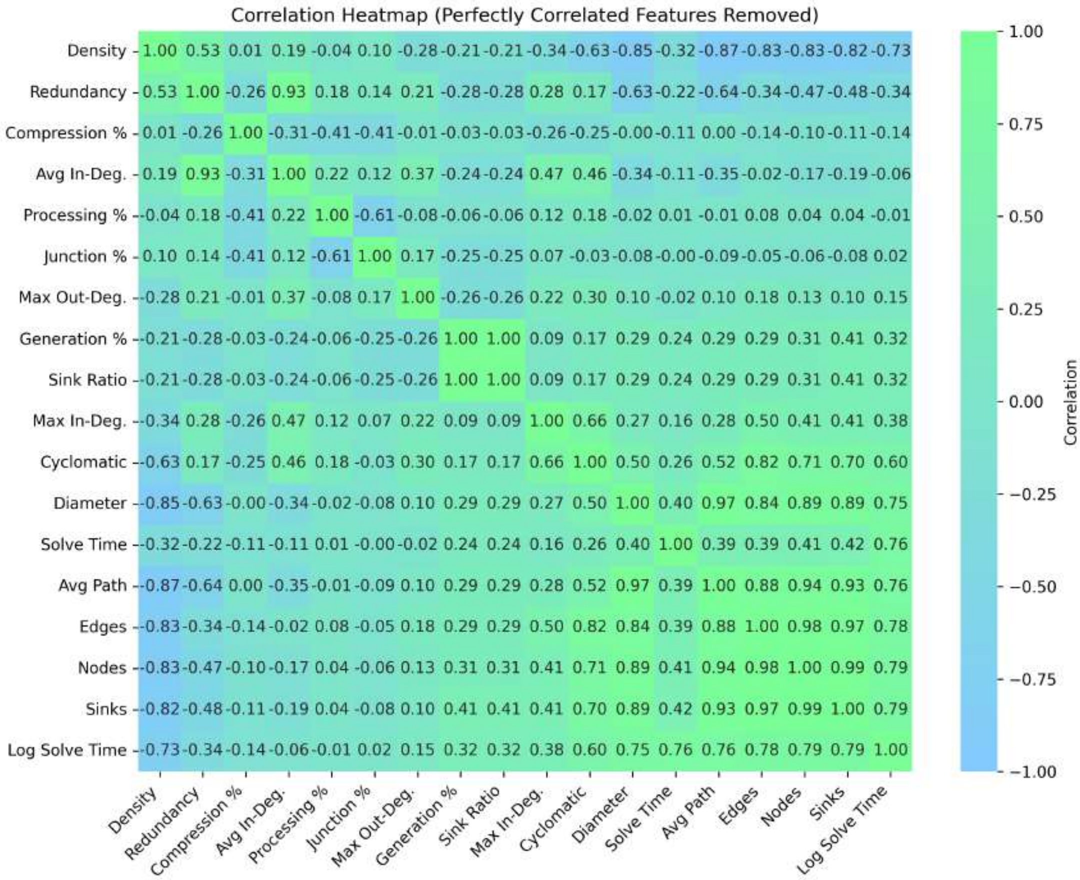

Figure 54: Correlation heatmap of the network features